UNIVERSITÉ DE YAOUNDÉ I
THE UNIVERSITY OF YAOUNDE I

FACULTÉ DES SCIENCES
FACULTY OF SCIENCE

DÉPARTEMENT DE PHYSIQUE
DEPARTMENT OF PHYSICS

ATTESTATION DE CORRECTION DE LA THÈSE DE DOCTORAT/Ph.D

Nous, Professeur **VONDOU Derbetini Appolinaire** et Professeur **NDJAKA Jean-Marie B.**, respectivement Examinateur et Président du jury de la Thèse de Doctorat/Ph.D de Monsieur **KEMGANG GHOMSI Franck Eitel**, Matricule **07W346**, préparée sous la codirection du Professeur **NGUIYA Sévérin** et du Professeur **NOUAYOU Robert,** intitulée : « **Reappraisal of the crustal configuration of three African hotspots from global gravity models constrained by seismic studies**», soutenue le **Lundi, 22 Mars 2021,** en vue de l'obtention du grade de Docteur/Ph.D en Physique, Spécialité **Physique de l'Environnement Terrestre,** Option **Géophysique et Geoexploration,** attestons que toutes les corrections demandées par le jury de soutenance ont été effectuées.

En foi de quoi, la présente attestation lui est délivrée pour servir et valoir ce que de droit.

Fait à Yaoundé le .....07 APR 2021.....

Examinateur	Le Chef de Département de Physique	Le Président du jury
Pr VONDOU Derbetini Appolinaire	Pr NDJAKA Jean-Marie Bienvenu	Pr NDJAKA Jean-Marie Bienvenu

Dedication

To my parents:

Mr. Ghomsi Jean Paul & Mrs. Domkem Alphonsine Epse Ghomsi

Acknowledgements

Above all, I am deeply grateful to God, the Almighty, for giving me the opportunity to bring forth the present study and for giving me the resources to do so. He has empowered me to believe in my passions to pursue my aspirations. Without this gift and the faith that comes with it, I would be powerless.

I thank the Institute for Geological and Mining Research through his General Director, Dr. Joseph Victor Hell and the Nansen Scientific Society through Prof. Ola Johannessen for the opportunity they gave me to complete one part of my doctorate in their Institute and research center respectively. I also thank the University of Yaoundé I and the Physics Department for granting me authority to travel abroad for capacity building through some international fellowship programs.

At this point I want to express my gratitude to several people who have been involved in the evolution of this thesis in one way or the other:

- I wish to express my gratitude to all members of the jury for agreeing to read the manuscript and to participate in the defense of this thesis;
- Prof. Robert Nouayou, my supervisor, who motivated me to tackle the PhD, proposed the field of investigations and was supporting and guiding me with his expertise;
- Special thank to Prof. Sévérin Nguiya, my thesis director, who gave me the freedom to pursue my research ambitions and was helping me with his tremendous knowledge whenever a question arose;
- I am deeply and indebted grateful to Dr. Animesh Mandal of the Indian Institute of Technology, Kanpur, India for his tutelage useful criticisms, guidance and review of my research work. I have no words to describe my gratefulness for all your invaluable contribution towards the completion of my PhD studies;
- Dr. Robert Tenzer, I would like to thank you for encouraging me to explore research areas that I feel most interested in, and to broaden my scientific vision despite the spatial distance;

- I thank tremendously Prof. Derbetini A. VONDOU for his academic support, guidance, review and support since my graduate admission, you have been for me a father, a Professor and an example, I owe my entire gratitude to you;

- I thank Prof. Philippe NDJANDJOCK, for his valuable academic support and review regarding my research work and more;

- My sincere gratitude to Dr. Alain P. TOKAM and Dr. Evariste NGATCHOU, my advisors, who motivated me to tackle the PhD, proposed the field of investigations and were supporting and guiding me with their expertise;

- I am also thankful to Dr. Mohamed SOBH and Dr. Jeannot NGALAMO for their useful discussions and tutoring on data processing;

- My gratitude goes also to all faculty members at the Physics Department of the University of Yaoundé I.

- I would like to express appreciation for the support I have received over the duration of my PhD journey to my lab mates Dommo, Tamoffo, Taguela, Kuete, Djeufa, Nonki, Fantah, Nana, Lemotio, Kamto and the Batch 07.

- But what would have been my PhD period and this thesis without the incredible support of Mr. Charles TEGUEM and Barrister Georges TEGUEM? Of course, the answer is obsolete, thanks to all of you who were always by my side, all along the way, whether you could follow it or not. Thank you very much for this incredible support. Thanks to you, these years have been complete and I look forward to continuing in the future what we began yesterday. My warmest thanks to Mummy Justine KAMMEGNE and Mr. Jean-Pierre GANSU, and to the wonderful MAGHA couple, especially to Joyce Brenda TEFANG for her delicacy and care.

- Last but not least, I would like to thank Guylaine, Sonia, Stéphane and Morel named the GHOMSI TEAM. My sincere thanks to my uncles, cousins and parents for their unconditional love and support. It is only because of their prayers, support and encouragement that I am able to complete this thesis. Their love, care and patience are indescribable and beyond words.

- Finally, special thanks go my nephews: Gabrielle, Daina, Evan, Aaron, Uriel, Jean-Baptiste, Eddy-Sylvain and Ivana, I love you more than anything and I appreciate all your patience and support during my Ph.D. journey.

Contents

List of Symbols vii

List of Figures viii

List of Tables xi

Abbreviations xii

Abstract xv

Resume xvii

General Introduction 1

Chapter 1 Geological and Geodynamic setting 7

1.1 Atlas configuration . . . 9

1.1.1 Geological setting of Atlas region . . . 9

1.1.2 Previous crustal studies of Atlas region . . . 11

1.2 Cameroon configuration . . . 14

1.2.1 Geological setting of Cameroon . . . 14

1.2.2 Previous Cameroon crustal studies . . . 17

1.3 East African configuration . . . 19

1.3.1 Geological setting of East African Rift System (EARS) . . . 19

1.3.2 Previous EARS crustal studies . . . 22

Chapter 2 Data and methodology 24

2.1 Data . . . 24

2.1.1 Sediment thickness . . . 24

2.1.2 Topography/Bathymetry and background datasets . . . 26

2.1.3 Africa Broadband seismic stations and seismic Moho estimates . . . 26

2.1.4 Crustal gravity based models . . . 31

2.1.5 Gravity data . . . 32

2.1.5.1 EIGEN-6C4 gravity model . . . 34

2.1.5.2 XGM2016 gravity model . . . 35
2.2 Methodology . . . 36
2.2.1 Gravitational Potential and Geoid . . . 36
2.2.2 Gravimetric anomalies . . . 37
2.2.2.1 Normal Gravity and Gravimetric Anomaly . . . 37
2.2.2.2 Free Air Anomaly . . . 38
2.2.2.3 Bouguer gravity anomaly . . . 39
2.2.3 Fundamental model of upward continuation . . . 40
2.2.4 Airy Isostasy . . . 42
2.3 Gravity inversion for crustal estimation . . . 43
2.3.1 Inversion algorithm . . . 43
2.3.2 Gravity modeling of a density layer in spherical coordinates . . . 45
2.3.3 Parameter estimation . . . 46
2.3.3.1 Estimating regularizing parameter . . . 47
2.3.3.2 Estimating the reference Moho depth and the density contrast . . . 47
2.4 Flowchart of the processing methodology . . . 48

Chapter 3 Results and discussions **50**
3.1 Crustal thickness beneath Atlas region from gravity, topographic, sediment and seismic data . . . 50
3.1.1 Free-air gravity data . . . 50
3.1.2 Bouguer gravity data . . . 51
3.1.3 Seismic data . . . 55
3.1.4 Comparison with seismic Moho depth estimates . . . 56
3.1.5 Comparison of regional Moho models . . . 59
3.1.6 Discussion of results . . . 59
3.1.6.1 Gravity maps . . . 61
3.1.6.2 Comparisons of Moho depth estimates . . . 62
3.1.6.3 Study profiles . . . 64
3.1.7 Summary and concluding remarks . . . 68
3.2 Cameroon's crustal configuration from global gravity and topographic models and seismic data . . . 69
3.2.1 Free-air gravity data . . . 69
3.2.2 Bouguer gravity data . . . 71
3.2.3 Seismic data . . . 74
3.2.4 Results . . . 76
3.2.4.1 Moho depth from gravity inversion . . . 76

3.2.4.2 Validation of result . . . 79
3.2.5 Discussion of results . . . 79
3.2.5.1 Gravity maps . . . 79
3.2.5.2 Bouguer gravity images at different elevations . . . 81
3.2.5.3 Moho models . . . 83
3.2.5.4 Cross comparisons of Moho models . . . 86
3.2.6 Summary and concluding remarks . . . 88
3.3 Equatorial east African crustal configuration from gravity and seismic data analysis . . . 92
3.3.1 Free-air gravity data . . . 92
3.3.2 Bouguer gravity data . . . 92
3.3.3 Upward gravity continuation . . . 96
3.3.4 Seismic data . . . 99
3.3.5 Results . . . 101
3.3.5.1 Optimal regularization parameters constraints . . . 101
3.3.5.2 Moho model . . . 103
3.3.6 Discussion of results . . . 107
3.3.6.1 Cross comparisons of Moho models . . . 107
3.3.6.2 Model performances . . . 109
3.3.6.3 Study profile . . . 111
3.3.7 Summary and concluding remarks . . . 112

Conclusion **114**

Bibliography **118**

List of Publications **132**

List of Symbols

ϕ: Latitude (°)

λ: Longitude (°)

r: Radius (km)

G: Constant of Universal Gravitation (6.67384×10^{-11} m/s^2)

g: Acceleration of normal gravity (mGal)

Δg_{fa}: Free Air Anomaly (mGal)

Δg_{bg}: Bouguer anomaly (mGal)

mGal: Acceleration unit, equivalent to 10^{-5}m/s^2

t: Normal crust width (km)

h: Topographic height (km)

ρ_t: Density of Topography (kg/m^3)

ρ_c: Density of the Crust (kg/m^3)

ρ_m: Density of the Mantle (kg/m^3)

List of Figures

Figure 1 Simplified geological map of Africa showing our three study areas: the Cameroon Volcanic Line, Rif-Tell-Atlas and the East African Rift System. 8

Figure 2 Regional geological and tectonic configuration of the Atlas region including seismicity. 10

Figure 3 Tectonic setting and regional geological map of Cameroon. 16

Figure 4 Sub-regions of previous crustal investigations overlaid on a simplified tectonic map of Cameroon. 18

Figure 5 Topographic (a) and regional geo-tectonic configuration (b) of the East African Rift System (EARS) region including seismicity. 20

Figure 6 Thickness of sediments in Africa from the global sediment thickness map from. . 25

Figure 7 Bathymetry and topography map of our three study areas (ETOPO1): the Cameroon Volcanic Line, Rif-Tell-Atlas and the East African Rift System. . . . 27

Figure 8 Map of Africa showing the seismic networks and stations involved in this study modify after (Ojo et al., 2019). 29

Figure 9 Crustal thickness in (a) Cameroon Volcanic Line, (b) East African Rift System, and (c) the Atlas orogen (Africa-Eurasia collision) constrained using receiver function analysis. 30

Figure 10 The juxtaposition of some existing crustal models for Africa. 33

Figure 11 Observed Gravity and Anomaly Observed for an example with Topography, Root and anomalous body in bark, measured in topography. 39

Figure 12 Free Air Anomaly and Simple Bouguer Anomaly for the same example as the Figure 11. 40

Figure 13 Upward continuation sketch map. 41

Figure 14 Lithospheric profile with topography, normal crust, isostatic Airy root and upper mantle. 43

Figure 15 A subsurface density layer consists of a grid of juxtaposed Tesseroid units in spherical coordinates with constant top and bottom surfaces. 45

Figure 16 Data splitting approach in which black points represent testing data and hallow points represent training data. 46

Figure 17 Schematic realization of the project. 49

Figure 18 Regional maps the free-air gravity anomalies computed on a $5' \times 5'$ grid of surface points. 51

Figure 19 Regional maps of: (a) the topographic-bathymetric and (b) sediment gravity corrections computed on a $5' \times 5'$ grid of surface points 52

Figure 20 Regional maps of the Bouguer gravity anomalies: (a) before and (b) after applying the sediment gravity correction computed on a $5' \times 5'$ grid of surface points. 54

Figure 21 Seismic Moho depth estimates from receiver functions analysis seismograph stations (circles), superimposed on a regional shaded topography. 56

Figure 22 Validation steps exploited to determine the Moho reference depth and the Moho density contrast. 57

Figure 23 Regional map of the Moho depth estimated based on a regularized non-linear inversion of the sediment-corrected Bouguer gravity data. 58

Figure 24 3D ensemble views of the crustal topography. Panels show the Moho geometry below depth of: (a) 40 (b) 30 (c) 20, and (d) 0 km. 60

Figure 25 The juxtaposition of existing crustal models for the Atlas region. The gravity-based models are GEMMA, Tugume13 and Tedla11. 60

Figure 26 Comparison between regional crustal thickness models and our model. 63

Figure 27 Study profiles for comparing values of the free-air and Bouguer gravity anomalies with the Moho depth and the topography across the Rif-Tell-Atlas orogenic region. 66

Figure 28 Regional map of the free-air gravity disturbances computed from the EIGEN-6C4 on a $5' \times 5'$ geographical grid. 70

Figure 29 Regional map of: (a) the topographic-bathymetric and (b) sediment gravity corrections computed on a $5' \times 5'$ grid of surface points. 72

Figure 30 Regional maps of the Bouguer gravity anomalies: (a) before and (b) after applying the sediment gravity correction computed on a $5' \times 5'$ grid of surface points. 73

Figure 31 Seismic Moho depth estimates from CBSE seismograph stations (circles) including 2 sites in Nigeria, superimposed on a regional shaded topography. 75

Figure 32 Validation steps exploited to determine the Moho reference level and the density contrast. 77

Figure 33 Bouguer gravity residuals (left panel) between the observed data (in Fig. 30a) and the predicted data (right panel) 78

Figure 34 Regional map of the Moho depth estimated based on a regularized non-linear inversion of the Bouguer gravity data. 78

Figure 35 Relation between the refined Bouguer gravity disturbance (uppermost), and (downwards) Gravity disturbance, Elevation, Moho. 80
Figure 36 Histogram of the Moho depth differences between the seismic and gravimetric estimates at the CBSE sites in Cameroon and 2 sites in Nigeria. 81
Figure 37 Regional maps of the Bouguer gravity disturbances continued upward at the constant elevations of: (a) 20 km, (b) 40 km, (c) 60 km, (d) 80 km, (e) 100 km, and (f) 120 km above the sea level. 82
Figure 38 The juxtaposition of existing crustal models for the Cameroon region. 86
Figure 39 Comparison of our model with (a) VMM model by (Bagherbandi et al., 2013), and (b) GEMMA model by (Reguzzoni and Sampietro, 2015). 87
Figure 40 EARS regional map of the free-air gravity disturbances. 93
Figure 41 Regional maps of: (a) the topographic-bathymetric and (b) sediment gravity effects. 94
Figure 42 Regional maps of the Bouguer gravity disturbances: (a) before and (b) after applying the sediment gravity correction. 95
Figure 43 Maps of the refined Bouguer gravity disturbances at elevations of: 20 (a), 40 (b), 60 (c), 80 (d), 100 (e), and 120 (f) km. 98
Figure 44 Seismic Moho depth estimates from receiver functions analysis at seismograph stations (circles), superimposed on a regional shaded topography. 100
Figure 45 Parameter estimation results. 102
Figure 46 EARS Regional Moho model 104
Figure 47 Comparison of our model with the published results: (a) GEMMA (Reguzzoni and Sampietro, 2015), (b) Tegume13 (Tugume et al., 2013), and (c) Tedla11 (Tedla et al., 2011). 108
Figure 48 Taylor diagram displaying statistics of comparison of our Moho model with GEMMA, Tegume13, and Tedla11. 110
Figure 49 West-East profile showing the Bouguer gravity disturbances, the free-air disturbances, and the Moho depth across Congo and southeast Kenya 111

List of Tables

Table 1 Moho depths of previous investigations for the Rif-Tell-Atlas orogenic system. . 13

Table 2 Statistics comparison between VMM, GEMMA, Tugume and Tedla crustal Models. 32

Table 3 Atlas Statistics of the referenced crustal models. 59

Table 4 Atlas statistics of differences between values of the new density model and the referenced crustal models. 64

Table 5 Characteristics of the studied sections drawn on the Moho depth, the free-air and sediment-free Bouguer gravity maps. 65

Table 6 Summary of the Cameroon's crustal structure by geological terrain compare between Moho depth estimates obtained. 85

Table 7 Cameroon's statistical comparison between VMM, GEMMA and the Referenced Crustal Models 88

Table 8 Statistical comparison between GEMMA, Tugume13, Tedla11 and the Referenced Crustal Models based on Taylor diagram. 110

Abbreviations

AAEASE: Africa Array Eastern Africa Broadband Seismic Experiment

AATBSE: Africa Array Tanzania Basin Seismic Experiment

CBSE: Cameroon Broadband Seismic Experiment

CC: Congo Craton

CHAMP: Challenging Minisatellite Payload

CVL: Cameroon Volcanic Line

DSS: Deep Seismic Sounding

D/O: Degree and Order

EAGLE: Ethiopia − Afar Geoscientific Lithospheric Experiment

EARS: East African Rift System

EIGEN: European Improved Gravity model of the Earth by New techniques

ESA: European Spatial Agency

GEMMA: GOCE Exploitation for Moho Modeling and Applications

GGM: Global Gravitational Models

GNSS: Global Navigation Satellite Systems

GOCE: Gravity Field and Steady-State Ocean Circulation Explorer

GOCO: Gravity Observation COmbination

GRACE: Gravity Recovery and Climate Experiment

KC: Kaapvaal Craton

KCF: Kribi Campo Fault

KiB: Kibaran Belt

KRISP: Kenya Rift International Seismic Project

LAB: Lithosphere − Asthenosphere Boundary

LADS: Laser Airborne Depth Sounder

LAGEOS: Laser Geodynamics Satellites

MAMBA: Geophysical Measurements Across the continental Margin of Namibia

MB: Massai Blocks

MnB: Manyara Rift

MDT: Mean Dynamic Topography

MoB: Mozambique Belt

MSE: Mean Square Error

Myr: Million years

PATSB: Pan-African Trans-Saharan Belt

PR: Pangani Rift

RwB: Rwenzori Belt

RF: Receiver Function

RMSE: Root Mean Square Error

RTA: Rif-Tell-Atlas

SASE: South Africa Seismic Experiment

SGG: Satellite Gravity Gradiometry

SMC: Sahara Meta-Craton

SSZ: Sanaga Shear Zone

STD: Standard Deviation

UbB: Ubendian Belt

UsB: Usagran Belt

TBSZ: Tchollire-Banyo Shear Zone

VMM: Vening−Meinesz Moritz

WAC: West African Craton

WAMZ: West African Mobile Zone

WGS84: World Geodetic System 1984

Abstract

The Mohorovičić discontinuity (or Moho) is the boundary between the Earth's crust and mantle. The Moho depth is primarily detected from seismic data. Unfortunately, seismic data coverage in large parts of Africa is low. Gravity data is used to determine the Moho depth where seismic surveys are insufficient. The progress in gravity data acquisition from multiple sources (terrestrial, airborne, shipborne and satellite) in compiling new promising generation of global gravitational model as EIGEN−6C4 and XGM2016 gravity data have been used in this work. In this regard, we compile a new Moho model of the Atlas Mountains, Cameroon Volcanic line and Tanzanian Craton, based on a gravimetric inversion constrained on seismic data respectively. The Bouguer gravity anomalies used for a gravimetric Moho recovery are obtained from the free-air gravity anomalies after subtracting the gravitational contributions of topography, bathymetry and sediments. The regional gravimetric Moho inversion constrained on seismic data have been carried out by applying a regularized inversion technique based on Gauss-Newton's formulation of improved Bott's method, while adopting a spherical approximation for the Earth. Along the Atlas mountains, our findings indicate a limited tectonic shortening of the High Atlas with the crustal thickness mostly within $36 - 42$ km. The Topographic discrepancies between the Rif Cordillera and the Atlas Mountains suggest that the hypothesis of isostatic compensation cannot be fully established. In Cameroon we found that the Yaoundé domain likely represents the crustal manifestation of the suture zone between the Adamawa-Yadé domain, acting as a micro-continent and the Congo Craton. Finally along the EARS, our result deciphers a thick lower crust beneath the Rwenzori Belt which seems to be associated with a crustal modification occurring during rifting episodes

that induced the delamination of the lithospheric mantle and consequently resulted in crustal uplift. These findings support a non-collisional origin of the central Rwenzori Mountains.

Key words: Atlas, Cameroon, East African Rift, GOCE, Gravity inversion, Moho, Seismic data.

Résumé

La discontinuité de Mohorovičić (ou Moho) est la limite entre la croûte terrestre et le manteau. La profondeur du Moho est principalement identifiée à partir des données sismiques. Malheureusement, la couverture des données sismiques est faible dans une grande partie de l'Afrique. Les données gravimétriques sont utilisées pour déterminer la profondeur du Moho lorsque les études sismiques sont insuffisantes. Les progrès réalisés dans l'acquisition de données gravimétriques provenant de sources multiples (terrestres, aériennes, navales et satellitaires) dans la compilation d'une nouvelle génération prometteuse de modèles gravimétriques mondiaux comme les données gravimétriques EIGEN−6C4 et XGM2016 ont été utilisées dans ce travail. À cet égard, nous compilons un nouveau modèle de Moho des montagnes de l'Atlas, du Cameroun et du Craton de Tanzanie, basé sur une inversion gravimétrique contrainte sur les données sismiques. Les anomalies gravimétriques de Bouguer utilisées pour une carte de Moho issue de l'inversion gravimétrique sont obtenues à partir des anomalies gravimétriques à l'air libre après soustraction des contributions gravimétriques de la topographie, de la bathymétrie et des sédiments. L'inversion gravimétrique régionale du Moho contrainte sur les données sismiques a été réalisée en appliquant une technique d'inversion régularisée basée sur la formulation de Gauss-Newton ainsi que de la méthode optimisée de Bott, tout en adoptant l'approximation sphérique de la Terre. Le long de l'Atlas, nos résultats indiquent un rétrécissement du Haut Atlas, avec une épaisseur de la croûte terrestre se situant principalement entre $36 - 42$ km. Les divergences de topographie entre la Cordillère du Rif et les montagnes de l'Atlas suggèrent que l'hypothèse de la compensation isostatique ne peut être entièrement établie. Au Cameroun, nous avons constaté que le domaine de Yaoundé représente

une manifestation crustale de la zone de suture entre le domaine l'Adamaoua-Yadé et le Craton du Congo, agissant comme un micro-continent. Enfin, le long du Rift Est-Africain, notre résultat décèle une épaisse croûte sous la ceinture des massifs du Rwenzori qui semble être associée à une modification crustale s'étant produite lors des épisodes de rifting qui ont induit la délamination de la couche lithosphérique et a donc provoqué un soulèvement de la croûte terrestre. Ces résultats confirment l'origine non-collisionnelle des montagnes centrales du Rwenzori.

Mots clés: Atlas, Cameroun, Rift Est-Africain, GOCE, Inversion gravimétrique, Moho, Données Sismiques.

General Introduction

Gravity techniques have been widely used as an exploration tool for oil and mining exploration. With the availability of airborne, marine, and latest gravitational models, compiled based on the combined analysis of satellite observations, gravimetric methods have been expanded to recognize salt-dome provinces, overthrusts, foothills and under-explored basins. Gravity data has played a role in the understanding of the Mohorovičić discontinuity geometry of the density variations from the crust to the upper mantle, especially when no other information is available, or when seismic data are scarce, when the seismic image of the lower crust is poor. The characterization of Moho geometry, and therefore of crustal structure, is fundamental for the understanding of the formation and evolution of potential sedimentary basins in the appropriate tectonic context.

The current crustal structure of the African continent is the result of a complex geodynamic history that dates back more than $3,700$ million years and includes: (i) the formation of juvenile crusts and craton stabilization in the Archean; (ii) a major crustal reworking in the Proterozoic; (iii) a Pan-African assemblage followed by a Mesozoic dislocation of the Gondwana supercontinent; and (iv) widespread volcanism, uplift and continental fracture in the Cenozoic. The structure of the African crust has been the subject of several continental and global studies, but many parts of the continent are still poorly known and insufficiently studied seismically.

In the past three decades over 1117 broadband seismic stations (Ojo et al., 2019) have been deployed in a number of permanent and temporal seismic networks across Africa (e.g. KRISP, EAGLE, MAMBA, Africa-Array, SASE). They were crucial for improving knowledge the crust and upper mantle geodynamic structure based on the

highly controversial processes that formed the African continent. We can denote the development of crusts and the stability of cratons during the Archean period, the African Superswell, the division of the crust/mantle into successive tectonic episodes, and the volcanism of the Cenozoic hotspots and the active rifting. The precise knowledge of the current variations in density and average thickness of the crust/mantle of the different tectonic units of the African continent is an essential contribution to the understanding of these processes.

Nevertheless, the most notable distributions of available seismic data come from stations that are distributed in four areas, namely the Cameroon region in West Africa, the Rif-Tell-Atlas in North Africa, the East African Rift System and the Kaapvaal-Zimbabwe Craton. There are many regional and continental scale crustal models for Africa, which can be built by extracting this knowledge from global models to fill the data gaps. Existing crust models, mainly seismological, gravity or a combination of both, provide uniform coverage but differ significantly depending on the modeling technique, resolution and type of data used to extrapolate the seismic estimates over large unsampled areas (Van der Meijde et al., 2015). However, they share the advantage of incorporating a variety of information on the properties of the Earth's crust with a high spatial resolution, which allows the depth of subsurface discontinuities, such as Moho and Lithosphere–Asthenosphere Boundary (LAB), to be estimated below the regions with no data.

First studies of the Moho depth beneath Africa were presented as a part of global models. The CRUST1.0 global seismic crustal model (Laske et al., 2013) is an upgraded version of the previous CRUST2.0 and CRUST5.1 models, where the Moho depth of unsampled regions (such as large parts of Africa) was statistically inferred according to basement age or tectonic setting. CRUST2.0 and CRUST1.0 were the most frequently used models in geodynamic and gravity modeling. Both these models have also been extensively used for crustal corrections in seismological studies. Recently, number of gravity-based global Moho depth models have been presented, which take advantage of a global coverage of the Earth's gravity field

measured by satellite gravity missions. Inverting gravity data for the Moho depth determination has been applied to generate models that are only based on gravity observations, such as the Veining Meinesz-Moritz model by Bagherbandi et al. (2013), as well as models that combine gravity observations with seismic data, such as the GEMMA model (Reguzzoni and Sampietro, 2015).

Indeed, these global studies have increased the knowledge about the Moho depth beneath Africa, but their associated resolution is still too coarse to be applied regionally. New continental-scale Moho depth estimates in Africa based on gravity modeling were presented by Tedla et al. (2011) and Tugume et al. (2013). Both studies provide the Moho depth models determined from gravity data and calibrated against seismic Moho depth estimates. The Moho depth model of Tugume et al. (2013) shows overall a shallower Moho depth than the model of Tedla et al. (2011) for eastern, southern and central Africa, with differences of more than 6 km for portions of western and northern Africa. Interestingly, the comparison between existing Moho depth models for Africa shows remarkable differences in regions where no seismic data are available, especially between global and continental models. Recently, Van der Meijde et al. (2013) pointed out that these differences may be up to 28 km in the Moho depth, and that gravity-based models show less variation between them than that seen when comparing seismic models or combined gravity-seismic models. As there is almost no control over the quality of resulting structures in regions with sparse seismic data coverage, these authors warn that the impact of these differences on geodynamic interpretations might be significant.

The current situation indicates the importance of a new Moho model for this continent based on accurate seismic data and incorporating the latest gravity models that allow improving the accuracy and resolution of the Moho model significantly. To address this issue, this thesis will deliver the latest Moho depth model of three major geodynamic areas , African areas such as Cameroon, Atlas, and East African Rift System, with approximately 10 km of spatial resolution and $3-5$ km of expected accuracy. The determination of the Moho depth requires information about

the crustal density distribution. Seismic data coverage in many parts of Africa is insufficient. The state-of-the-art computational methods for gravimetric forward and inverse modeling will be developed and implemented to determine the Moho depth from gravity data in these regions with adequate seismic data coverage. These methods will be based on the regularized non-linear gravity inversion method developed by Uieda and Barbosa (2016) for the Earth sphericals approximation and solved by employing the tesseroids technique (Anderson, 1976). This method, modified for the Earth's spherical approximation will allow solving the gravity inversion for the Moho depth over much larger regions than the existing planar form of this method that is suitable only for local applications. The regularized non-linear gravity inversion technique allows high-speed computations when dealing with detailed gravity data covering large areas. The resulting thickness maps have been compared with recent continental and global scale models of crustal thickness.

Thesis objectives

The main objective of this thesis is to develop crustal thickness maps of active deformation zones in Africa that are consistent with available seismic estimates in conjunction with topographic and sediment data, in order to ensure their validity, where existing crustal models predict contrasting results.

In this respect, the following specific objectives have been set:

- Provide the first high-resolution sediment-corrected Bouguer gravity maps, constraining with topographic-bathymetric and sediment gravity corrections for three African active deformation zones which can serve as a base of geodetic and geophysical applications.
- Make a complete compilation of the seismic crustal thickness: compiling information on Moho depth in Africa from available deep seismic sounding (DSS) and receiver function (RF) to better evaluate the relevance of the crust thickness model.

- Provide crustal thickness map of the Cameroon, Rif-Tell-Atlas and East African Rift System (EARS) including some cratonic features such as Congo Craton, Sahametacraton and West African Craton that are consistent with the available seismic data.
- Comparing the obtained crustal thickness model with most recent African gravity-based models and discuss the differences and their geodynamic implications.

Thesis Structure

Beside the general introduction and the conclusion, the rest of the thesis is organized as follows:

Chapter 1 summarizes the geological record of the African continent, especially significant events that occurred during the Archaean episodes when the West African, Congo, and Tanzanian cratons formed, followed by Palaeoproterozoic accretion of cratons. Thus, including the collisional belts of NW Africa and the recent magmatism, which has modified crustal structure beneath West-Central Africa along the Cameroon Volcanic Line (CVL).

Chapter 2 introduces the set of input data, topography and sediment that are used in the gravimetric forward modeling and a Moho inversion procedure. Furthermore, available crustal parameters such as sediment thickness and topographic gravity correction are presented together with an extensive review of the actual knowledge of the crustal structure and available point estimates of crustal thickness in Africa from seismic experiments. This chapter also contains a section on geopotential theory, global geopotential models on Earth, and descriptions of various gravity fields such as geoid, gravity disturbance, gravity anomaly. Finally, this chapter also illustrates the method estimates the depth of the crust-mantle interface (the Moho) from observed gravity data using a spherical Earth approximation.

Chapter 3 consists of results and discussions of the significance of the obtained results within a critical comparison with existing crustal, deduced from the gravity and passive seismic data along the three selected African hotspots.

Chapter 1

Geological and Geodynamic setting

Africa is an old continent with a large area occupied by Precambrian shields. It assembled as a single continent about 600 Myr ago with the formation of the African plate (Begg et al., 2009), one of largest relatively stable crustal blocks, as seen in Figure 1. The plate occupies almost whole Africa except for the northwestern (Altas mountains in Morocco) and southern (Capó region, South African Republic) parts. It formed by amalgamation of the Congo, Kalahari, Somali, Central African and West African plates (Pasyanos and Nyblade, 2007). It consists of several large Archean cratons with the Congo Craton ($\backsim$ 40×10^5 km^2) and the West African Craton (29×10^5 km^2) being the largest with an average crustal thickness of 40 km. Much smaller cratons, including the Kaapvaal Craton (5.5×10^5 km^2), the Tanzanian Craton (4×10^5 km^2) and the Zimbabwe Craton (2.4×10^5 km^2) have a similar Moho depth varying from $39 - 40$ km (Baranov and Bobrov, 2018). In comparison to many other continents, the knowledge of the Precambrian crustal structure of Africa, including rift systems and supersweell is very limited. In the following subsections, we will briefly describe the most notable tectonic features of these three atypical regions, highlighting their importance in relation to the current structure of Africa's crust and anomalous topographic features.

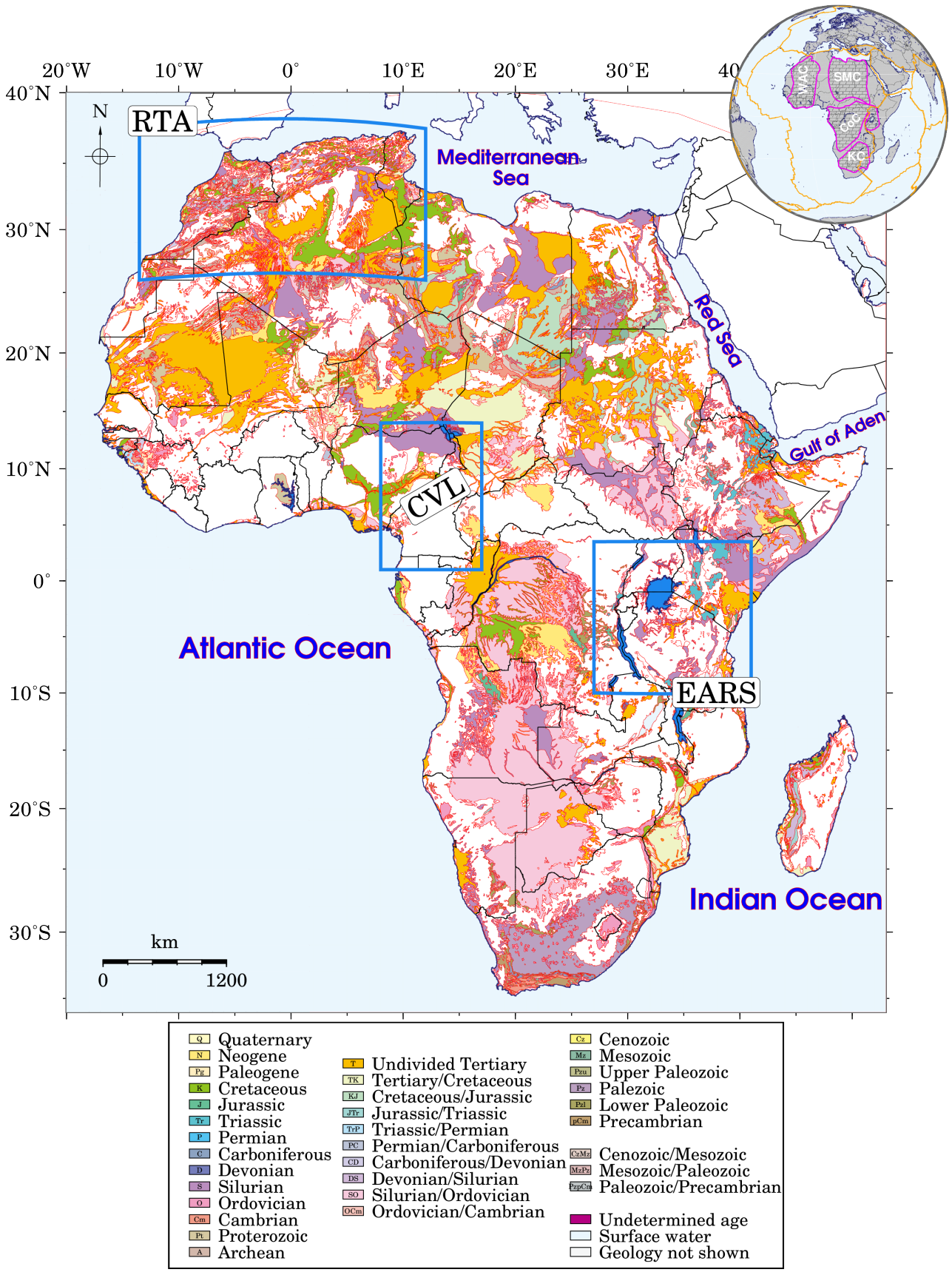

Figure 1: Simplified geological map of Africa showing our three study areas: the Cameroon Volcanic Line, Rif-Tell-Atlas and the East African Rift System. The inset shows in purple the location and extent of the Archean Cratons and intracratonic basins. The orange lines indicate plate boundaries according to Bird (2003). Notation used: West African Craton (WAC), Congo Craton (CC), Sahara Meta-Craton (SMC) and Kaapvaal Craton (KC).

1.1 Atlas configuration

1.1.1 Geological setting of Atlas region

The Atlas Mountains extend over 2000 km from Morocco, through Algeria to Tunisia. The topography of these mountain ranges is modest in their east part, while gradually elevates towards west in the High and Middle Atlas. The Atlas system comprises the Rif Cordillera and the Tell Mountains, rigid blocks, High Plateaus of Algeria, the Atlas Mountains (the Anti, Middle, High, Saharan and Tunisian Atlas) and the Sahara Platform. The Rif Cordillera and the Tell Mountains form a part of an Alpine thrust system that extends from the Beltic Mountains (in south Spain) to Tunisia and the Atlantic margin (Fig. 2). The current geological configuration of this region is mainly the result of the Cenozoic and Mesozoic extensional and compressional tectonic events, related to the opening and subsequent closing of the Mediterranean Sea (Blundell et al., 1992; Mickus and Jallouli, 1999). The region of the High Plateaus of Algeria is typically divided into the Saharan Atlas and the Tell Atlas, while geologically the whole region belongs to the Atlas domain. A tectonic style of the Algerian Atlas, consisting of broad synclinal basins and narrow anticlinal pinches, is similar to that of the Moroccan Atlas. The folds, with the N45°E axial strike, are oblique to the general N60°E trend of the Atlas. These folds are seldom symmetrical and, as in Morocco, the anticlines grade into stretch-thrusts at depth. The faults are well expressed throughout the domain. Asfirane and Galdeano (1995) have characterized its south part by a succession of epicontinental deposits (the Mesozoic sandstone representing its sedimentary layer) and in the north part by thinner sediments (Triassic to Neogene). The northern fringe of the West African Craton is located between the northwest edge of the Saharan Desert and series of hills of the High Atlas in south Morocco mainly behind the Anti-Atlas Mountains (Jessell et al., 2016).

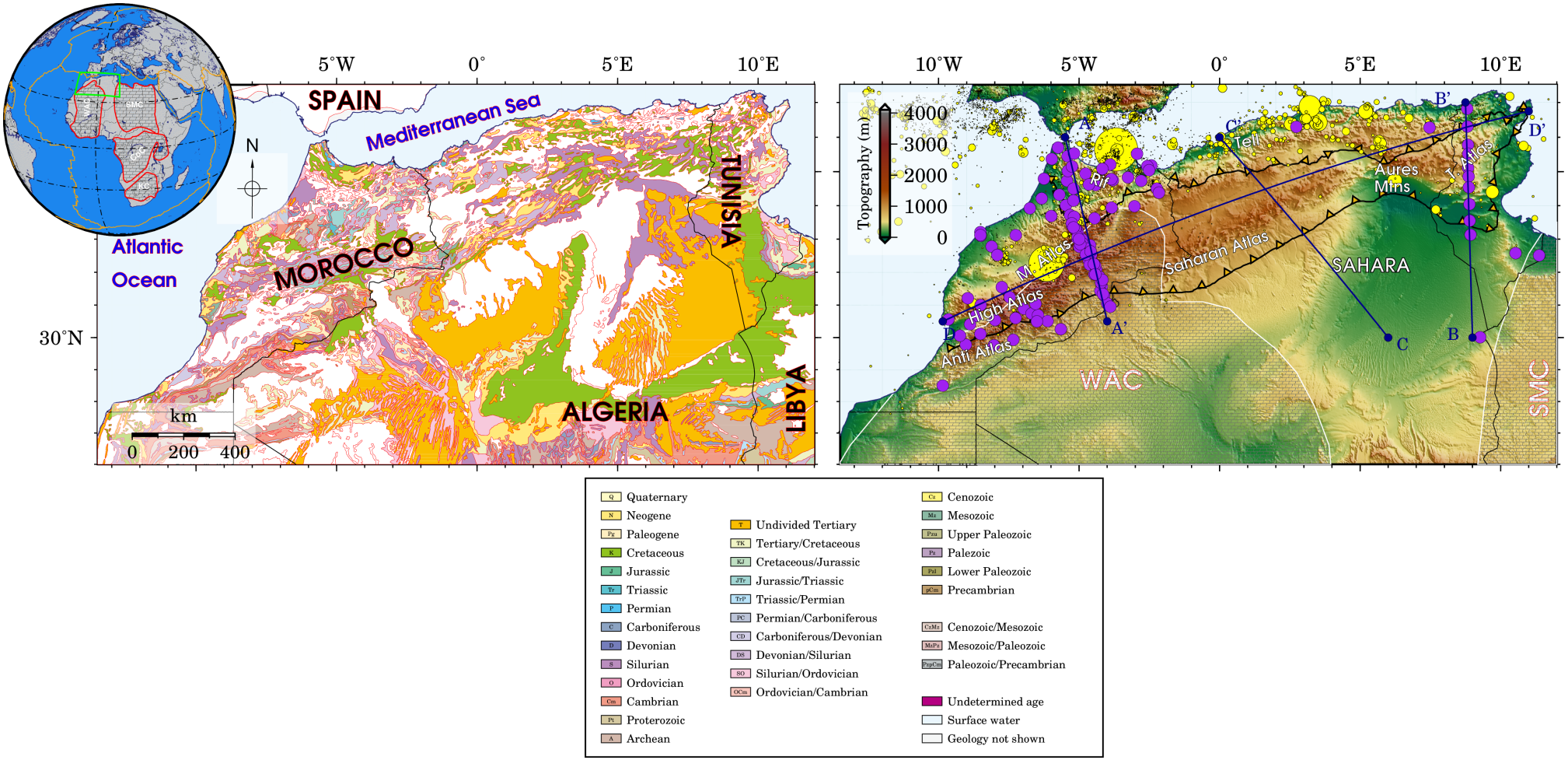

Figure 2: Regional geological and tectonic configuration of the Atlas region including seismicity. AA', BB', CC' and DD' indicate four selected profiles. The inset shows the location of the Rif-Tell-Atlas orogenic region along the Eurasian-African plate boundary. The orange lines indicate plate boundaries according to Bird (2003). Notation used: West African Craton (WAC), Pan-African Trans-Saharan Belt (PATSB) and Sahara Meta-Craton (SMC).

The West African Craton represents the main geological unit of the study area, underlying various late rocks of the Neoproterozoic and Palaeozoic orogenic mobile belts. The Saharan Meta-Craton and the West African Craton are bounded by the Pan-African Trans-Saharan Belt, forming the Archean core of north Africa, extending from the Hoggar in Algeria to the Gulf of Guinea (Ennih and Liégeois, 2008). The geological configuration of Algeria is essentially formed by the Pan-African Trans-Saharan Belt with predominantly linear north-south trend all over the West African Craton and a higher metamorphic grade. In the Atlas orogen, localized magmatism follows the strike of the Atlas Mountains from the Canary Islands hotspot towards the Alboran Sea. The Tunisian Atlas and the Saharan Atlas mountains are intracontinental orogenic belts formed within the stable Proterozoic-Paleozoic Sahara Platform that belongs to the old African basement. These orogenic belts consist of the Mesozoic rift sediments that were deformed into a series of large step folds. In the Saharan Atlas (the Tell and Atlas zones), the Mesozoic rift sediments were inverted into a major mountain range by thrust faults and block uplift tectonics, whereas the Tunisian Atlas was formed by thin-skin tectonics (Anderson, 1996; Gomez et al., 1998). The nearest Archaean granitic basement outcrop appears in east Algeria, which may be in concordance with the basement of north Tunisia.

1.1.2 Previous crustal studies of Atlas region

As evident from earlier seismic and gravimetric studies of the Atlas region (summarized in Table 1), most authors focused on the northern and western parts of the region along the Atlantic Ocean and the Mediterranean Sea based on the analysis of seismic refraction, receiver functions and terrestrial gravity measurements. Mickus and Jallouli (1999) and Jallouli and Mickus (2000) detected a crustal thickness of $38-40$ km under the Saharan Atlas and $34-36$ km under the Tunisian Atlas. Using Woollard (1959) empirical formula, Arfaoui et al. (2015) estimated the Moho depth in Tunisia. Their result revealed that the Moho depth there varies between 29 and 39 km, with maxima under the Tunisian Atlas, where the Moho deepens gradually

westwards. This crustal thickening continues under the Saharan Atlas in Algeria. They also identified the localized Moho deepening in north Tunisia (29 km) and in the Sahel (31 km). Using deep seismic sounding surveys, Diaz et al. (2016) detected a maximum crustal thickness beneath the Rif Cordillera with the Moho depth there exceeding 45 km. They also demonstrated that the Atlas Mountains, and in particular the High Atlas are characterized by crustal thickness variations roughly within $35-40$ km. They detected a thin crust along continental margins (the Mediterranean domain and the Atlantic margins) with the Moho depth typically $\backsim$ 5 km and a gradual Moho deepening towards inland with maxima exceeding 50 km beneath the Rif Cordillera. This estimate is significantly larger than the result presented earlier by Urchulutegui et al. (2006).

According to their result, using a simple approach based on the analysis of regional topographic and geoidal data, the Moho deepens only to $\backsim$ 34 km under the Rif Cordillera and to $\backsim$ 38 km beneath the Atlas Mountains. A similar estimate for the Rif Cordillera was given by Giese and Jacobshagen (1992). They reported a maximum crustal thickness of 40 km. Mancilla and Diaz (2015), based on the P-receiver function analysis, detected significant variations in the Moho geometry in north Morocco that could be characterized by three distinctive regions. A thick crust beneath the Rif Cordillera. A thinned crust in northeast Morocco, and the region of $30-35$ km thick crust in the transition to the Meseta domain. Further south, moderate crustal roots with the Moho roughly 40 km deep are clearly identified under the High Atlas. Ayarza et al. (2005), using geological evidence and terrestrial gravity data, detected the under thrusting slab of the Saharan Atlas. They also identified a dense lower crust of local crustal roots with the Moho deepening to $38-41$ km beneath the central High Atlas. These results have reinforced models of crustal under-compensation and a Moho involvement in the deformation that have implications for a deep structure of intracontinental mountain belts.

Beneath the Tell and Atlas orogenic belts including adjoining parts of the West African Craton most studies have used seismic data to resolve the crustal structure

Table 1: Moho depths of previous investigations for the Rif-Tell-Atlas orogenic system.

Area	**References**	**Methods**	**Depth Estimates (km)**
Rif	Gil et al. (2014)	Deep Seismic Sounding (DSS)	29 – 42
	Mancilla et al. (2012) Van der Meijde et al. (2013)	Receiver Functions (RF)	21.6 – 44.4
	Urchulutegui et al. (2006)	Regional elevation and geoid data	34
Atlas	Ayarza et al. (2014) Wigger et al. (1992) Makris et al. (1985)	Deep Seismic Sounding (DSS)	33 – 41
	Mancilla et al. (2012) Sandvol et al. (1998) Spieker et al. (2014) Cooper and Miller (2014)	Receiver Functions (RF)	23 – 44.7
	Mickus and Jallouli (1999) Jallouli and Mickus (2000)	Gravity	26 – 38
	Urchulutegui et al. (2006)	Regional elevation and geoid data	38 – 40
	Arfaoui et al. (2015)	Gravity	29 – 39
Meseta	Makris et al. (1985)	Deep Seismic Sounding (DSS)	35
	Mancilla et al. (2012)	Receiver Functions (RF)	30.7 – 37.6
	Diaz et al. (2016)	P-receiver function (PRF)	30 – 35
North-western Morocco Margin	Contrucci et al. (2004)	Deep Seismic Sounding (DSS)	34 – 35
South-western Morocco Margin	Makris et al. (1985)		27 – 29
West African Craton	Sandvol et al. (1998) Kosarian (2006) Leo et al. (2015)	Receiver Functions (RF)	41 – 42.6

(Civiero et al., 2018). The Atlas region is not an exception, with fewer gravity studies than continental-scale seismic studies. A limitation of seismically derived crustal thickness maps is an inherent uncertainty about crustal structures in areas with limited or low-quality data coverage. To our knowledge, continental-scale crustal thickness models of the Atlas region are generally constructed from seismic studies (e.g., Jessell et al., 2016; Ebinger et al., 2017; Civiero et al., 2018) with only a handful of models derived from gravity studies (e.g., Mickus and Jallouli, 1999; Jallouli and Mickus, 2000; Jallouli et al., 2013). In all instances, however, the limited availability of both seismic and ground-based gravity measurements has resulted in unconstrained crustal structure models in the Atlas. To partially these deficiencies, we estimated the Moho depth based on the gravity (from global model) inversion constrained on available seismic data.

1.2 Cameroon configuration

1.2.1 Geological setting of Cameroon

Located on the west side of central Africa bordering the easternmost part of the Gulf of Guinea, between Nigeria and Equatorial Guinea, slightly above the equator, Cameroon lies between parallels two and thirteen north latitude, and meridians 9° 34′ and 16° 15′ east longitude (Fig. 3). With a landmass of $472,710$ km^2 and $2,730$ km^2 of water, it covers an overall area of $475,440$ km^2. Together with neighbouring countries, Cameroon shares the northern edge of the largest African Archean Craton ($3.4 - 2.5$ Ga): the Congo Craton (Baranov and Bobrov, 2018). The Ntem Complex mainly composed of early Proterozoic syenites constitutes the northern edge of the Archean Congo Craton domain in the southern part of Cameroon (Vicat et al., 1996; Tchameni et al., 2000). The geology of the study area (and adjunct geological regions) could generally be divided into the Precambrian basement and Archean structure (Fitton, 1987; Poudjom et al., 1997; Toteu et al., 2004). Both these major geological features are associated with the Oubanguides Belt, formed during the

Atlantic opening from the continental collision of Archean Congo and West African Cratons in Africa together with the São Francisco Craton in South America (Ngako, 1999; Tchameni et al., 2000; Toteu et al., 2004; Nkoumbou et al., 2014).

The Cameroon Volcanic Line, located northwest of the Craton Congo, is about 100 km wide and stretches for 1600 km along a NE−SW axis (Fitton, 1987; Coulon et al., 1996). This rift consists of highland massifs, plateaus, and islands of volcanic and anorogenic plutonic origin. Its northern edge consists of the Mandara Mountains, southwest of Lake Chad and extends to the southwest by the Atlantika Mountains (spanning the border between Nigeria and Cameroon), Shebshi Mountains, Adamawa plateau, the Cameroonian Ridge (in the west, with the Mounts Oku and Mekoua) and Mount Cameroon.

From these mountain chains, the Cameroon Volcanic Line sinks under the Atlantic Ocean through the Bight of Biafra and emerges with the islands Bioko, São Tomé and Principe then Annobón at its southern end. The southern part of the Cameroon Volcanic Line is punctuated by volcanoes born from the hotspot of Cameroon (Lee et al., 1994). The Benue Trough is a large geological formation, underlying a significant part of Nigeria that formed at the beginning of the early Cretaceous Rift ($145 - 66$ Ma) and extends over 1000 km from Gulf of Benin to Lake Chad known as the Mamfe Basin in southwest of Cameroon and Garoua Rift in north (Burke and Wilson, 1972; Liu, 1977; Gallacher and Bastow, 2012). It is an aborted rift forming part of a broader system of Central and West Africa stretching from the Darfur region to the Adamawa Plateau name the Central African Shear Zones constituted by the Tchollire-Banyo Shear Zone (TBSZ), Adamawa Fault, Foumban Shear Zone and the ENE−WSW Sanaga Shear Zone (SSZ). Similarities in shape and composition (alkali basalt) of the Benue Trough and the Cameroon Volcanic Line indicates a common geodynamic control of their formation. Wilson and Guiraud (1992) and Ngako et al. (2006) illustrated that the Africa Rift Systems were related to magmatism during its evolution; particularly in the Benue Trough. Moreover, there is also an existing evidence of dipping of this zone under the Benue Trough, suggesting heating from

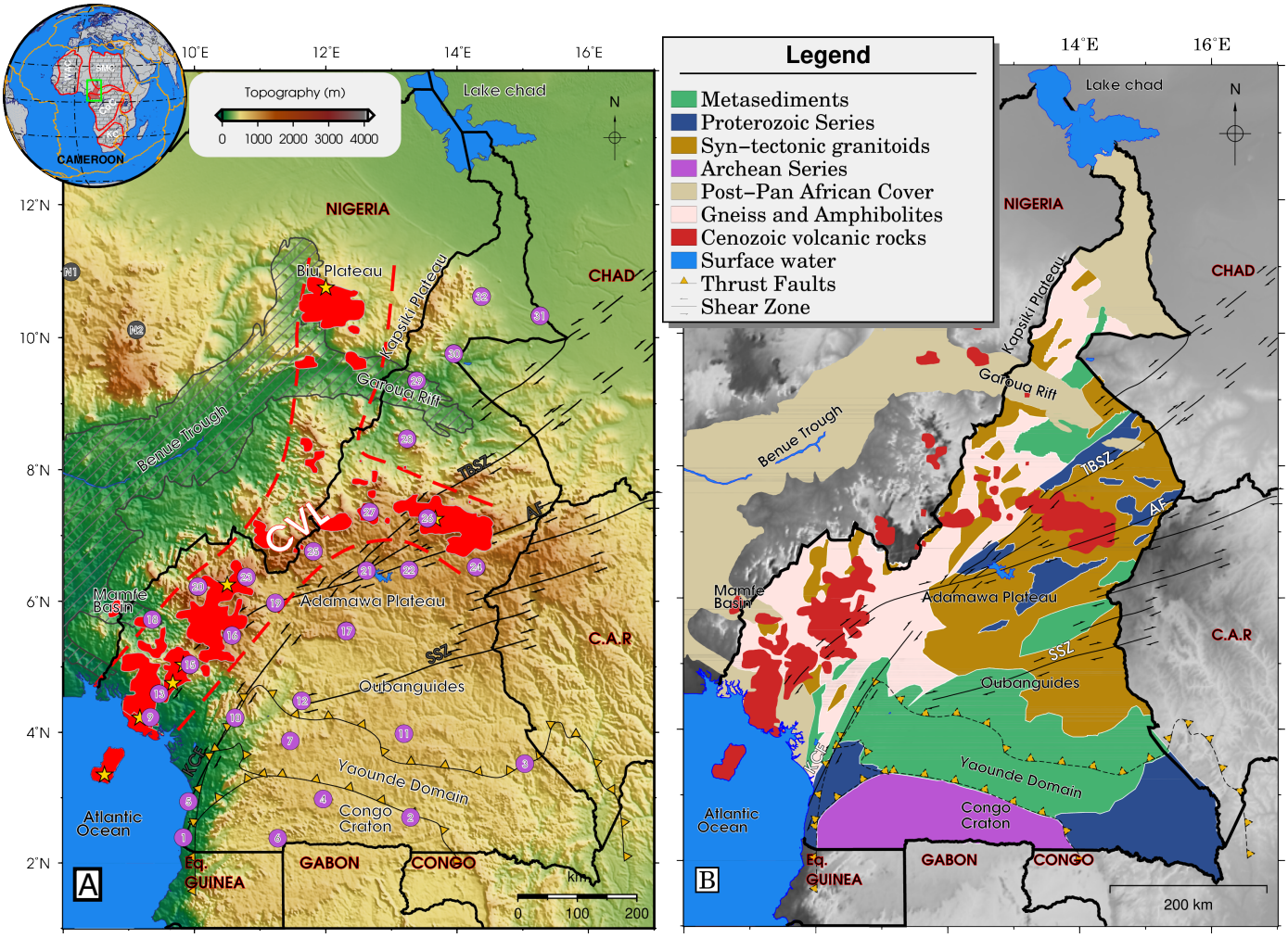

Figure 3: Tectonic setting (left panel) and regional geological map (right panel) of Cameroon. Major geological units according to studies by Toteu et al. (2004), Nzenti et al. (2006), Reusch et al. (2010), Tokam et al. (2010) and Anderson et al. (2014) involve the Cameroon Volcanic Lines (CVL), Mamfe Basin, Benue Trough, Biu Plateau, Garoua Rift, Kapsiki Plateau, Adamawa Plateau (Paleoproterozoic), Oubanguides Belt, Yaoundé Domain (Neoproterozoic), and Congo Craton (Archean). The red areas are regions of Cenozoic volcanism along the CVL. Stars are the main volcanoes found along with the CVL. The Foumban shear zone (FSZ), Tchollire-Banyo Shear Zone (TBSZ), Sanaga Shear Zone (SSZ), Kribi Campo Fault (KCF) and Adamawa Fault (AF) are shown as light black thick lines. The location of the Cameroon Broadband Seismic Experiment (CBSE) sites and two seismic sites in Nigeria are shown by grey circles. The inset shows the location of Cameroon and neighbouring countries along with the cratonic units. The orange lines indicate plate boundaries according to Bird (2003). The notation used: West African Craton (WAC), Congo Craton (CC) and Sahara Meta-Craton (SMC).

below the lithosphere (Coulon et al., 1996; Elsheikh et al., 2014).

1.2.2 Previous Cameroon crustal studies

Numerous studies have been conducted using seismic and gravity data to detect the Moho interface in Africa. The lithospheric and crustal structures in Cameroon have also been investigated quite extensively (Fig.4). Stuart et al. (1985) estimated the crustal thickness of the Adamawa Plateau (33 km) and the Garoua Rift (23 km) based on the analysis of seismic refraction studies. Poudjom et al. (1995) used spectral analysis for $\backsim$ 32000 ground gravity measurements in Cameroon to suggest that the thickness of the continental crust decreases from $\backsim$ 50 km in the south to $\backsim$ 18 km to the north.

They suggested progressive northward thinning of the crust from $\backsim$ 22 to 50 km beneath the Congo craton, the Yaoundé domain and the Adamawa-Yade domain, to $22-18$ km beneath the West Cameroon domain. Using terrestrial gravity data, Nnange et al. (2000) found similar variations between the northern part of the Cameroon Volcanic Line, the Adamawa Plateau and the southern part of the Cameroon Volcanic Line. Tokam et al. (2010) obtained the Moho depth ($35-39$ km) using 32 portable broadband seismometers installed across the country. Tugume et al. (2013) used the combined gravimetric and calibrated 377 passive seismic data with a three-dimensional (3D) inversion to decipher the crustal thickness of the whole African continent. Using the EGM2008 (Pavlis et al., 2012) global gravitational model, Eyike and Ebbing (2015) determined a crustal thinning (< 30 km) in the Yola-Bornu basin from a regional $3-$D gravity modelling, while assuming the Airy (1855) isostatic theory. Ngatchou et al. (2014) employed a wavelet analysis method and a power spectrum technique to evaluate depths of various gravity sources. According to their results, the sediment depth in the Adamawa area was found to be in the range between 4.5 and 7 km based on the gravity disturbances and a crust-mantle transition zone varying from 25 to $\backsim$ 50 km. They illustrated at the Moho discontinuity and at the intermediate depth a pre-Cenozoic geologic body. Ngalamo et al. (2018) applied the

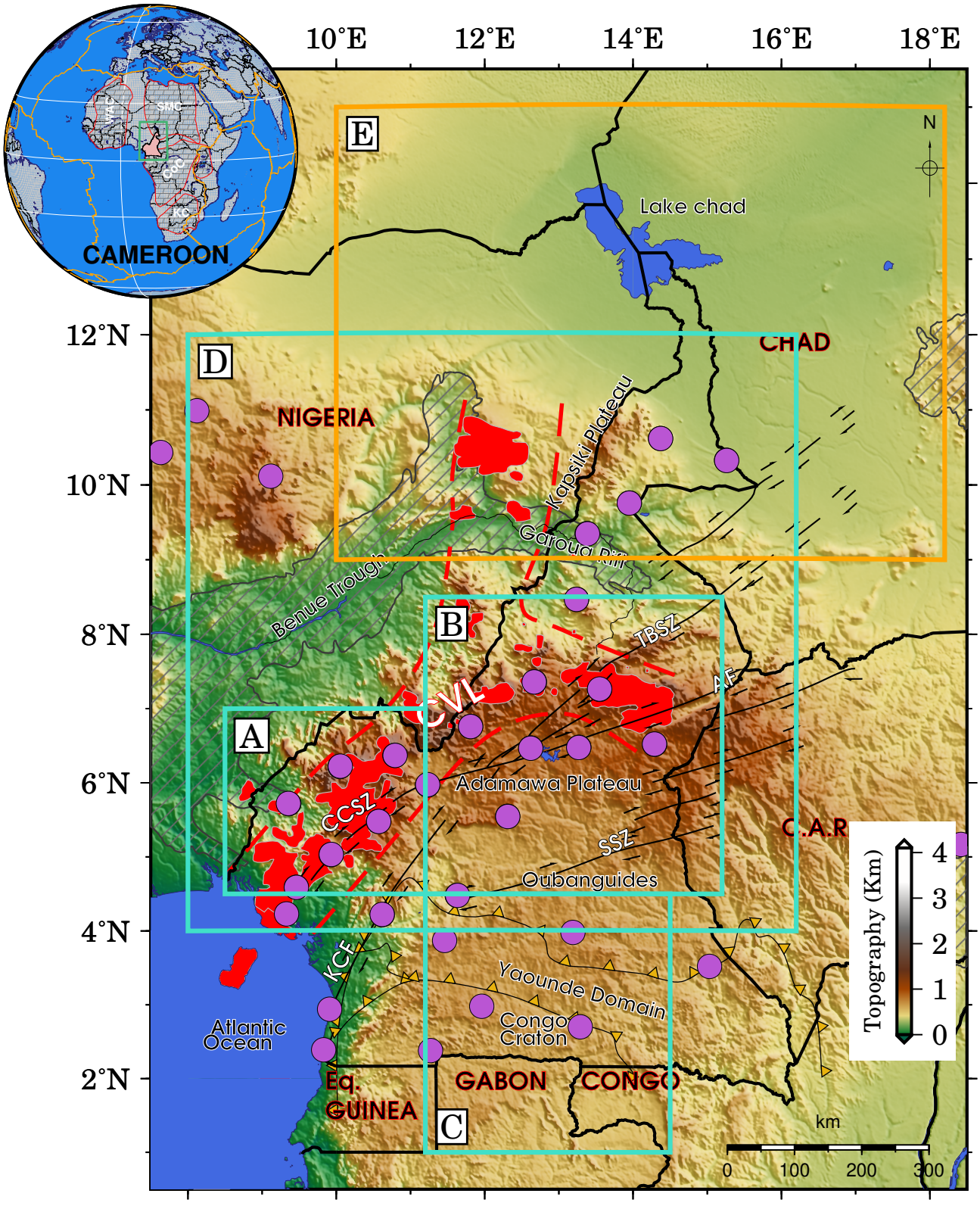

Figure 4: Sub-regions of previous crustal investigations overlay on a simplified tectonic map of Cameroon. The Turquoise boxes (A, B, C and D) represents areas in which power spectra have been determined according to Nnange et al. (2000). to estimate crustal thickness. The orange box labeled "E" defines the location of the sub-region used by Eyike and Ebbing (2015) to image the crustal thickness using gravity inversion. The purple dots represent the locations of the passive seismic station used by Tokam et al. (2010), Gallacher and Bastow (2012) and recently by Ojo et al. (2019).

World Gravity Map (WGM 2012) data to study the Pan-African Orogenic Belt and the Congo Craton by applying a spectral analysis. More recently, Ojo et al. (2019) simultaneously invert Rayleigh wave group and phase velocity dispersion, P-wave receiver function and Rayleigh wave ellipticity measurements using a joint inversion method based on the Neighbourhood Algorithm.

1.3 East African configuration

1.3.1 Geological setting of East African Rift System (EARS)

The study area is situated in prominent part of the East African Rift System, between meridians of 28°E and 40°E longitudes and parallels of 3°N and −11°S latitudes (Fig. 5). The East African Rift System forms part of the largest Tertiary-Quaternary rift system (McConnell, 1972). It is divided around the Tanzanian Craton into the eastern and western branches (called thereafter the East and West Rifts) with the Paleoproterozoic Usagaran and Ubendian orogenic belts to the southeast and southwest of the craton respectively, and the Neoproterozoic Mozambique Belt and the Mesoproterozoic Kibaran Belt to the east and west of the craton respectively. These two Cenozoic rifts show incongruous tectonic behaviour which seems to be linked to their specific locations with respect to asthenospheric mantle plumes (upwelling processes) and structural variations in the pre-existing basement framework (Albaric et al., 2009).

The Cenozoic rift valleys expanded entirely inside mobile belts, largely bordering the cratonic nucleus. Within northeast Tanzania, the rift faults splay out over an area extending some 200 km eastwards from the craton margin (Nyblade et al., 1996). In the southern portion, the Usagaran orogenic domain has been interpreted to be derived from the Archean Tanzania Craton (2.7 Ga) and equilibrated with the whole rocks during the Usagaran-Ubendian orogeny at $1.8 - 2.0$ Ga (Priem et al., 1979). The Usagaran Belt was reworked during the East African Orogeny associated with the collision of the East and West Gondwana (Viele et al., 1998; Möller et al., 2000).

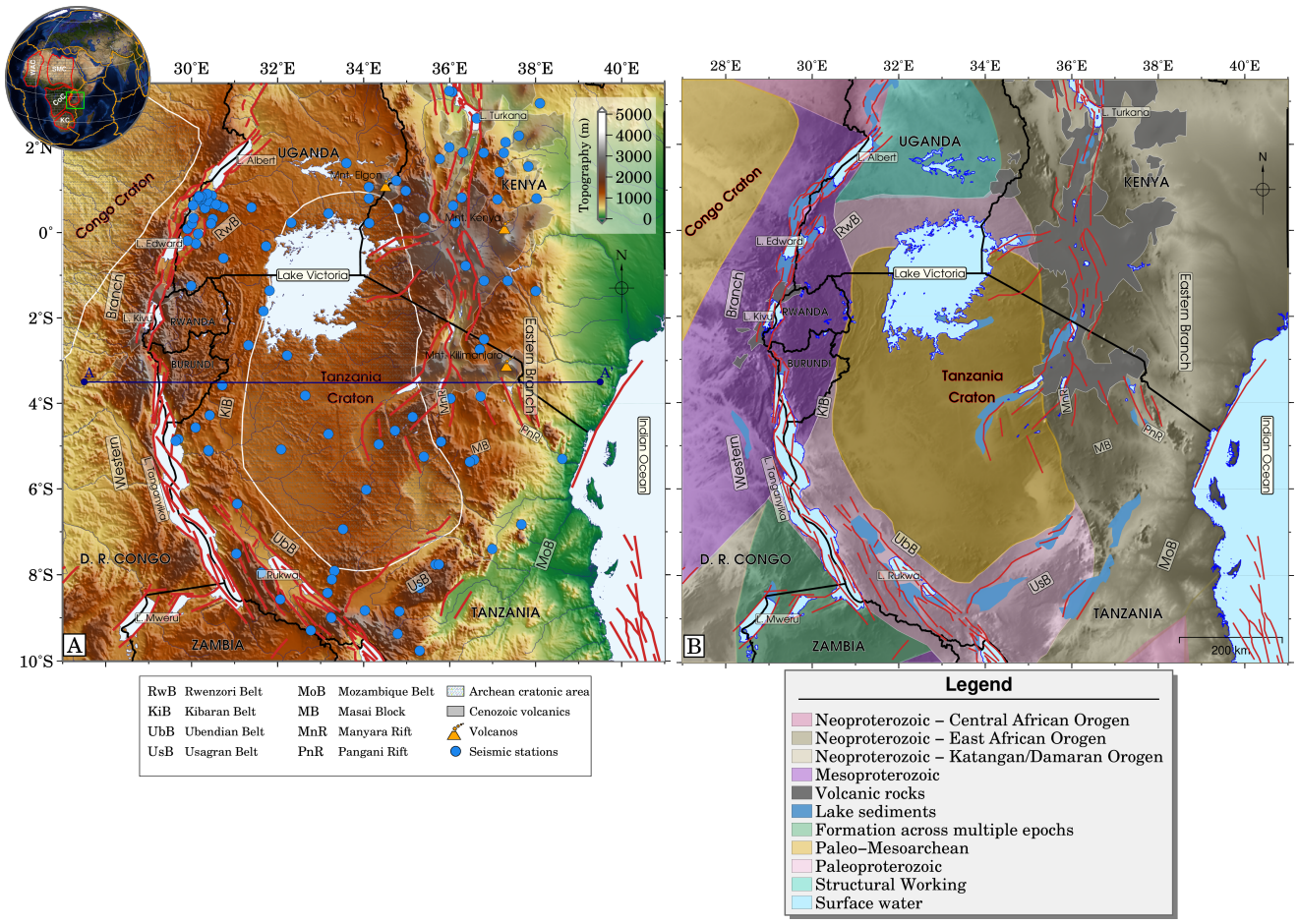

Figure 5: Topographic and regional tectonic configuration of the East African Rift System (EARS) region including seismicity. Fire brick colour lines represent main faults related to the West and East Rifts of EARS. The Congo and Tanzanian Cratons are depicted with white lines. The abbreviation used: the Proterozoic mobile belts (UsB: Usagran Belt, UbB: Ubendian Belt, KiB: Kibaran Belt and MoB: Mozambique Belt) encompassing the Tanzanian Craton, the major Cenozoic rift faults (MNR: Manyara Rift, PR: Pangani Rift) and the rift segments. Lake Albert, Lake Edward, Lake Kivu, Lake Mweru, Lake Rukwa, MB: Massai Blocks, RwB: Rwenzori Belt. Orange spot symbols highlight mountains along the Eastern Rift. AA' (Fig. 49) indicates selected profile. The inset shows the location of the EARS region along the Somalian plate boundary. The orange lines indicate plate boundaries according to Bird (2003). Notation used in inset: West African Craton (WAC), Congo Craton (CoC), and Sahara Meta-Craton (SMC).

A question remains as to whether the Usagaran Belt has affected or rejuvenated the craton (Fritz et al., 2005). The Cenozoic rift system observed to the southwest and south of the Tanzanian Craton expanded near or within the Permian and Triassic (Karoo) Rift System, filled by alluvial deposits and sedimentary rocks in response to compressional and transpressional deformations in east-central Africa (Delvaux, 2001).

The rift system is embedded between the East and West Rifts enclosing the Tanzanian Craton in its central part. In north Tanzania, the East Rift basins are identified by minor extension, suggesting that most of the extension in equatorial Africa is accommodated along the West Rift (Ring, 2008). The West Rift displays a sigmoidal geometry and spreads from the Rwenzori Mountains. These mountains, with maximum elevations reaching $\backsim$ 5.1 km above sea level, are the highest non-volcanic rift mountains on Earth.

The Kenya Rift is defined by its atypical rift faults and volcanoes (not older than $5-8$ Ma) which became gradually younger to the south, ending in northeast Tanzania in a wide (300 km) zone of block faulting, stretching from the Lake Eyasi Graben in the west to the Pangani Graben in the east (Dawson, 1992). The East Rift (also called the Kenya Rift), marked by the highest mountains in Africa, passes through Lake Turkana within the Mozambique Belt into north Tanzania with intensive volcanic activity. These mountains comprise the Mount Kilimanjaro (5, 895 m), the Mount Kenya (5, 199 m) and the Mount Elgon (4, 321 m). The hills of Chyulu, considered as one of the world's youngest volcanic mountain ranges (Wadge et al., 2016), are nestled in the eastern arm of the Kenyan Rift, located $\backsim 150-200$ km east of the rift axis and $\backsim$ 50 km northeast of Kilimanjaro, near the Tanzanian border. The Proterozoic orogenic belts and volcanic zones of this rift system surround the Archean cratons of central (i.e. the Congo Craton) and eastern Africa (Kampunzu et al., 1998). The Tanzanian Craton (with average elevation $\backsim$ 1.2 km) is possibly a manifestation of dynamic topography (plume activity) formed since 2.9-2.5 Ga (Manya and Maboko, 2003).

1.3.2 Previous EARS crustal studies

The crustal structure beneath east Africa has been investigated in numerous studies based on the analysis of surface and body wave tomography or gravity data. Many authors focused on the crustal structure of the rift systems while only a few studies were carried out to investigate the whole region. Among the first studies of this region, we could mention the works by Bonjer et al. (1970), Mueller and Bonjer (1973), Nolet and Mueller (1982), or Hebert and Langston (1985). They examined the Moho geometry using seismic refraction data, regional earthquakes and in situ teleseismic data. They reported large crustal thickness variations, with a typical Moho depth of $40-48$ km beneath the Precambrian crust and an expected much thinner crust along rift basins with the Moho depth mostly within $20-32$ km. A more inclusive image of the crustal structure was obtained from refraction profiles conducted as a part of the Kenya Rift International Seismic Project (KRISP). These results were published, for instance, by Prodehl et al. (1994), Fuchs (1997), Simiyu and Keller (1998, 2001), or more recently by Sippel et al. (2017). They reported the Moho depth beneath the Mozambique Belt in the range of $\backsim 35-42$ km, and $34-40$ km beneath the Tanzanian Craton, with uncertainties of ± 2 km in both regional Moho depth estimates. Nyblade et al. (1996) and Nyblade (2002) upgraded information about cratonic and orogenic formations in these regions based on a more recent analysis by using P-wave receiver functions and Rayleigh wave dispersion data from Tanzania and Kenya broadband seismic experiments; see also Last et al. (1997), Dugda (2005), and Julià et al. (2005).

Last et al. (1997) detected the Moho depth of $37-42$ km beneath the Tanzanian Craton, and $36-39$ km beneath the Mozambique Belt. These results closely agree with those reported by Julià et al. (2005) and Dugda (2005) obtained from the KRISP experiments. In the southwest part of the West Rift, especially around the Ubendian Belt, they obtained the Moho depth variations between 40 and 45 km. In its northern branch, for the Rwenzori region (in Uganda), they reported the Moho depth of $20-28$ km, and 30 km along the eastern side of the Albertine Rift.

Under the Lake Magadi Rift (southernmost lake in the Kenyan Rift Valley), Birt et al. (1997) reported a slight crustal thinning, with a Moho depth of $\backsim$ 35 km based on the KRISP94 seismic results. Novak et al. (1997) observed a Moho depth of 42 km beneath the Chyulu Hills in the east part of the rift valley.

Owens et al. (2000) found a transition zone from 30 to 40 km under the East Rift narrower than under the Tanzanian Craton within the eastern African plateau, which is not affected by rift, a result that was later confirmed by Huerta et al. (2009) using a denser dataset from stations in Kenya and Tanzania. The mantle transition zone discontinuities are located deep beneath the south part of the Tanzanian Craton that has not been affected by rift faulting. Weeraratne et al. (2003), using surface wave tomography, decipher also a low-velocity anomaly contrast beneath the Tanzanian Craton and the East Rift. More recently, Adams et al. (2012) demonstrated that the high seismic velocity upper-mantle structure under the Tanzanian Craton extends to the north beneath the basement complex in north Uganda. They also reported anomalously low velocity beneath volcanic centres along the West Rift. A crustal study of this region using seismic, deep drilling profiles and satellite gravity data was conducted also by Tedla et al. (2011).

Chapter 2

Data and methodology

In this chapter, the crustal thickness beneath our areas of interest in Africa is modeled by combining geophysical observations that provide additional information on the density-contrast variation within the depth: Bathymetry/Topography and thickness of the sediments. The integration of these data sets into a consistent model allows the study of crustal structure and requires a numerical framework based on certain geophysical concepts and assumptions. Therefore, the most appropriate crust model will be defined and compared with the modelled crustal thickness map to highlight its strengths and weaknesses.

2.1 Data

2.1.1 Sediment thickness

To model the gravitational signature of topography and crustal density heterogeneities, the global seismic crustal model CRUST1.0 (Laske et al., 2013) will be used as the a priori model, because the continental-scale crustal density model is not available for Africa. CRUST1.0 provides information on a 1×1 arc-deg global grid for several layers comprising the ice, water, (upper, middle and lower) sediments and (upper, middle and lower) consolidated (crystalline) crustal layers. In addition, the lateral density structure of the upper mantle was included into the CRUST1.0 model (Fig. 6). The globally averaged data from active seismic methods and deep drilling profiles were used to predict the crustal structure where no seismic measurements were

available (most of Africa, South America, Greenland and large parts of oceans) by a generalization to similar geological and tectonic settings. Since this global crustal model does not meet accuracy requirements for this thesis purpose, we will refine this model.

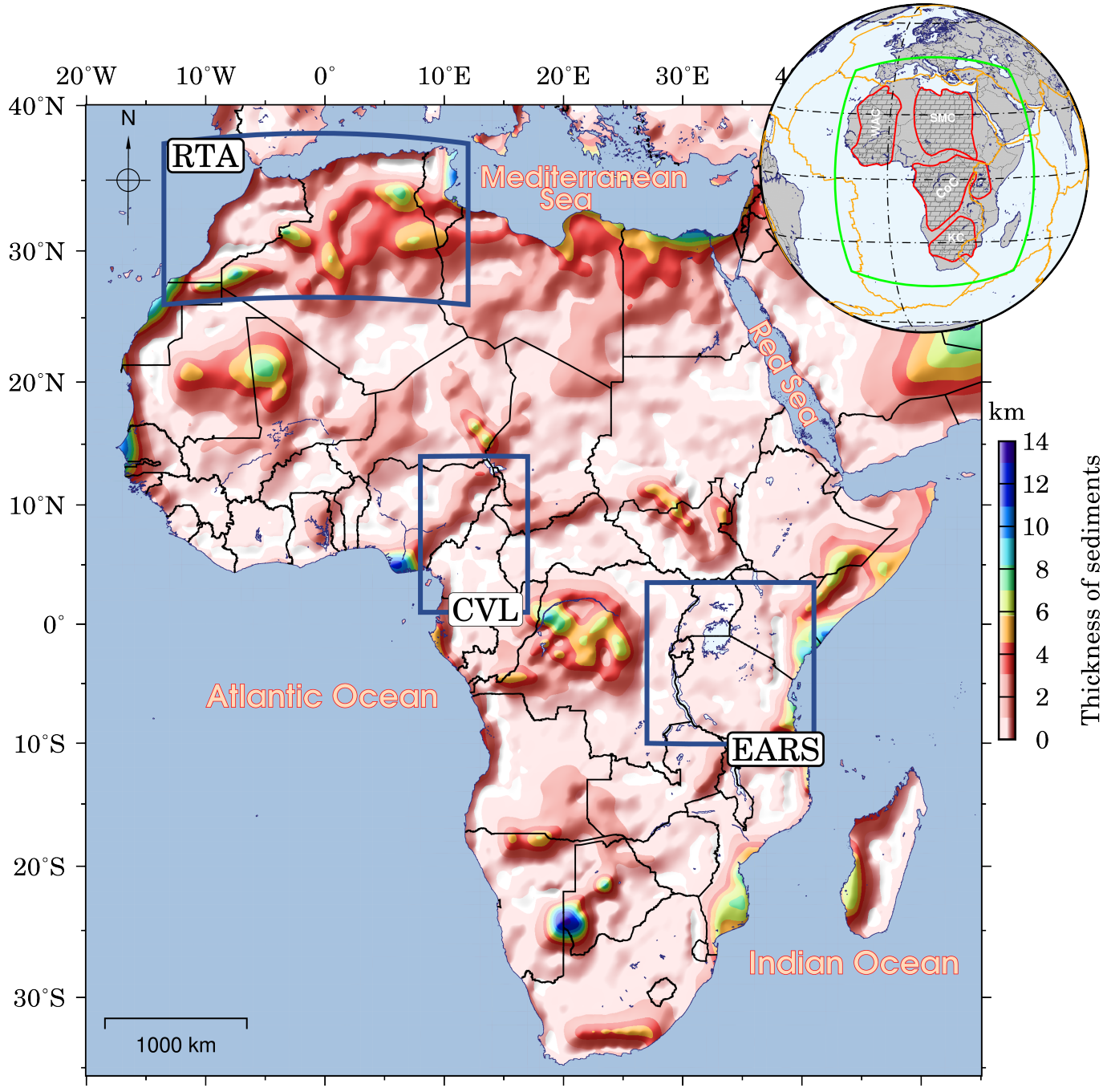

Figure 6: Thickness of sediments in Africa from the global sediment thickness map from (Laske et al., 2013). The orange lines indicate plate boundaries according to Bird (2003). Notation used: West African Craton (WAC), Congo Craton (CC), Sahara Meta-Craton (SMC) and Kaapvaal Craton (KC).

2.1.2 Topography/Bathymetry and background datasets

For this purpose, we will utilize the 1×1 arc-min data from the ETOPO1 (Amante and Eakins, 2009) datasets of topography, bathymetry, inland bathymetry (major lakes). In this dataset, the elevation (Topography/Bathymetry) component of the data is based primarily on satellite altimetry measurements tied to ocean soundings (Fig. 7). These grids lack much of the detailed data source in local surveys but provide excellent background data sources for the development of the higher resolution grid for regional areas. In the 2009 grid, lower resolution ETOPO2 and ETOPO1 data has been used to fill those off-shelf areas (approximately -200 metres or deeper) where higher resolution survey datasets (such as swath, fairsheets and Laser Airborne Depth Sounder (LADS)) were not available. The result in off-shelf areas is a combination grid of high resolution data where it is available and lower resolution ETOPO data elsewhere. There is also a visual difference between the ETOPO dataset in the 2005 grid compared with the 2009 grid.

For on-shelf areas (approximately -200 metres or shallower) surveys completed over the last few years have greatly improved the overall accuracy and resolution of the data. In some cases there were notable discrepancies between the survey data and ETOPO datasets. These were where the difference in resolution and accuracy caused anomalous valleys or ridges as the higher resolution survey data cut through the lower resolution ETOPO data. These differences also resulted in edge effects where the edges of the different datasets did not meet at the same height. In such cases, an interpolation process was used to smooth the data artefacts.

2.1.3 Africa Broadband seismic stations and seismic Moho estimates

Studies of the Moho depth address several important aspects of geoscience applications. These studies are used to facilitate the inversion of seismic-related data in order to obtain important information about sedimentary basins. They are also needed in geodynamic modeling of Earth's heat flux and for predicting and mitigating geohazards (e.g., earthquakes), as well as for better identification of margins between

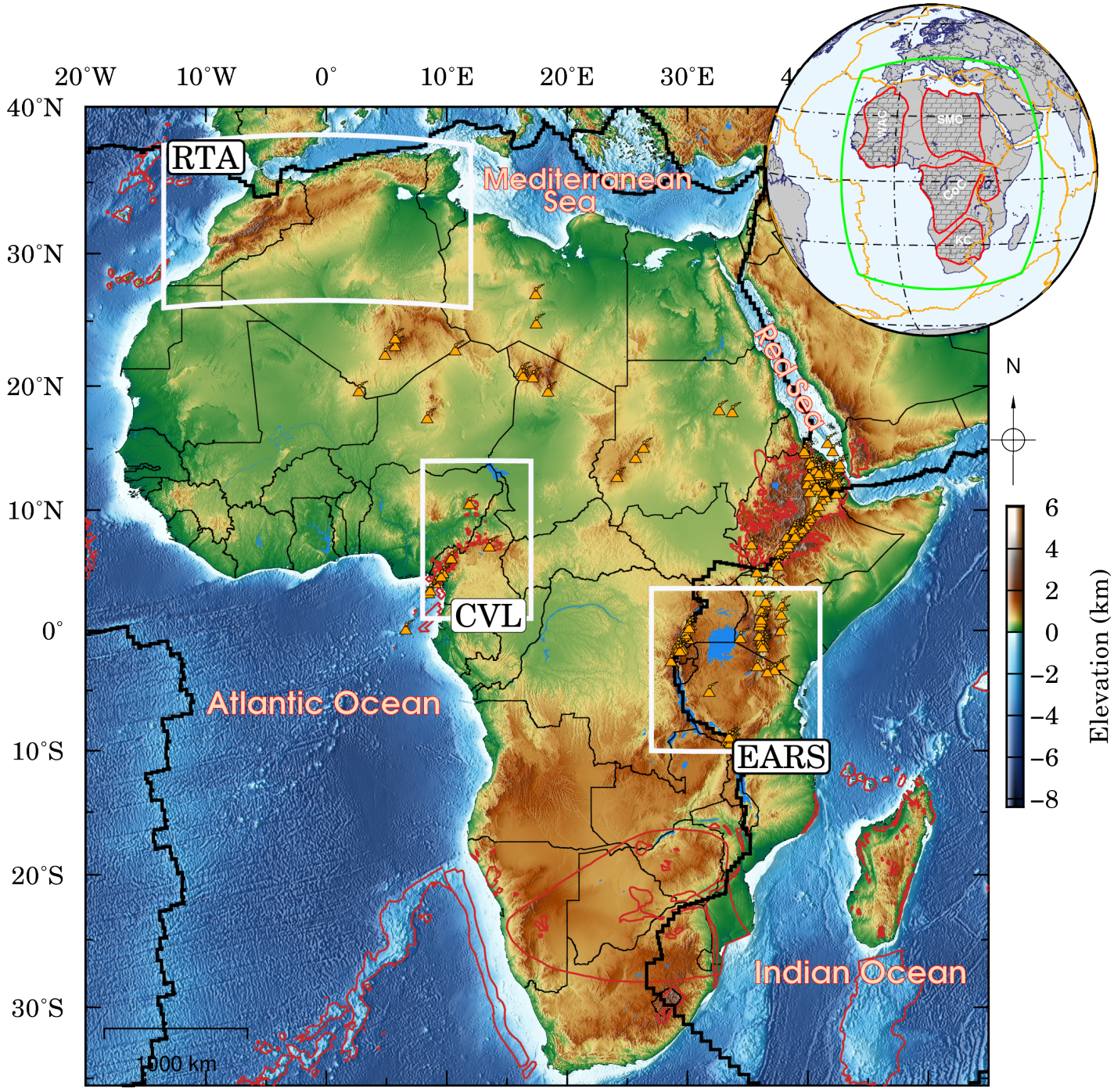

Figure 7: Bathymetry and topography map of our three study areas (ETOPO1) (Amante and Eakins, 2009): the Cameroon Volcanic Line, Rif-Tell-Atlas and the East African Rift System. The inset shows in purple the location and extent of the Archean Cratons and intracratonic basins. The orange lines indicate plate boundaries according to Bird (2003). Notation used: West African Craton (WAC), Congo Craton (CC), Sahara Meta-Craton (SMC) and Kaapvaal Craton (KC). The domains inside the red lines represent the large volcanic provinces.

geological units of different structure and age, which is essential in geophysics for better distribution of natural resources in exploration.

Despite the existence of enormous natural resources in Africa, most of this continent has not yet been covered by seismic surveys. Consequently, the current knowledge on the Moho depth (determined from seismic data) and Earth's inner structure under this continent is relatively vague. Existing studies have mainly focused on geophysically significant areas, while the Moho depth beneath large parts of the continent is not yet fully understood. The Moho depth model will provide a new inside about Earth's inner structure of this continent, especially in regions without seismic data coverage. Since active seismic experiments are relatively expensive, large parts of the world are not yet covered sufficiently by seismic surveys, such as most of Africa (Fig. 8). Nevertheless, the Moho depth estimates from seismic data are essential to constraint the Moho depth model determined based on the gravity data inversion. In the thesis, we will use all available seismic estimates of the Moho depth in Africa that have been published in scientific reports and journal articles.

Over the last couple of decades, quite a number of join international collaborative large-scale seismic projects have been proceeded in Africa (Fig. 8). Mainly, in East and northern Africa to understand the lithospheric structure and to search for the source regions and reason for the wide-spread earthquake activity using methods as the seismic refraction profiles on 1075 broadband seismic networks installed in Africa and surrounding regions with a special focus on: Cameroon (Tokam et al., 2010; Gallacher and Bastow, 2012), Rif-Tell-Atlas region (Jallouli and Mickus, 2000; Arfaoui et al., 2015; Diaz et al., 2016), Tanzania (Prodehl et al., 1994; Fuchs, 1997), Kenya (Nyblade et al., 1996; Nyblade, 2002), and Ethiopia as seen in Figure 9. The compiled seismic data and current knowledge of crustal thickness in Africa displays very well their uneven distribution and absence of seismic coverage for vast areas of the continent (e.g., WAC, Sahara Metacraton, Congo Craton). For a brief review of passive-source seismic studies in Africa the reader is referred to Fishwick and Bastow (2011).

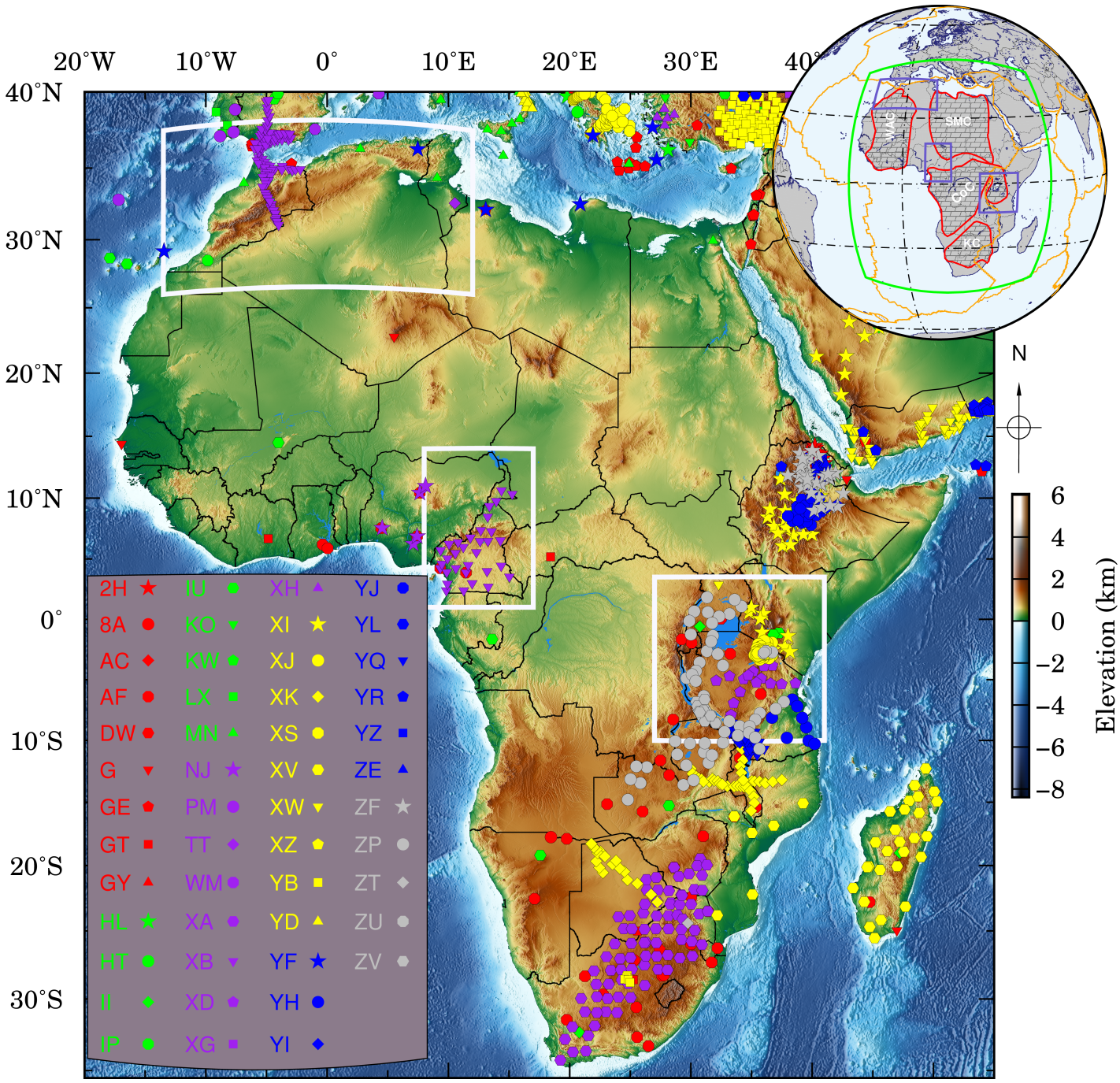

Figure 8: Map of Africa showing the seismic networks and stations involved in this study after (Ojo et al., 2019). The one- and two-letter labels in the legend denote the network codes, whereas the shape and color indicate the stations belonging to different seismic networks. Country names where the stations are installed are denoted. The inset shows in purple the location and extent of the Archean Cratons and intracratonic basins. The orange lines indicate plate boundaries according to Bird (2003). Notation used: West African Craton (WAC), Congo Craton (CC), Sahara Meta-Craton (SMC) and Kaapvaal Craton (KC).

Several decades of seismic studies have indicated the unique characteristics of the thickness of the earth's crust beneath Africa and the uniqueness of the variations in the depth of Moho linked to various cratons, mobile belts, Cenozoic volcanism, and the recent continental rift. In summary, the thickest crust in Africa is found under the cratons and belts (> 38 km) and the thinnest (< 25 km) under the rifts in West and East Africa, as well as in the coastal areas.

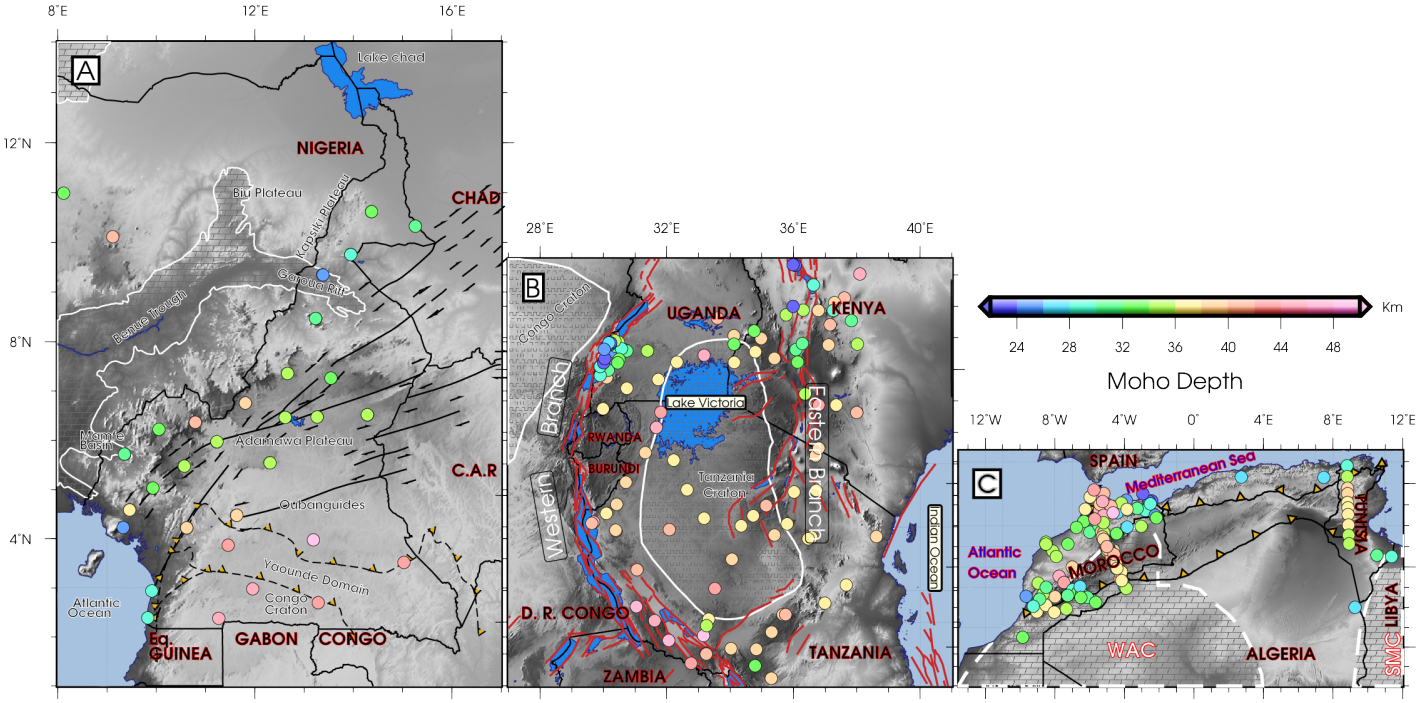

Figure 9: Crustal thickness in (a) Cameroon Volcanic Line, (b) East African Rift System, and (c) the Atlas orogen (Africa-Eurasia collision) constrained using receiver function analysis. Data from Figure 9a are Mancilla et al. (2012), Cooper and Miller (2014), Spieker et al. (2014), and Jessell et al. (2016), Figure 9b are sourced from Tokam et al. (2010) and Gallacher and Bastow (2012) , and Figure 9c are from Dugda (2005), Tugume et al. (2013), Wölbern et al. (2010), and Hodgson et al. (2017).

Gao et al. (2013) and Hodgson et al. (2017) found that the receiver functions give restrictions on velocity contrasts at the level of Moho and, in some regions, including intracrustal and intramantle reflectors located below each permanent or temporary seismic station (Fig. 9). Tokam et al. (2010) had reached the same observation when he studied the crustal structure beneath Cameroon through the Cameroon Broadband Seismic Experiment (CBSE).

They found an increase in crust thickness of $36 - 43$ km in the Oubanguides belt and crust thickness values of $33 - 26$ km in the Garoua rift and a crust thickness of

about 28 km in the coastal plains. For large areas with detailed knowledge of the crustal thickness under the West African Mobile Zone (WAMZ), West African Craton (WAC), and Sahara metacraton are non-existent.

2.1.4 Crustal gravity based models

Several gravity-based crustal models (Fig. 10 and Table 2) have been proposed recently taking advantage of the high precision and high spatial resolution measurements of the Earth's gravitational field and geoid provided by the GOCE (Gravity Field and Steady-State Ocean Circulation Explorer) and GRACE (Gravity Recovery and Climate Experiment) satellite missions (Pail et al., 2010; der Meijde and Pail, 2020). The inversion of gravity data for crustal thickness has been used to generate models based exclusively on these gravity observations. Of course, although these global models have advanced our knowledge of crustal structure, the accuracy of their resolution is still too low to be applied to regional studies.

The Vening-Meinesz Moritz (VMM) (Fig.10a) model is based on the Vening Meinesz inverse isostasy problem, relying on the generation of the zero isostatic gravity disturbances. The Moho depth is estimated from Bouguer's gravitational anomalies and under the assumption of variable Moho depths and the use of a constant Moho density contrast. After correction of the gravitational signal for topography, bathymetry, ice and sediments, the computed isostatic disturbances are assumed to be the sum of the gravitational disturbances of the earth's crust plus the gravitational attraction of the isostatic compensation masses.

The GEMMA (GOCE Exploitation for Moho Modeling and Applications) model developped by Reguzzoni and Sampietro (2015) is a combination of the CRUST2.0 seismic model and the gravitational observations from the GOCE satellite mission. The GEMMA model (Fig.10b) has been reduced to a two-layer model by eliminating the effects of topography, bathymetry and densities, and can be considered as "an update of the CRUST2.0 Moho model" with a resolution of $0.5° \times 0.5°$.

The model by Tugume et al. (2013) is based on an iterative 3D Parker−Oldenburg

inversion (Oldenburg, 1974) of the EIGEN−6C gravitational data (Shako et al., 2013) using Bouguer's sediment-corrected anomalies to obtain a simple two-layer model with Moho as the only subsurface interface (Fig.10c).

Tedla et al. (2011) (Fig.10d) performed a deconvolution of Euler's gravity to estimate the depth of Moho at a resolution of 0.25°. The method consists in studying the spectral analysis of the gravitational field to detect the subsurface interfaces with an estimation limit in regions where the crust is strongly thinned (Van der Meijde et al., 2015). In addition, the thinner crust of Tedla is located at about 33.25 km, indicating a cut in Euler's solutions at this depth (Tugume et al., 2013). In addition, Tedla et al. (2011) do not take into account seismic data when referring to their crust model to reduce compromises. However, the application of this method and its validity for the African continent has been widely questioned (Reid et al., 2012; der Meijde and Nyblade, 2013).

Table 2: Statistics comparison between VMM, GEMMA, Tugume and Tedla crustal Models.

Models	Coverage	Method	Resolution	References
VMM	Global	Isostatic model	1°	Bagherbandi et al. (2013)
GEMMA	Global	Combined gravity and seismic model	0.5°	Reguzzoni and Sampietro (2015)
Tedla	Continental	Gravity, 3−D Euler deconvolution	0.225°	Tedla et al. (2011)
Tugume	Continental	Gravity, Parker-Oldenburg inversion	0.25°	Tugume et al. (2013)

2.1.5 Gravity data

Gravity data from the global gravity model EIGEN−6C4 (Förste et al., 2014) and XGM2016 (Mayer-Guerr, 2015; Pail et al., 2016) are used in this study.

Global Gravitational Models (GGMs) are commonly divided into two different types:

1. The Satellite-only models and combined. Satellite-only models are derived from the artificial earth satellite data such as CHAMP (Challenging Minisatellite Payload), GRACE, GOCE (Balmino et al., 1999; Gerlach et al., 2003) and LAGEOS

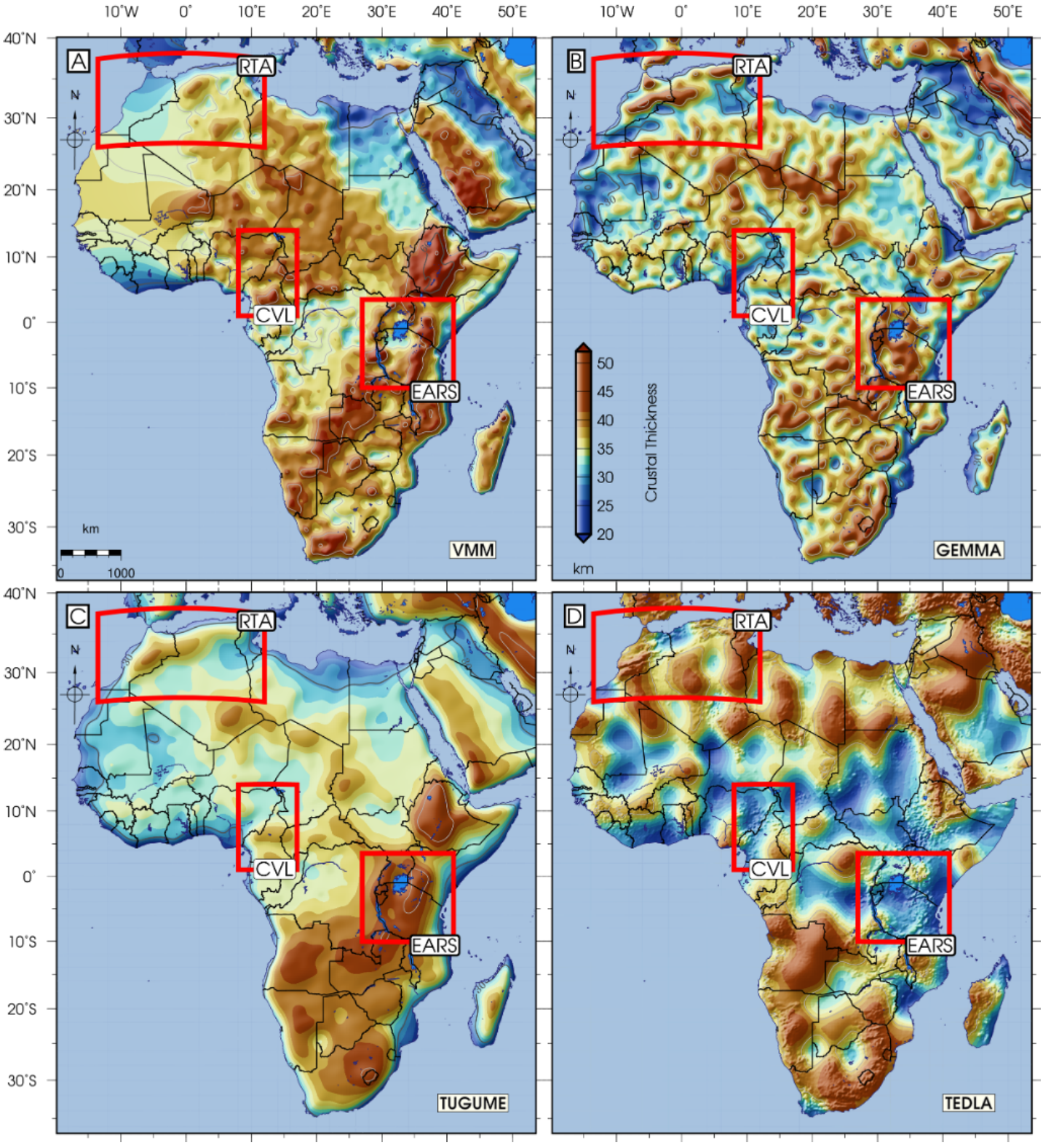

Figure 10: The juxtaposition of some existing crustal models for Africa. The gravity-based models are VMM (Vening-Meinesz Moritz) model by Bagherbandi et al. (2013), (b) GEMMA model by Reguzzoni and Sampietro (2015), (c) Tugume model by Tugume et al. (2013), and (d) Tedla model by Tedla et al. (2011).

(Laser Geodynamics Satellites) (Yoder et al., 1983). They are independent from any terrestrial data and their degree is low.

2. The combined models are generated through merging/combining satellite data, airborne gravimetry with ground-based observation data over the continental areas and altimetry data over the ocean areas (Rapp, 1998). The combined EGMs have much higher degrees and more accurate data compared to satellite-only models.

2.1.5.1 EIGEN-6C4 gravity model

The EIGEN−6C4 (European Improved Gravity model of the Earth by New techniques) data are based on the gravity observations by the GRACE (Tapley, 2004) and GOCE satellites, and gravity models EGM2008 (Pavlis et al., 2012) and DTU10 (Andersen et al., 2009) solutions. The EGM2008 and DTU10 gravity data are global models. EGM2008 uses the data from ground, airborne and satellite measurements, and DTU10 is a combination of the EGM2008 model over the continents and altimetry data on the oceans.

EIGEN−6C4 is a static global combined gravity field model up to degree and order 2190. It has been elaborated jointly by GFZ Potsdam and GRGS Toulouse and contains the following satellite and ground data:

- LAGEOS−1/2 (deg. $2-30$): Satellite Laser Ranging data $1985-2010$
- GRACE, GNSS-SST and K-band range-rate data, processing according to RL03 GRGS (deg. $2-130$): ten years $2003-2012$
- GOCE, Satellite Gravity Gradiometry (SGG) data, processed by the direct approach including the gravity gradient components T_{xx}, T_{yy}, T_{zz} and T_{xz} out of the following time spans: 837 days out of the nominal mission time span $20091101-20120801$, 422 days out of the lower orbit phase between $20120801-20131020$. These GOCE data as well as the LAGEOS and GRACE data are the same as used for the 5^{th} release of ESA's satellite only gravity field model via the direct

approach (Pail et al., 2010; Bruinsma et al., 2014).

- Terrestrial data (max degree 370): DTU12 ocean geoid data and an EGM2008 geoid height grid for the continents.

2.1.5.2 XGM2016 gravity model

The XGM2016 model (Pail et al., 2016) has been used as the state-of-the-art high-resolution GGM in order to assess the considered GOCE-only as well as combined GGMs. The XGM2016 is a preparation release of the planned Earth Gravitational Model 2020 (EGM2020) that will succeed the EGM2008 (Pavlis et al., 2012).

The XGM2016 model is parameterized as a spherical harmonic series expansion resolved to degree and order (d/o) 719, which is the maximum resolution supported by the $15' \times 15'$ terrestrial gravity grid (720 blocks in latitude direction enable the estimation of 720 zonal coefficients, which corresponds to the coefficients from degree $0 - 719$). For XGM2016, a significant focus is the optimal combination of the new terrestrial data with the latest satellite gravity information. The combination is based on the rigorous solution of a full normal equation system up to the maximum d/o 719 (corresponding to $518,400$ gravity parameters), and a regionally dependent weighting strategy is applied to cope with the varying data quality of the ground data. The stochastic model of the ground data grid is inferred from comparison with satellite-only solutions in the long–medium wavelength range. Finally, the resulting XGM2016 is validated against existing global gravity field models in terms of geoid/height anomaly and MDT (Mean Dynamic Topography) comparisons.

The combination of these different satellite and surface data sets has been done by a bandlimited combination of normal equations (to maximum degree/order 370), which are generated from observation equations for the spherical harmonic coefficients (Shako et al., 2013). The resulted solution to degree/order 370 has been extended to degree/order 2190 by a block diagonal solution using the DTU10 global gravity anomaly data grid.

The gravity signal is calculated using the unit mGal, which is equivalent to 10^{-5}

m/s ^{2}.

2.2 Methodology

2.2.1 Gravitational Potential and Geoid

According to Newton's Law of Universal Gravitation, the gravitational potential generated by a mass differential at a point at a distance r is given by:

$$dV = +G\frac{dm}{r} \tag{2.1}$$

where G is the universal gravitation constant[1].

Therefore, the potential generated by a mass distribution with density $\rho(\vec{r})$ and volume V can be written as:

$$W_a(\vec{r}) = G\int_V \frac{\rho(\vec{r}\,')}{|\vec{r}-\vec{r}\,'|}d\vec{r}\,' \tag{2.2}$$

It can be shown that this potential satisfies the Poisson's equation:

$$\nabla^2 W_a = -4\pi G\rho \tag{2.3}$$

Outside the masses, the density ρ is canceled and the potential satisfies the Laplace equation:

$$\nabla^2 W_a = 0 \tag{2.4}$$

and therefore, W_a is a harmonic function.

In the case that the body that generates this potential is the Earth, we must not stop considering the effect of rotation of the same, which generates a centrifugal potential Φ.

$$\Phi(\vec{r}) = \frac{1}{2}\omega^2 d_z^2 \tag{2.5}$$

where ω is the angular velocity of the Earth and $d_z = \sqrt{x^2+y^2}$ the distance from the point $\vec{r}$ to the rotational axis (z).

[1]Note that the convention of the positive sign is used for the definition of the potential.

In conclusion, the gravitational potential generated by the Earth outside its masses can be written as the sum of a harmonic potential and a centrifugal potential.

$$W = W_a + \Phi \tag{2.6}$$

However, we can rethink this potential as the sum of two potentials: one that we will call "normal" U and another one called "perturbative" T. We will define the first one in such a way that the equipotential surface given by $U(\vec{r}) = U_0$ has the same form as the Ellipsoid of revolution. While the second one will be the disturbing potential necessary to reach the potential W.

Rewriting the potentials in the ellipsoidal coordinates (h, λ, ϕ), and taking into account that U does not depend on λ, we can express W as:

$$W(h, \lambda, \phi) = U(h, \phi) + T(h, \lambda, \phi) \tag{2.7}$$

Finally, we will define the geoid as that equipotential surface defined by $W(h, \lambda, \phi) = U_0$ and geoid ripple to function $N(\lambda, \phi)$ such that:

$$W(h{=}N(\lambda, \phi),\ \lambda,\ \phi) = U(h{=}0, \phi) = U_0 \tag{2.8}$$

2.2.2 Gravimetric anomalies

2.2.2.1 Normal Gravity and Gravimetric Anomaly

Before being able to refer to a gravimetric anomaly it is necessary to define the "normal" scenario from which such anomaly deviates. The concept of normal gravity is used for this purpose.

The acceleration vector of gravity can be obtained from the potential that generates it. For example, the gravity vector generated by the terrestrial potential W can be obtained in the following way[2]:

$$\vec{g} = +\nabla W \tag{2.9}$$

And from here we obtain the radial component of the acceleration:

$$g_z = \frac{\partial W}{\partial r} \tag{2.10}$$

[2]Note that the convention of the positive sign for the definition of the potential gradient is used.

Now, we can define normal gravity as the radial component of the normal U gradient evaluated on the surface of the Ellipsoid.

$$g_0 = \frac{\partial U}{\partial r}\Big|_{h=0} \tag{2.11}$$

Taking advantage of the potential U is harmonic, it is possible to perform a development in spherical harmonics and then obtain the value of g_0 as a function of ϕ. For Ellipsoid WGS84 g_0 adopts the following:

$$g_0(\phi) = 9.7803267714 \frac{1 + 0.00193185138639 \sin^2(\phi)}{\sqrt{1 - 0.00669437999013 \sin^2(\phi)}} \tag{2.12}$$

Finally, we can define the gravitational anomaly observed as the difference between observed and normal gravity:

$$\Delta g(h, \lambda, \phi) = g_z(h, \lambda, \phi) - g_0(\phi) \tag{2.13}$$

Figure 11 presents a simple example of a lithosphere model that includes the mantle, the crust, a given topography along with the root it generates and includes an anomalous body immersed in a bark. In the first graph we can see the observed gravity, that is, the one generated by the complete model together with the rest of the Earth. While the second graph shows how it is modified by removing the normal gravity to that magnitude. The effect that this has on the model is to remove the normal cortex and the mantle, leaving a root with a negative density contrast and part of the anomalous body with positive density contrast.

2.2.2.2 Free Air Anomaly

Note that the observed gravity anomaly has a dependency on h. For example, if the measurement was made in topography, h will come to take the value of the topographic dimension. Such dependence is unnecessary, so it is beneficial to eliminate it. To do this we will use what is known as Free Air correction.

This consists in removing the effect produced by the normal potential U by raising the measurement point from the geoid to the height h. It is obtained by making an approximation by Taylor series of the acceleration of gravity:

$$g(h) \simeq g_0 + \frac{\partial g(h)}{\partial r} h \simeq g_0 - 0.3086 \cdot 10^{-5} h \tag{2.14}$$

where the constant 0.3086 is expressed in s^{-2}.

We then define the Free Air correction term as:

$$g_{fa}(h) = -0.3086 \cdot 10^{-5}\, h \tag{2.15}$$

And the Free Air anomaly will not be more than the Observed Gravity Anomaly minus said correction:

$$\Delta g_{fa} = g_z - g_0 - g_{fa} \tag{2.16}$$

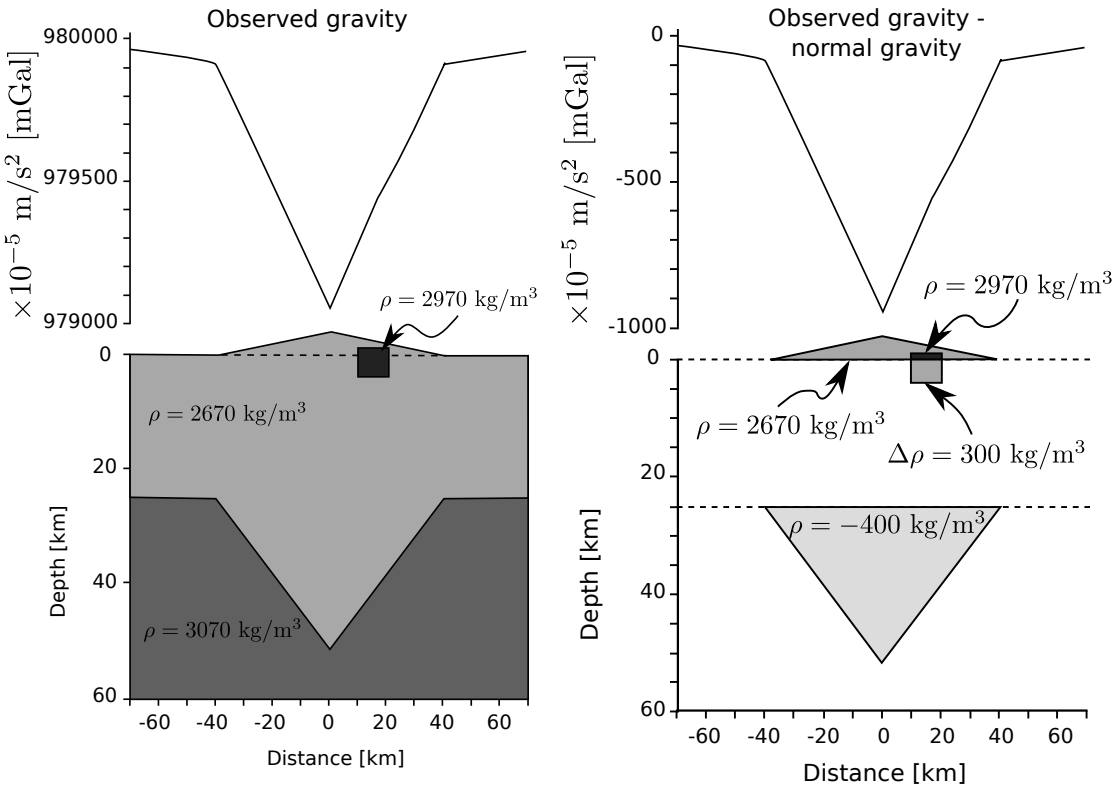

Figure 11: Observed Gravity and Anomaly Observed for an example with Topography, Root and anomalous body in bark, measured in topography.

2.2.2.3 Bouguer gravity anomaly

In addition to the Free Air correction, another correction is usually made to eliminate the effect that the topography produces on a said anomaly. This is known as the Bouguer anomaly.

$$g_{bg} = 2\pi g_0 \rho_c h \simeq 0.1119 \cdot 10^{-5}\, h \tag{2.17}$$

where $\rho_c = 2670$ kg/m^3 is the standard density of the topographic masses and the constant of proportionality is expressed in s^{-2}.

Finally, we define the Bouguer Anomaly as:

$$\Delta g_{bg} = \Delta g_{fa} - g_{bg} = g_z - g_0 - g_{fa} - g_{bg} \tag{2.18}$$

In Figure 12 the Free Air and Bouguer anomalies are exposed for the same example as that of the Figure 11.

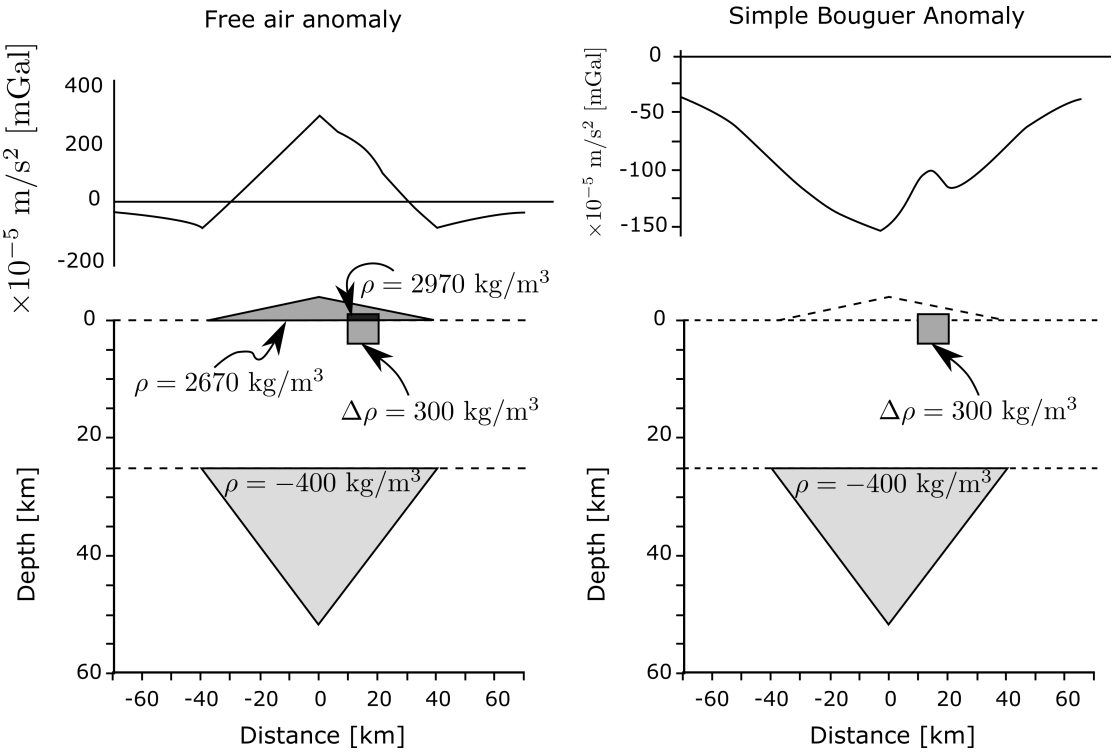

Figure 12: Free Air Anomaly and Simple Bouguer Anomaly for the same example as the Figure 11.

In the first graph, we see that the Free Air correction removes the effect produced by having obtained the measurements in height, however it does not produce any modification to the model. While in the second graph we observe how the Bouguer correction eliminates the gravimetric effect produced by the topography.

2.2.3 Fundamental model of upward continuation

The fundamental principle of downward continuation is shown in Fig.13. In Fig.13, $u_0(x, y)$ are the gravity surveying data on the observation plane and $u_h(\xi, \eta)$ are the gravimetric data on the continuation plane. According to the upward continuation

formula, the plane approximation relationship between gravimetric surveying data on the observation plane and gravimetric data on the continuation plane (Jacobsen, 1987; Leonov, 2011).

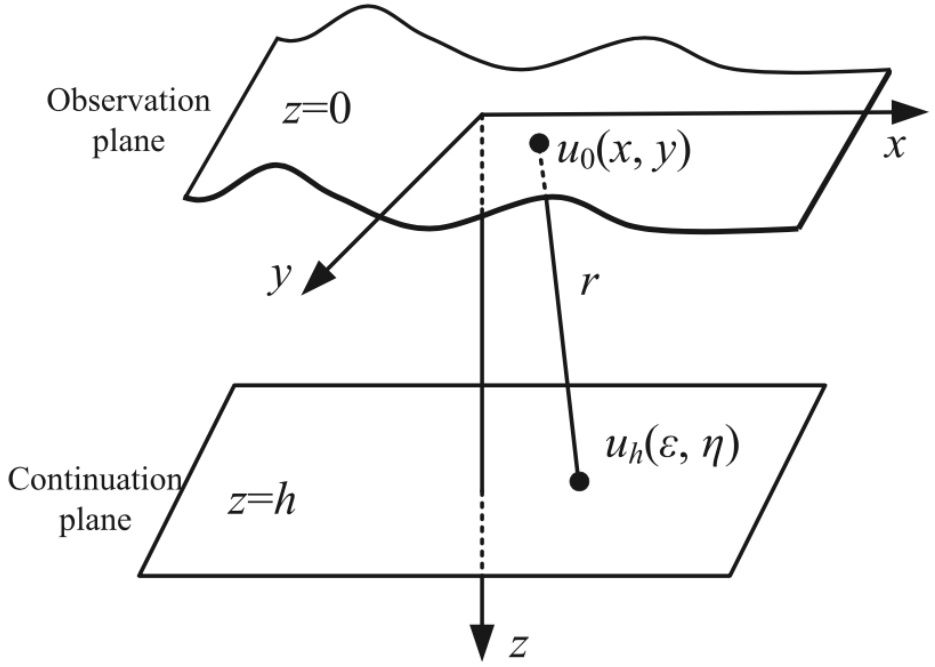

Figure 13: Upward continuation sketch map.

$$\begin{aligned} u_0(\mathrm{x},\mathrm{y}) &= \frac{h}{2\pi}\iint_{-\infty}^{+\infty}\frac{u_h(\xi,\eta)}{r^3}\mathrm{d}\xi\mathrm{d}\eta \\ &= \frac{h}{2\pi}\iint_{-\infty}^{+\infty}\frac{u_h(\xi,\eta)}{[(\mathrm{x}-\xi)^2+(y-\eta)^2+h^2]^{3/2}}\mathrm{d}\xi\mathrm{d}\eta \end{aligned} \tag{2.19}$$

where h is the upward continuation depth and r is the distance between point(ξ, η, h) on the continuation plane and point $(x, y, 0)$ on the observation plane.

By Fourier transform of equation 2.19, the fundamental formula of upward continuation can be obtained as follows:

$$u_h(\mathrm{x},\mathrm{y}) = \mathrm{F}^{-1}\left[\mathrm{e}^{2\pi fh}\mathrm{U}_0(u,\mathrm{v})\right] \tag{2.20}$$

From equation 2.20, we can infer that the high-frequency noise in gravimetric data because of the instability of upward continuation operator $e^{2\pi fh}$.

2.2.4 Airy Isostasy

Isostasy is the state of equilibrium between the crust and the terrestrial mantle due, among other factors, to the difference of densities between both. The terrestrial crust is generally less dense than the mantle, with which, due to the principle of Archimedes, it can be interpreted that the first fleet on the second.

There is a classic isostatic model known as the Airy-Heiskanen model isostatic or Isostasy of Airy, which predicts that a topographic elevation produces a root that is inserted into the mantle at a depth that depends on that elevation. The balance is produced with competition from the gravitational force of the cortex and the thrust generated by the difference of the densities of the mantle and the root.

Given an arbitrary topography, consider a column of the entire lithosphere (from the topography to the upper mantle), as can be seen in Figure 14. According to the Airy model, the weight of the cortical part of the column (first member of the equation 2.21) must be annulled with the thrust generated by the mantle displacement due to the intrusion of the root (second member of the equation 2.21).

$$\rho_t \, g \, h + \rho_c \, t \, g + \rho_c \, w \, g = \rho_m \, w \, g + \rho_c \, t \, g \tag{2.21}$$

Regrouping the terms, the Airy isostatic equilibrium equation is obtained:

$$w = \frac{\rho_t}{\rho_m - \rho_c} \, h \tag{2.22}$$

By applying the said equation to each point of the profile or grid it is possible to obtain the isostatic root. As an observation, taking normal values of topography, bark and mantle densities ($\rho_t = 2670$ kg/m^3, $\rho_t = 2900$ kg/m^3, $\rho_m = 3300$ kg/m^3) the relation of proportionality between the intrusion of the mantle bark and the topography is:

$$w \simeq 6,675 \, h \tag{2.23}$$

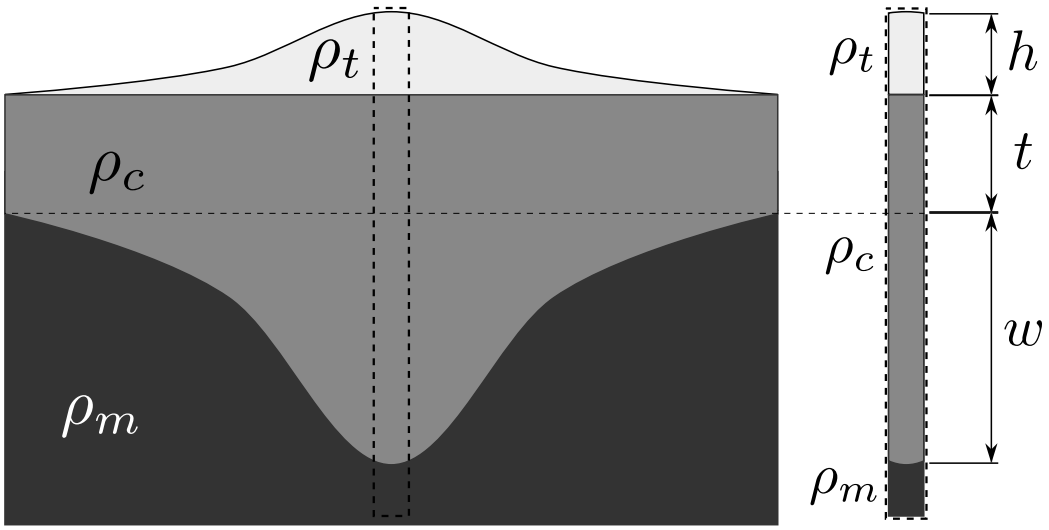

Figure 14: Lithospheric profile with topography, normal crust, isostatic Airy root and upper mantle. In the chosen column the topography has a height h and the root a depth w measured from the lower limit of the normal crust, defined with a width t.

2.3 Gravity inversion for crustal estimation

Estimating Moho depth from gravity data is a non-linear inverse problem. One can generalize this problem of estimating the depths of an interface separating two media, such as the sediment-basement interface of a sedimentary basin or the crust- mantle interface (Moho).

2.3.1 Inversion algorithm

Different gravity inversion methods have been developed over the years for the determination of the Moho topography. This study followed an approach of Van der Meijde et al. (2013), using an algorithm proposed by Uieda and Barbosa (2016) based on the Gauss-Newton formulation of Bott's equation (Silva et al., 2014). The algorithm takes into account the earth curvature by using tesseroids for forward modeling. The forward modeling is achieved through numerically solving the Gauss-Legendre quadrature (GLQ) integration problem (Asgharzadeh et al., 2007). In this approach, the numerical instability is overcome by an improved adaptive discretization of the anomalous Moho (Uieda et al., 2016). Bott (1960) presented an iterative approach for estimating a relief in a two-layer model with contrasting densities on the inter-

face, $\mathrm{p}(\mathrm{x}_i) : i = 1, 2, \ldots, \mathrm{N}$ where x_i is a set of horizontal coordinates of N-gravity observations. The approximation of $p^{\mathrm{k}}(\mathrm{x}_i)$ for iteration at a k^{th} point is given by:

$$p^k(x_i) = p^{k-1}(x_i) + \frac{g^o(x_i) - g\left(x_i, \rho, p^{k-1}\right)}{2\pi G \Delta\rho}, i = 1, 2, \ldots, N \tag{2.24}$$

where G is the gravitational constant, ρ is the density contrast on the interface, $g^o(x_i)$ is the gravity anomaly, and $g\left(x_i, \rho, p^{k-1}\right)$ is the computed gravity anomaly at a point calculated from the depth model.

Bott's method had several limitations, such as the non-optimized step sizes of the iterative corrections and an inherent subjectivity in the criteria for stopping the iterative process (Silva et al., 2014). Silva et al. (2014) extended Bott's method as a Gauss-Newton formulation method by changing the Jacobian matrix $(N \times M)$ to $A = 2\pi G \Delta\rho I$, where I is the identity matrix. However, despite this improvement, Bott's method still suffers from instability during inversion. Thus, a smoothing filter is required especially when handling unstable depth estimates.Uieda and Barbosa (2016) introduced a regularized method for Bott's approach that inverts gravity data in spherical coordinates in two ways:

1. the rectangular prism was replaced by the spherical prisms, or tesseroids (Uieda et al., 2016) .

2. they deployed a regularization parameter to control the smoothness of the inversion results while maintaining the fit between solutions and the observed data, using the Tikhonov regularization (Tikhonov and Arsenin, 1977).

In this approach, the ill-posed inverse problem is transformed into a well-posed inverse matrix. Inversion results from the regularized Bott's method, i.e. the Moho depth estimates, at k^{th} iteration, are obtained by solving a parameter perturbation vector, Δp^k;

$$\left[A^{kT} A^k + \mu R^T R\right] \Delta p^k = A^{kT} \left[g^o(x_i) - g\left(x_i, \rho, p^{k-1}\right)\right] - \mu R^T R p^k, i = 1, 2, \ldots, N \tag{2.25}$$

Where

* A^{k} is a Jacobian matrix defined as $A_{ij}^{k} = \frac{\partial f_i}{\partial p_j}\left(\mathrm{p}^{k}\right)$,
* μ is a regularization parameter,
* R is an $L \times M$ finite-difference matrix representing an L first-order difference between adjacent tesseroids,
* p^{k} is the M-dimensional parameter vector containing M-Moho depth.

2.3.2 Gravity modeling of a density layer in spherical coordinates

Considering a **3D** subsurface density layer, whose top and bottom surfaces are constant or variable in spherical coordinates, we divide the layer into a gird of M and N segments with equal mesh interval of $\Delta\lambda, \Delta\varphi$ in longitude and latitude directions. The total Tesseroid unit number of the layer is $\mathbf{N}_{\mathrm{tess}} = \mathbf{M} \times \mathbf{N}$.

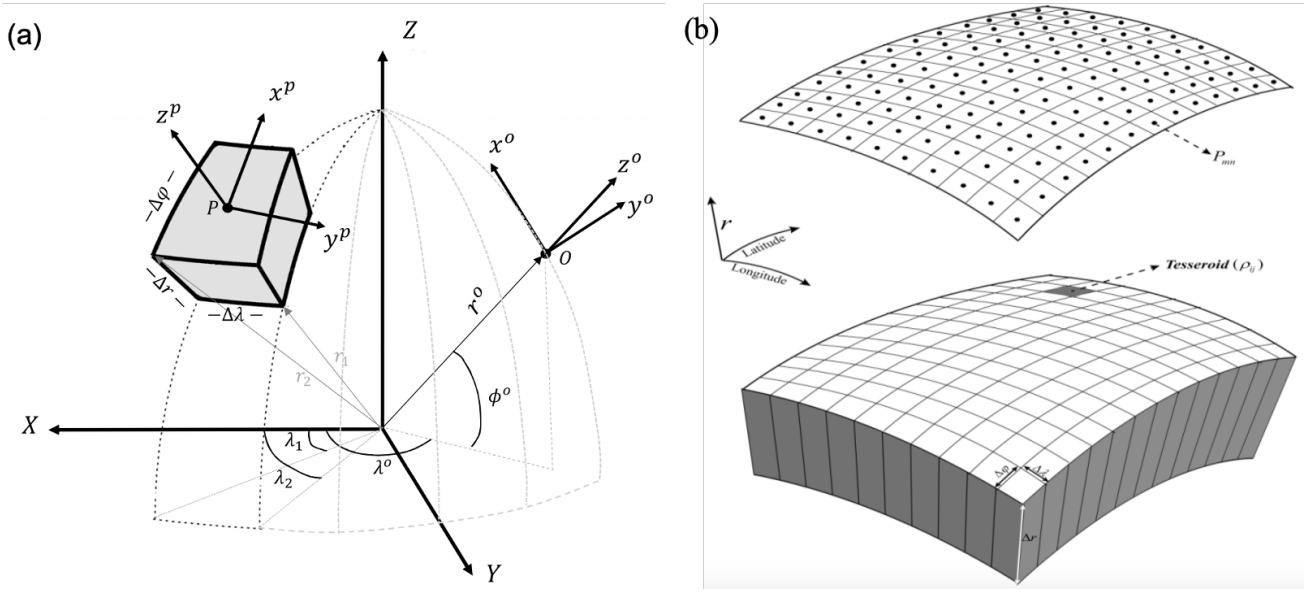

Figure 15: A subsurface density layer consists of a grid of juxtaposed Tesseroid units in spherical coordinates with constant top and bottom surfaces. (a) Geometry of a spherical tesseroid showing global (X, Y, Z) and local $(x^p, y^p, z^p; x^o, y^o, z^o)$ coordinate systems. (b) $\Delta\lambda, \Delta\varphi$ are mesh intervals in longitude and latitude directions, Δr is the thickness of the layer, $P_{(m,n)}$ is a computation point of observation surface in spherical coordinates, ρ_{ij} is the density of the Tesseroid numbered (i, j) in longitude and latitude directions.

For the convenience of display, the top and bottom surfaces of the layer, and the observation surface are assummed to be constant in Figure15. The density of each Tesseroid is constant, which means only lateral difference of the spatial density distribution is available.

2.3.3 Parameter estimation

The regularized Bott's method requires a regularization parameter, a reference Moho depth and a density contrast as parameters. These were estimated using the hold-out method Kim (2009). The gravity data was split into a training dataset (t^o_{inv}), and a testing dataset (t^o_{test}), using the approach as shown in Fig.16.

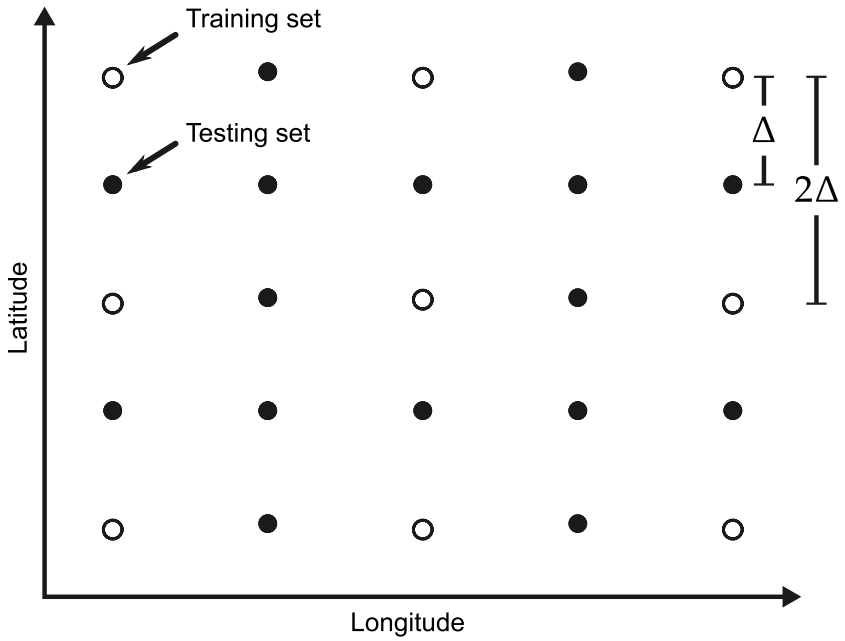

Figure 16: Data splitting approach in which black points represent testing data and hallow points represent training data. The training data set is still displayed on a regular grid but with twice the grid spacing of the original data grid.

Training data were used to estimate the optimal regularization parameter, the reference Moho depth and the density contrast. Testing data were used to check the quality of the chosen value for the regularization parameter (μ) while seismic constraints were used to validate the reference Moho depth and the density contrast. Parameter estimation was done in two steps.

2.3.3.1 Estimating regularizing parameter

The metric chosen to evaluate μ_n is the mean square error (MSE) of the misfit between the observed and predicted testing data sets,

$$MSE_n = \frac{\|\mathrm{t}^o_{test} - \mathrm{t}^n_{test}\|^2}{N_{test}} \tag{2.26}$$

in which N_{test} is the number of data in the testing set. The optimal value of μ will be the one that minimizes the MSE, i.e. the one that best predicts the testing data. Note that the inversion is only made on all training data. The algorithm for the hold-out cross-validation is outlined as described below:

1. Divide the observed data into the training (t^o_{inv}) and testing (t^o_{test}) sets.
2. For each $\mu_n \in [\mu_1, \mu_2, \ldots, \mu_{N_\mu}]$:
   (a) Estimate the regularization parameter by inverting the training set t^o_{inv}.
   (b) Use the regularization parameter to calculate the predicted testing set t^n_{test}.
   (c) Calculate the mean square error MSE_n using Eq. 2.26.
3. The final solution correspond to the smallest MSE_n.

2.3.3.2 Estimating the reference Moho depth and the density contrast

In this study, we use point estimates of the Moho depth to determine the optimal values of the Normal Earth Moho (z_{ref}) and the anomalous Moho ($\Delta\rho$). These points will generally come from seismological studies, like receiver functions, surface wave dispersion and deep refraction experiments.

Let z^o_s be a vector of N_s known Moho depths. We use the mean square error (MSE) as a measure of how well a given inversion output $\hat{\mathrm{p}}^{l,m}$ fits the know depths. The optimal values of z_{ref} and $\Delta\rho$ are the ones that best fit the independent known Moho depths (i.e., produce the smallest MSE). However, the points do not necessarily coincide with the model elements of the inversion. Before computing the MSE, we interpolate $\hat{\mathrm{p}}^{l,m}$ on the known points to obtain the predicted depths $\mathrm{z}^{l,m}_s$.

The MSE is defined as

$$MSE = \frac{\|\mathrm{z}_s^o - \mathrm{z}_s^{l,m}\|^2}{N_s}. \tag{2.27}$$

The algorithm for estimating z_{ref} and $\Delta\rho$ is:

1. For every combination of $z_{ref,l} \in [z_{ref,1}, z_{ref,2}, \ldots, z_{ref,N_z}]$ and

   $\Delta\rho_m \in [\Delta\rho_1, \Delta\rho_2, \ldots, \Delta\rho_{N_\rho}]$:

   (a) Perform the inversion on the training data set d_{inv}^o using $z_{ref,l}$, $\Delta\rho_m$, and the previously estimated value of μ. The inversion output is the vector $\hat{\mathrm{p}}^{l,m}$.

   (b) Interpolate $\hat{\mathrm{p}}^{l,m}$ on the known points to obtain the predicted depths $\mathrm{z}_s^{l,m}$.

   (c) Calculate the MSE between z_s^o and $\mathrm{z}_s^{l,m}$ using Eq. 2.27.

2. The final solution is the $\hat{\mathrm{p}}^{l,m}$ corresponding to the smallest MSE.

2.4 Flowchart of the processing methodology

As mentioned, the aim of this thesis is to determine the new Moho depth model for peculiar areas of Africa with high accuracy ($3-5$ km) and detailed resolution (about 10 km). The new and improved methods will be applied to determine the Moho depth from the gravity model EIGEN$-$6C4/XGM2016 in these atypical regions where seismic data are missing, sparse or uneven. The integrated data approach will require additional topography, bathymetry and sediment models. The determination of the Moho depth model will be carried out in three individual steps (for a schematic illustration, see Fig. 17). First, the gravimetric forward modelling will be applied to model the gravitational signature of major known anomalous density structures within the crust. In the second step, the gravimetric inversion will be applied to estimate the Moho depth from Bouguer gravity data obtained from observed gravity data after subtracting the gravitational signature of topography and crustal density heterogeneities. In the final step, the combined processing of gravimetric and seismic results will be conducted to fit the Moho depth model determined from gravity

data with the seismic estimates of the Moho depth at seismic sites. Numerical steps involved has been extensively reviewed above.

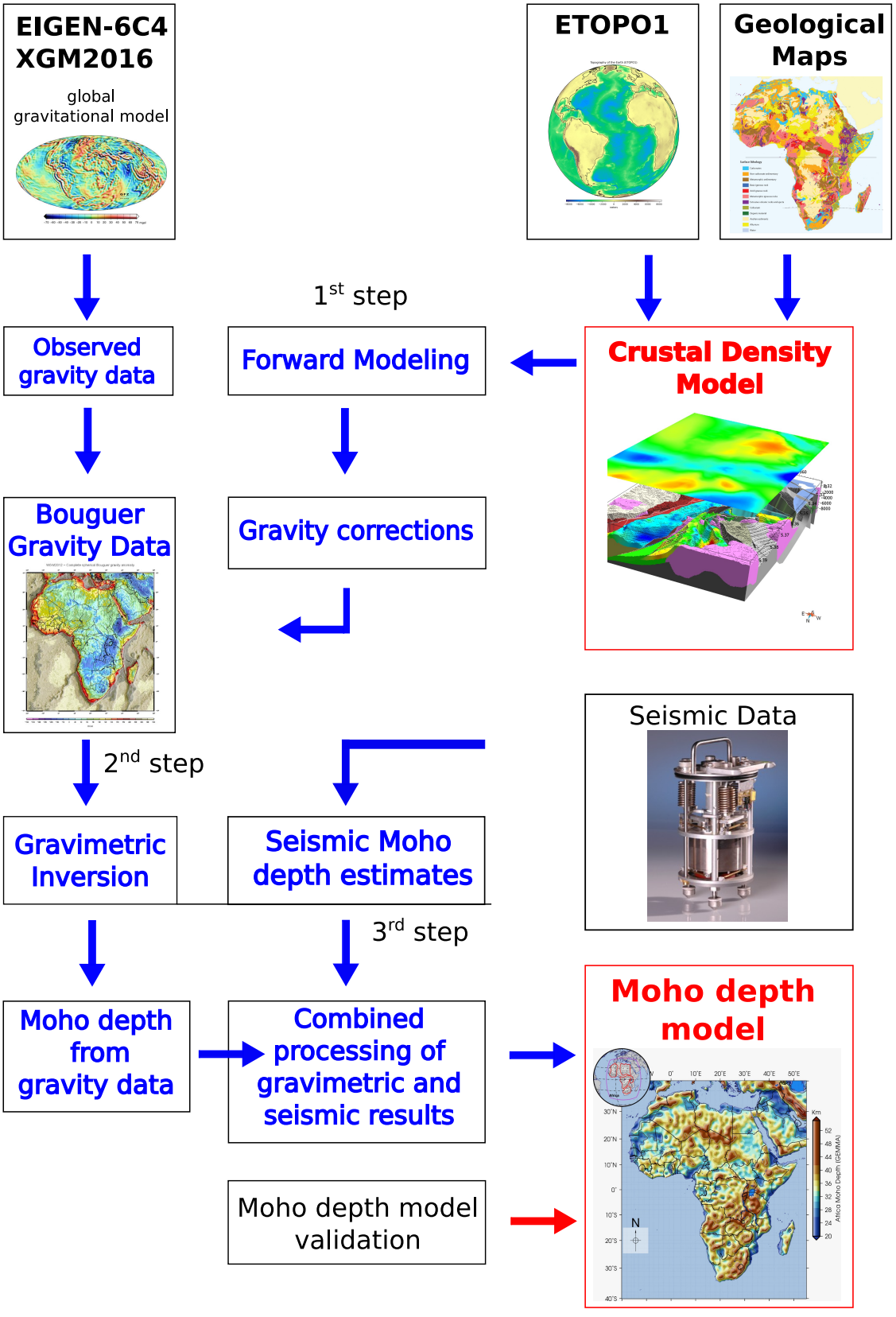

Figure 17: Schematic realization of the project.

Chapter 3

Results and discussions

The purpose of this chapter is to present the results of the gravimetric forward modelling obtained along the African hotspots configuration based on satellite gravity, topographic and seismic data. We will present sequentially the results obtained along the Rif-Tell-Atlas (Section 3.1), then along the Cameroon Volcanic Line (Section 3.2), and finally over the Eastern African rift System (Section 3.3).

3.1 Crustal thickness beneath Atlas region from gravity, topographic, sediment and seismic data

3.1.1 Free-air gravity data

The free-air gravity anomalies computed on a $5' \times 5'$ geographic grid of surface points are shown in Fig. 18. At the study area, these gravity anomalies vary mostly between -100 and 250 mGal. Positive values prevail over most of moderately elevated and mountainous regions. Over lowlands, the values are mostly negative. In the central High Atlas, the contours of the free-air gravity anomalies strike roughly N55°E direction, reflecting the direction of most elevated regions. This observation obviously agrees with the expected high spatial correlation between the free-air gravity anomalies and the topography. However, this trend is slightly oblique to the general structural direction of the High Atlas, which is approximately in N75°E direction. Maxima of the free-air gravity anomalies reaching $\backsim$ 250 mGal in west part of the central High Atlas correlate with the highest summits that exceed elevations of 4000

m. Over lowlands to north and south of the High Atlas, the free-air gravity anomalies decrease substantially, with most of values within ±50 mGal. Over the north part of continental margins from Morocco to Tunisia, except for the coastal area along the Rif Cordillera, the free-air gravity anomalies are typically positive, while mostly negative in south of the Aures Mountains (−100 mGal), the Sahara (−75 mGal), the central (−25 mGal) and east parts (−80 mGal) of the West African Craton. In the central part of the Pan-African Trans-Saharan Belt, the free-air gravity anomalies vary roughly from −60 to −90 mGal, while gradually decrease westwards along the West African Craton with negative values below −100 mGal.

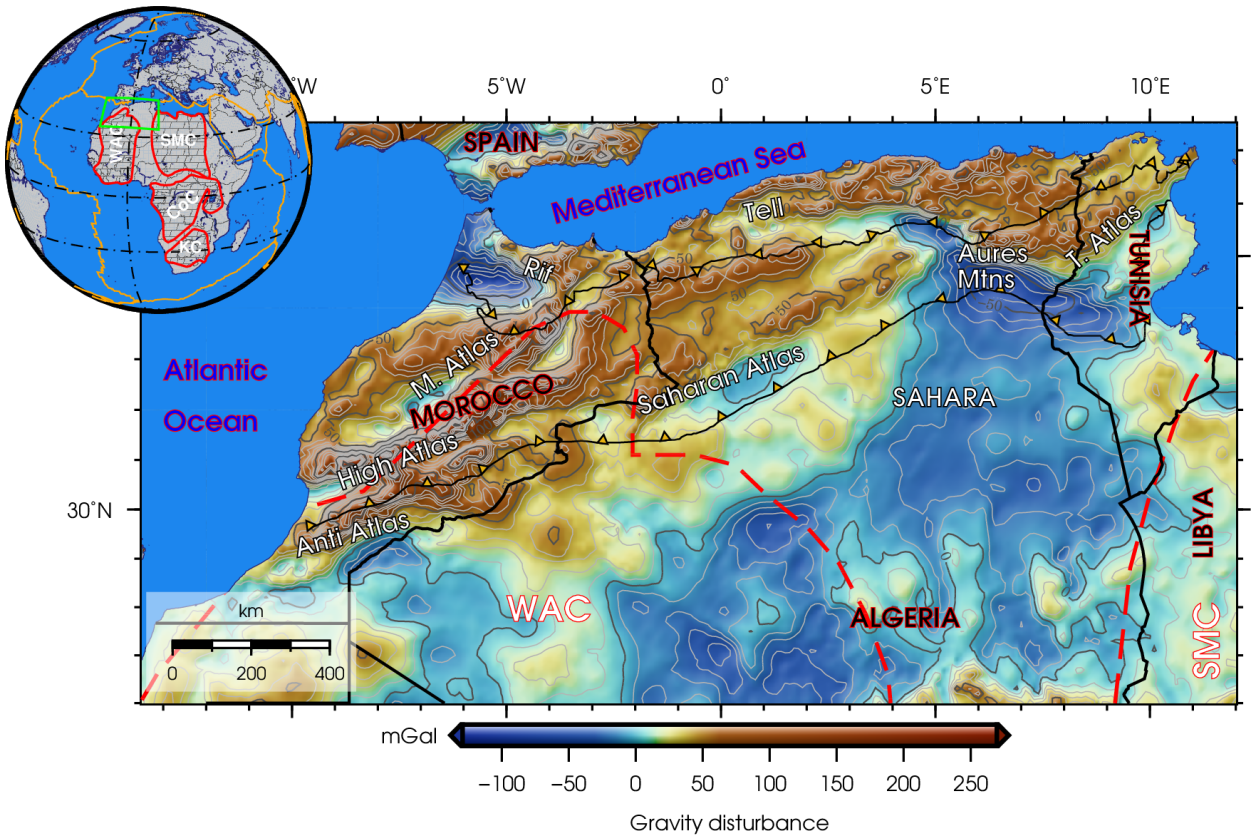

Figure 18: Regional maps the free-air gravity anomalies computed on a $5' \times 5'$ grid of surface points

3.1.2 Bouguer gravity data

We used the ETOPO1 (Amante and Eakins, 2009) global (solid) topography data to compute the topographic and bathymetric gravity corrections with the same spectral resolution as used for the free-air gravity data. Both gravity corrections were computed simultaneously by applying the tesseroid method (Uieda et al., 2016). The

topographic gravity correction was estimated for a homogeneous density distribution due to a lack of knowledge on the distribution of topographic density in most parts of north-west Africa. In particular, we used the density value of 2670 kg.m^{-3} that is typically adopted to represent the upper continental crustal density (Hinze, 2003). The bathymetric gravity correction was computed for the ocean density contrast of 1630 kg.m^{-3}. It is worth mentioning that for a more accurate computation of the bathymetric gravity correction, the depth-dependent seawater density model developed by Gladkikh and Tenzer (2011) could be used; see also Tenzer et al. (2010, 2011, 2012). We further used the sediment data from the CRUST1.0 global seismic crustal model (Laske et al., 2013) to compute the sediment gravity correction. In regions with a well-known geological stratigraphy, additional gravity corrections can also be applied to model and subtract the gravitational signature of deeper lithospheric structures (Tenzer et al., 2009; Tenzer and Gladkikh, 2014; Tenzer et al., 2014; Tenzer and Chen, 2019).

The combined topographic-bathymetric gravity correction computed on a $5' \times 5'$ geographic grid of surface points is shown in Fig. 19.

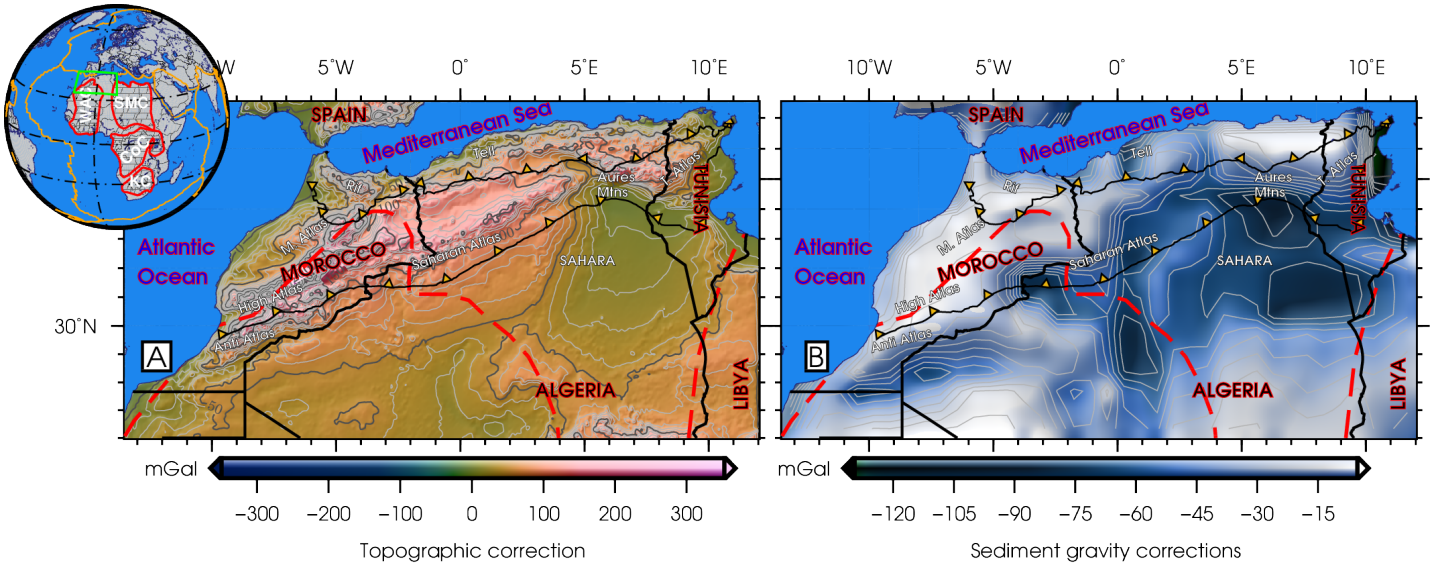

Figure 19: Regional maps of: (a) the topographic-bathymetric and (b) sediment gravity corrections computed on a $5' \times 5'$ grid of surface points

This combined gravity correction is spatially correlated with the topography. Within the study area, it varies roughly between ±300 mGal. Large positive values apply for

the High, Middle, Saharan and Tunisian Atlas mountain ranges with localized maxima exceeding even 300 mGal over the Middle Atlas. Lowlands and shoreline regions of the Aures Mountains and the Moroccan coast are characterized by small negative values (to about −20 mGal). The sediment gravity correction is shown in Fig. 19b. Values of this gravity correction are everywhere negative with absolute maxima along the Pan-African Trans-Saharan Belt south of the Aures Mountains. We applied the topographic-bathymetric gravity correction to the free-air gravity anomalies.

The Bouguer gravity map is shown in Fig. 20. Subsequently, we applied the sediment gravity correction to the Bouguer gravity anomalies. The sediment-corrected Bouguer gravity anomalies are shown in Fig. 20b. From comparing Figs. 18 and 20a, we see that the application of the combined topographic-bathymetric gravity correction significantly modified the free-air gravity pattern. Some substantial changes are also recognized in the Bouguer gravity map after applying the sediment gravity correction, particularly along the east coast of Tunisia and over the Sahara Plateau. The application of the sediment gravity correction increased the long-wavelength negative Bouguer gravity anomalies in Morocco along the Central and Middle Atlas, where values of this correction varies approximately between −50 and −100 mGal. Other significant modification of the Bouguer gravity pattern by this correction is to the south of the Aures Mountains.

As seen in Fig. 20b, the sediment-corrected Bouguer gravity anomalies range from −120 to 250 mGal. Over the central High Atlas, these values are mostly negative between −40 and −120 mGal, with the largest negative values close to the southern border of central and west parts of the central High Atlas. Despite large negative values are mostly distributed over the elevated topography, these values do not coincide with the highest summits that are located further north. Similarly, in the high plains between the Middle and High Atlas mountain ranges, the highest topographic elevations do not coincide with minima of the sediment-corrected Bouguer gravity anomalies. Consequently, the expected spatial correlation between the Bouguer gravity anomalies and the topography is not clearly manifested in the High Atlas. Instead, we see

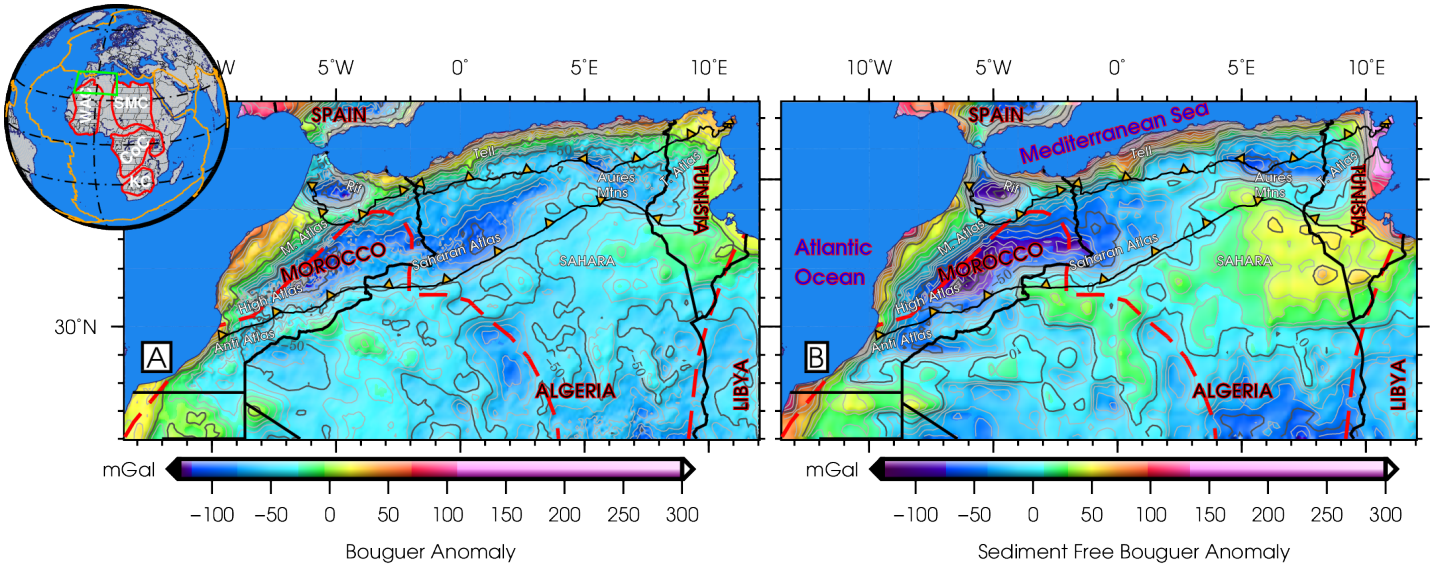

Figure 20: Regional maps of the Bouguer gravity anomalies: (a) before and (b) after applying the sediment gravity correction computed on a $5' \times 5'$ grid of surface points.

misfits, suggesting a lack of local isostatic equilibrium at a crustal level. Moreover, the Bouguer gravity anomalies in the Atlas Mountains are not clearly pronounced with respect to bordering lowlands to the north and the south that are otherwise exhibited in the free-air gravity map, characterized by a significant contrast between gravity anomaly highs over the elevated topography and gravity anomaly lows over lowlands.

The long-wavelength pattern of negative values of the sediment-corrected Bouguer gravity anomalies is along the Tunisian Atlas. In contrast, the long-wavelength pattern of positive values prevails over the Tell Atlas, the Sahel as well as the southeast coastal zones. Other region with large negative values (-100 mGal) is detected in the Algerian anticlinorium, characterized by significant structural high gradients (north-south axis) that are associated with a significant structural alignment. In agreement with findings by Jallouli and Mickus (2000), we see that the sediment-corrected Bouguer gravity anomalies are largely spatially correlated with major geological units in Tunisia. Positive values over the Sahel are limited to the west by the high gradient defining the north-south axis. This axis is observed throughout the Sahel. Arfaoui et al. (2015) argued that it is not simply a response of the Bouguer gravity anomalies to a change in density of the Mio-Plio-Quaternary outcrops dominating this region.

Instead, this gravity pattern is more likely due to a rising of the basement towards the east and to a crustal thinning. Negative anomalies over the Tunisian Atlas Mountains coupled by positive anomalies along coastal regions and lowlands indicate that the long-wavelength Bouguer anomalies correlate inversely with major topographic features.

This finding suggests that the Tunisian Atlas is isostatically compensated. In other worlds, the gravitational contribution of the elevated topography is compensated at depth by a mass deficit, reflecting a thick crust with a density that is relatively lower compared to an underlying uppermost mantle density. The effects of mass deficits at the base of the crust generally mask the gravity signal associated with shallower crustal sources. The Atlas Mountains (−130 mGal) and the Rif Cordillera (−100 mGal) in north Morocco are characterized by similar Bouguer gravity minima, while much less elevated topography. The cause of this steady anomaly has been suggested by Fullea et al. (2008) to be mainly due to the thickening (up to 6 km) of the Phanerozoic sediments present in this region. The overall anomaly observed along the West African Craton is negative mainly on its northern edge.

3.1.3 Seismic data

We used the Moho depth estimates regionally concentrated along the Rif-Tell-Atlas orogenic system from available deep seismic sounding (Makris et al., 1985; Contrucci et al., 2004; Ayarza et al., 2014) and receiver function (Mancilla et al., 2012; Spieker et al., 2014; Leo et al., 2015) studies. Our total database includes 111 seismic points from these referred works. The seismic data distribution and the seismic Moho depth estimates are visualized in Fig. 21. We see a relatively dense seismic data distribution in Morocco and Tunisia, in contrast to their absence in most parts of Algeria. In these cases, the observations were assessed qualitatively based on the reliability or accuracy of the crustal thickness observations. For a brief review of passive source seismic studies in Africa, and especially in the study area, we refer readers to study by Fishwick and Bastow (2011). The seismic Moho depths are within the interval

from 20 to 52 km, with a mean of 32 km.

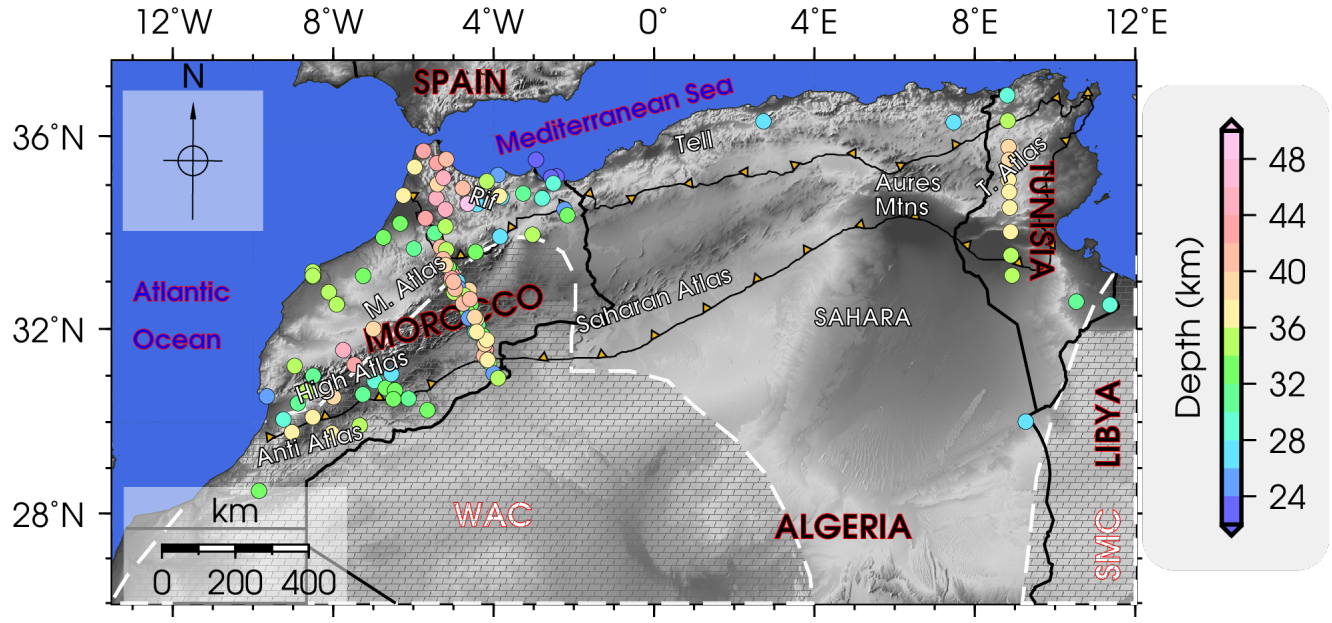

Figure 21: Seismic Moho depth estimates from receiver functions analysis seismograph stations (circles), superimposed on a regional shaded topography.

3.1.4 Comparison with seismic Moho depth estimates

Results of the gravity inversion are controlled by two parameters, namely by the Moho reference depth and the Moho density contrast. We used previous seismic studies to validate gravimetric results by examining all possible combinations for the Moho reference depth values at the range from 20 to 40 km with a 0.5 km step, and for the Moho density contrast values between 200 and 500 kg.m^{-3} with a 50 kg.m^{-3} step. The best fit by means of minimizing the mean-square-error (MSE) of the Moho depth differences between the gravimetric and seismic solutions was attained for the values of 32.5 km and 500 kg.m^{-3} of the mean Moho depth and the Moho density contrast respectively (Fig. 22).

The result of a regional Moho recovery is shown in Fig. 23. We also plotted (in Fig. 23b) the histogram of Moho depth differences between seismic and gravimetric estimates. At a regional scale, we see a good MSE fit between gravimetric and seismic results. Nevertheless, some large localized discrepancies also exist. In the Rif Cordillera in north Morocco, the comparison with seismic data is somewhat am-

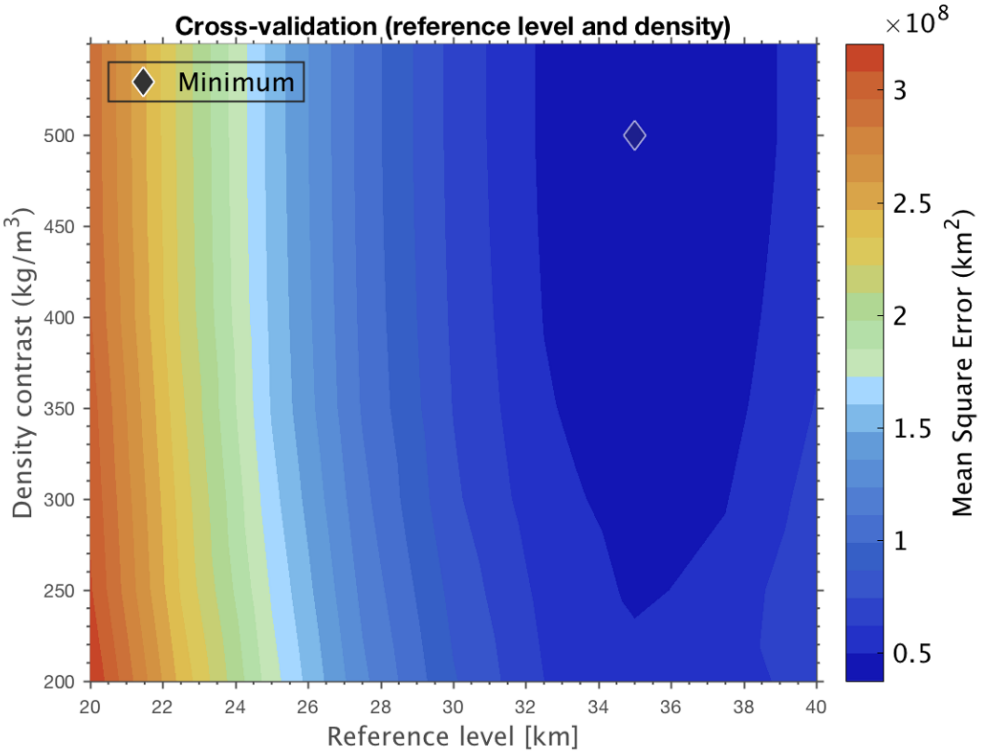

Figure 22: Validation steps exploited to determine the Moho reference depth and the Moho density contrast. The colour scale represents the Mean Square Error. The best-fit model is marked by a grey rectangular (for the Moho density contrast of 500 kg.m^{-3} and the Moho reference depth of 35 km).

biguous with a strong heterogeneous crust, with the presence of large crustal roots beneath this mountain range and a thinned Moho to the east, close to the Algerian border. In the west part of the Atlas Mountains, we observe a crustal root beneath the High Atlas reaching 44 km. As seen in Fig. 23b, the Moho depth differences are roughly between −19 and 15 km with a bias of only 0.14 km and a STD of 3.5 km. These values indicate that the gravity-derived Moho is in a relatively good agreement with the Moho depth derived from receiver function analysis. Fig. 24 displays remarkable crustal thickness variations deduced in the study area by presenting the crustal thickness of the final 3D model and below different given depths.

The Moho depth in the Rif-Tell-Atlas orogenic system varies between 16 and 53 km. The deepest Moho is observed beneath the Rif Cordillera, with values exceeding 40 km under the Aures Mountains and reaching maxima 53 km at some locations (Fig. 24a).

The crustal roots beneath of the west basin of the Tunisian Atlas, the High and

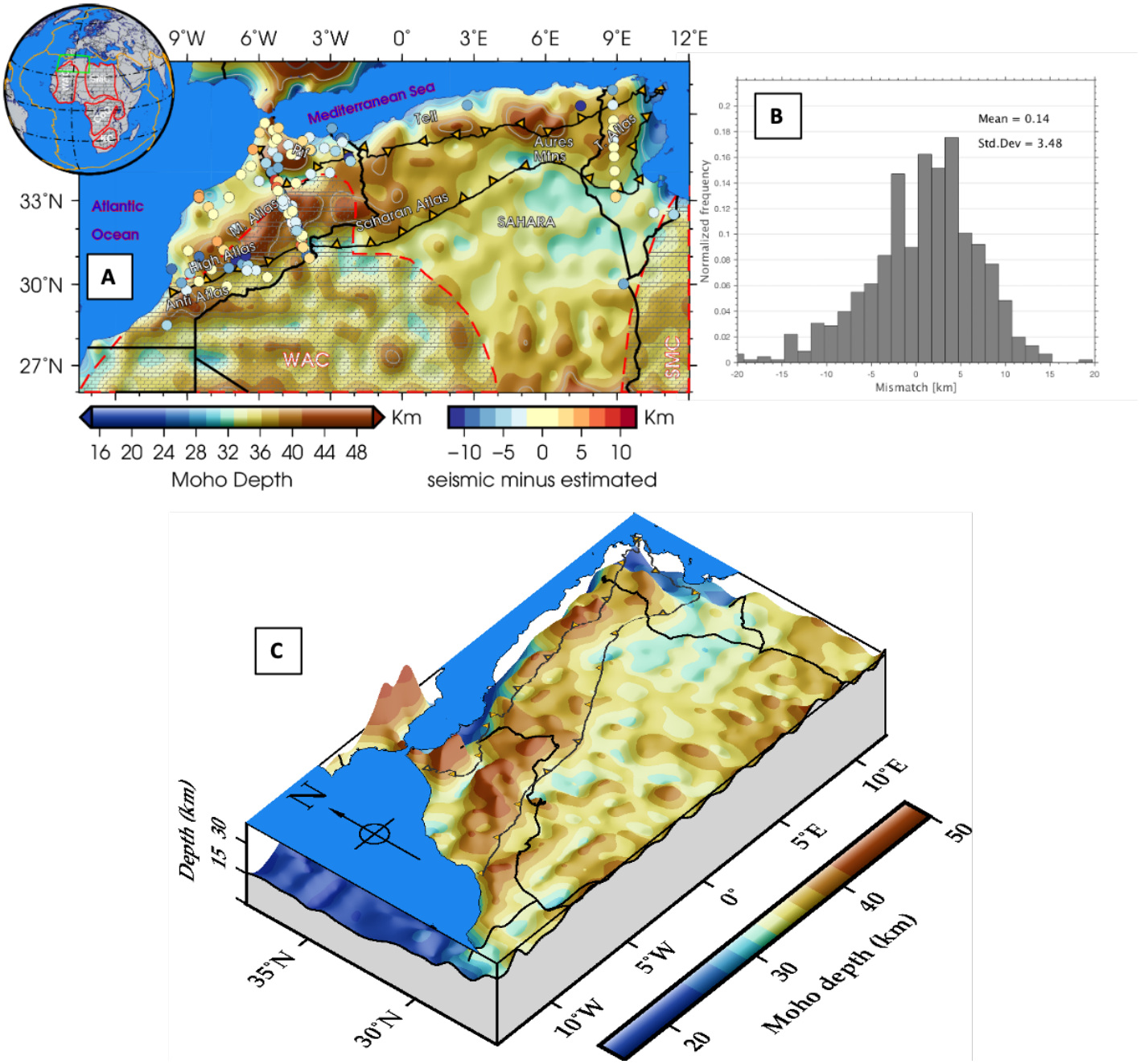

Figure 23: Regional map of the Moho depth estimated based on a regularized non-linear inversion of the sediment-corrected Bouguer gravity data. The Moho depth differences between seismic and gravimetric solutions is shown at seismic sites. Figure also includes the histogram of these differences.

Middle Atlas are clearly exhibited, with the Moho depth there varying from 30 to about 40 km (Fig. 24b). As seen in Figs. 24b-c, the Moho depth shallows gradually eastwards to 25 km. A similar trend is also detected in north Tunisia (26 km) and the north part of the Pan-African Trans-Saharan Belt, particularly in the Sahel (28 km). The Moho topography beneath the Tunisian Atlas is marked by a flexure between the depression and uplift zones, exhibiting some major faults in east and south. The West African Craton, including the Atlas Mountains and in particular the Anti, High and Middle Atlas in its northern edge, have some topographic elevations exceeding 4100 m while its Moho depths varying mostly within $32 - 44$ km. An opposite situation characterizes the Rif Cordillera, with low topographic elevations below 2000 m and the deep Moho exceeding even 50 km. A thinner crust ranging from $29 - 37$ km is, on the other hand, depicted along the eastern margin of the West African Craton.

3.1.5 Comparison of regional Moho models

We compared our Moho model with three gravity-derived models, namely, the GEMMA (Reguzzoni and Sampietro, 2015), Tugume13 model (Tugume et al., 2013) and the Tedla11 model (Tedla et al., 2011); see Fig. 25 and Table 3. The Moho depth differences are plotted in Fig. 26 and Table3, with their statistical summaries given in Table 4. We see that the TUGUME13 and GEMMA models are clustered and closer to our model than Tedla11.

Table 3: Atlas Statistics of the referenced crustal models.

Models	Coverage	Methods	Min (km)	Max (km)	Mean (km)	STD (km)
GEMMA	Global	Combined gravity and seismic model	4.8	105.19	22.36	12.12
Tugume2013	Continenetal	Gravity, Parker-Oldenburg iterative inversion	3.97	44.48	23.62	11.43
Tedla 2011	Continental	Gravity, 3-D Euler deconvolution	32.99	47.7	39.45	2.36

3.1.6 Discussion of results

The results of gravimetric forward modelling (presented in Section 3.1.1) and the result of gravimetric Moho recovery (shown in Section 3.1.4) are discussed in the context of geological and tectonic setting of the study area.

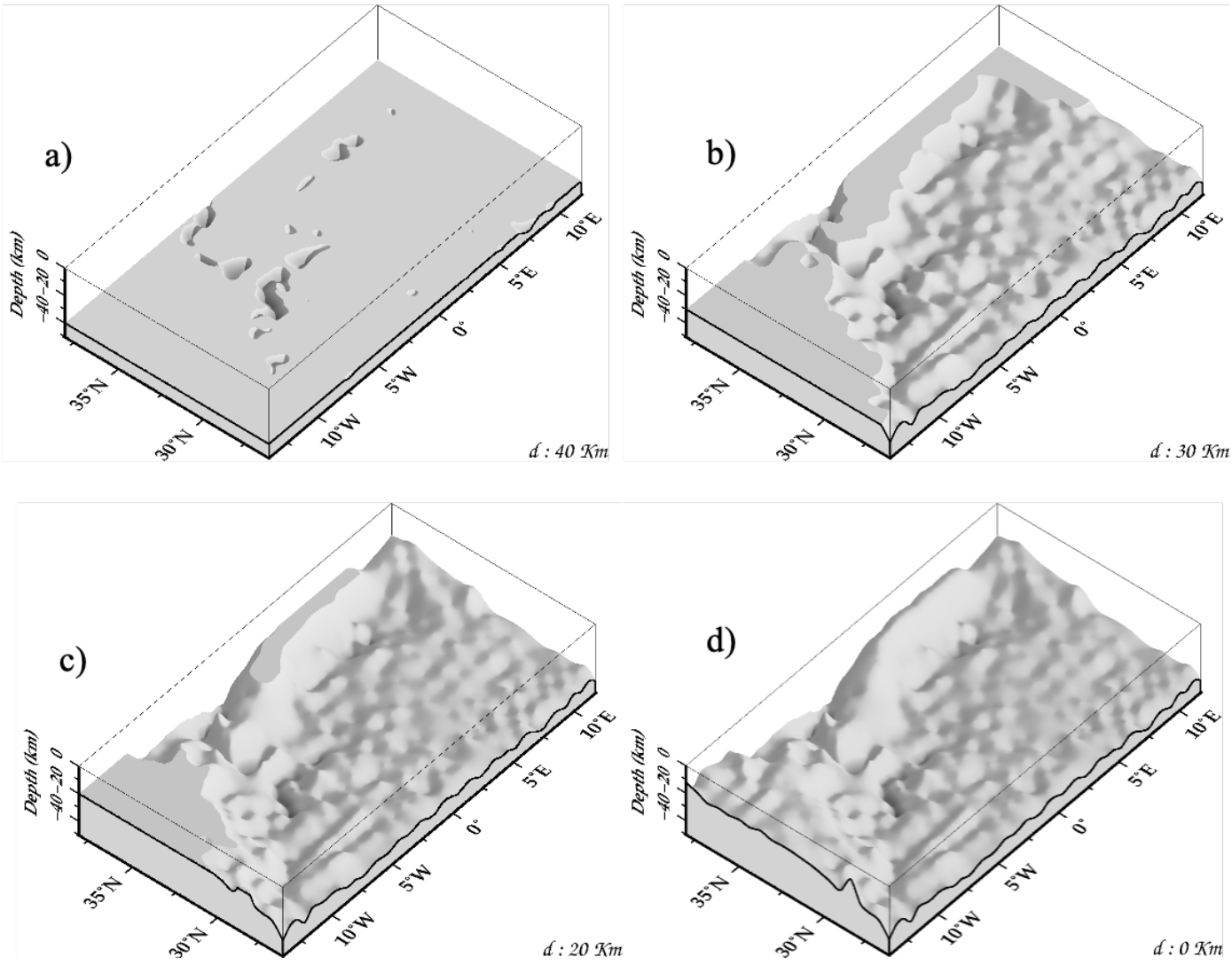

Figure 24: 3D ensemble views of the crustal topography. Panels show the Moho geometry below depth of: (a) 40 (b) 30 (c) 20, and (d) 0 km.

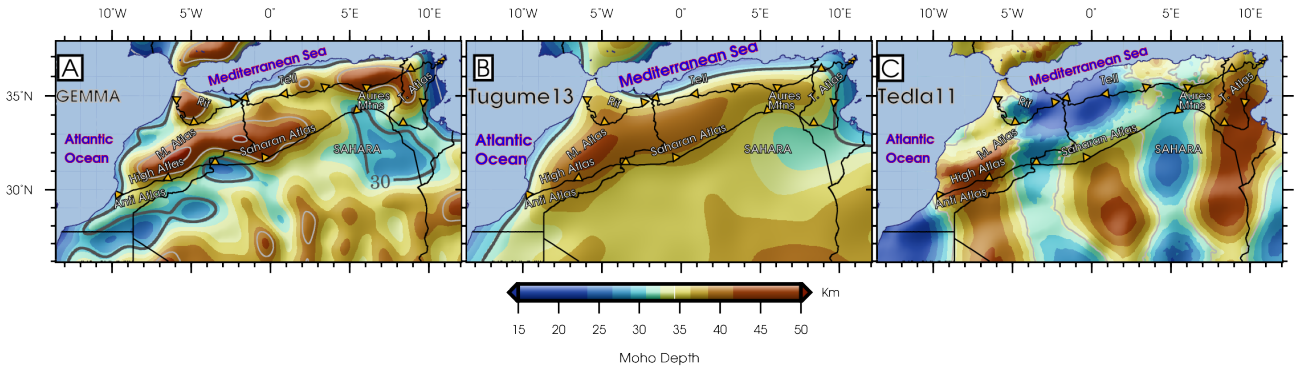

Figure 25: The juxtaposition of existing crustal models for the Atlas region. The gravity-based models are GEMMA, Tugume13 and Tedla11.

3.1.6.1 Gravity maps

The sediment-corrected Bouguer gravity map presented in Fig. 20b exhibits clearly the gravitational signature of different geological units within north Morocco, Algeria and Tunisia. Values of the sediment-corrected Bouguer gravity anomalies range from -140 mGal in the High Atlas Mountains of Morocco to 200 mGal along the northeast coast of Algeria. The Bouguer gravity map (corrected for the sediment effect) is likely more realistic than the Bouguer gravity map presented by Mickus and Jallouli (1999); Jallouli et al. (2013); Arfaoui et al. (2015). Most of spatial features in our Bouguer gravity map reflects largely crustal thickness variations and a low density of sedimentary basins. Additional gravity variations are attributed to a density structure within the deep lithosphere. More specifically, sources of gravity anomalies within the Atlas Mountains involve crustal thickness variations as well as sedimentary rocks overlying the Precambrian and younger basement rocks and crustal thickness changes. Minima of the sediment-corrected Bouguer gravity anomalies are over the High Atlas at the intersection of the Tell Atlas with the Tunisian Atlas Mountains and the Rif Cordillera.

These gravity anomaly lows are possibly attributed to the isostatic signature of a significant Moho deepening under these mountain ranges. The Saharan Atlas Mountains in Algeria are associated with broad-scale, southwest-trending minima in the sediment-corrected Bouguer gravity map. These minima extend beyond surface boundaries of the Saharan Atlas Mountains northwards over the High Plateau region and southwards over the South Atlas Front and the Sahara Platform. This large-scale gravity anomaly low may be explained by a crustal thickening caused by the loading of the Saharan Atlas onto the continental crust that is similar with the source of gravity anomaly over the High Atlas. Our estimate of the crustal thickness confirmed the existence of a thick crust ($36 - 40$ km) across the Saharan Atlas.

A general idea about the isostatic compensation of the entire Tell and Atlas Mountains can be seen by comparing the sediment-corrected Bouguer gravity map (Fig. 20b), the free-air gravity map (Fig. 18) and the topographic relief (Fig. 2b). (Arfaoui

et al., 2015) noticed that the Tunisian Atlas is associated with the positive free-air gravity anomalies that, in general, mirror the topography.

Our result agrees with their finding. Nonetheless, the Saharan Atlas comprises also regions with the negative free-air gravity anomalies and with the corresponding negative values of the sediment-corrected Bouguer gravity anomalies that indicate a possible overcompensation. The rest of the Saharan Atlas appears to be compensated, except near the boundary with the Tunisian Atlas. This may imply again an overcompensation, but such conclusion could be an oversimplification, as a thick low-density material may be the cause of these anomalies, as is the case for the Rif Cordillera.

3.1.6.2 Comparisons of Moho depth estimates

New continental-scale Moho estimates beneath Africa, based on gravity modelling, were presented by Tedla et al. (2011) and Tugume et al. (2013). Both studies provide gravity-derived crustal thickness maps, calibrated against seismic Moho estimates. These results exhibit only minor variations in crustal thickness between terranes of the Archean and Proterozoic age Tedla et al. (2011). The crustal model of Tugume et al. (2013) shows overall a thinner crust than the model presented by Tedla et al. (2011), with differences exceeding 6 km in the part covered by our study area. A feature common to all three models mentioned above is a relatively thick crust (35 to 45 km) beneath the High and Middle Atlas. GEMMA is more prominent and reliable than models presented by Tedla et al. (2011) and Tugume et al. (2013). The calculated differences using a heterogeneous density structure in the crustal thickness with respect to the constant density model are shown in Fig. 25.

The comparison of the Moho depth differences of these three models with our solution (see Fig. 26) shows that significant Moho differences are observed for all three models, although differences between our model and GEMMA and Tugume et al. (2013) models are acceptable for most parts of the study area with ± 4 km for the Moho. In the study area, the maximum Moho depths ($42 - 48$ km) correspond to the West African Craton and to the Rif Cordillera. The maximum Moho deepening

in northwest Africa is detected in the Atlas Mountains (∽ 37 km) with local maxima under the High Atlas (45 km). Compared to the Moho depth estimates from active seismic experiments in Morocco (Wigger et al., 1992; Ayarza et al., 2014; Gil et al., 2014), our model is in a good agreement with the crustal structure across the Atlas Mountains. In the northwest Moroccan platform, the Moho depth estimate of ∽ 32.5 km is slightly lower than the Moho depth of ∽ 35 km reported by Contrucci et al. (2004).

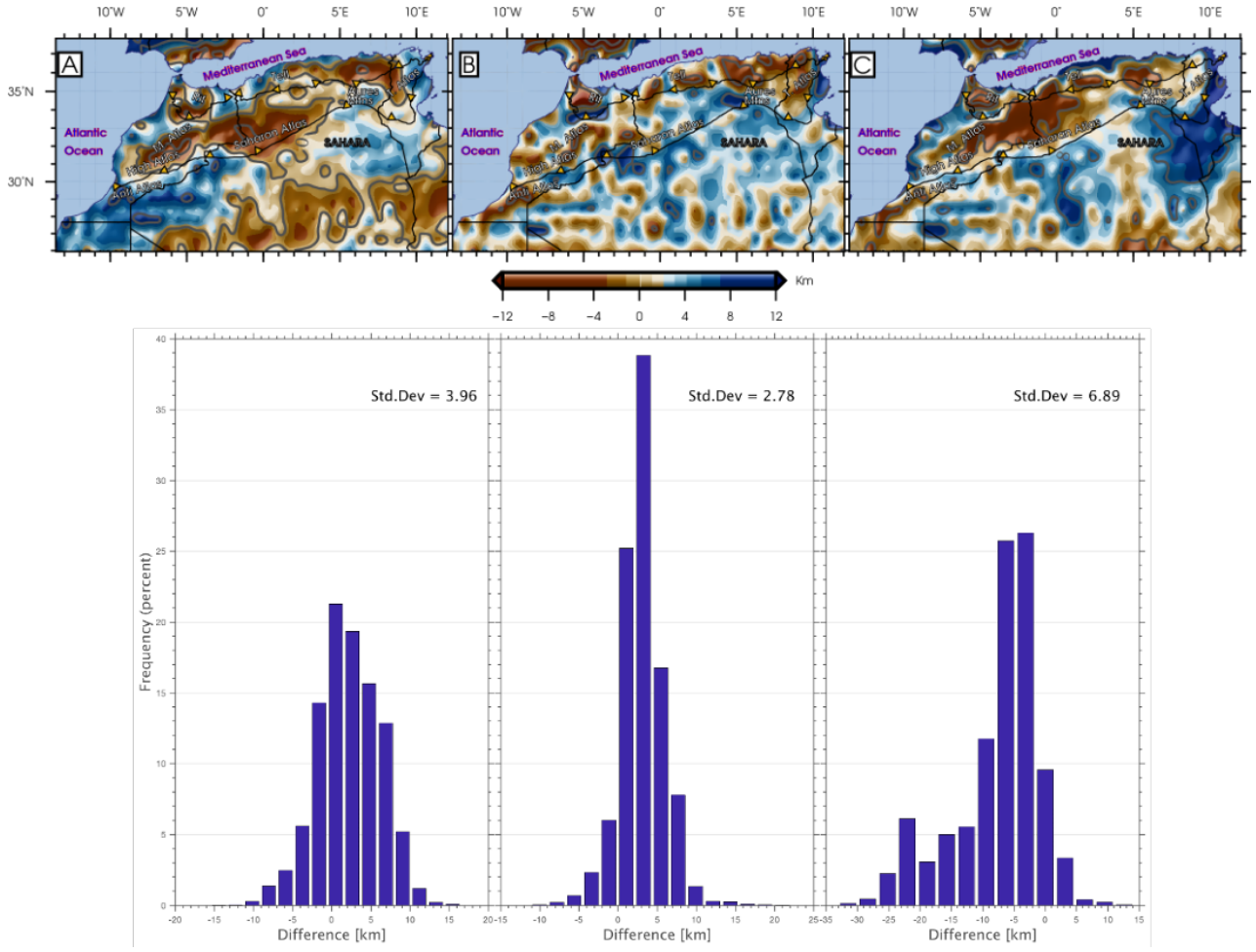

Figure 26: Comparison between regional crustal thickness models and our model. The Moho depth differences with respect to: (a) GEMMA model by Reguzzoni and Sampietro (2015), (b) Tugume13 model by Tugume et al. (2013), and (C) Tedla11 model by Tedla et al. (2011).

Our estimate, also very closely agrees with the result published by(Globig et al., 2016). Tadili et al. (1986) found that the crustal thickness varies from 25 km along the Atlantic coast to 40 km in the central High Atlas, which argues for a possibly thinner crust less than 35 km along the Moroccan margin. According to our estimate,

Table 4: Atlas statistics of differences between values of the new density model and the referenced crustal models.

Differences	Min (km)	Max (km)	Mean (km)	STD (km)
GEMMA	−15.50	16.51	2.16	3.96
Tugume2013	−11.15	22.09	3.06	2.78
Tedla2011	−33.06	14.19	−7.57	6.89

in the west parts of the High and Middle Atlas Mountains, the Moho depth varies within $34-42$ km and closely spatially agrees with GEMMA, Tedla et al. (2011) and Tugume et al. (2013) models. Our model, however, disagrees with these models in the very southwest part of the High Atlas. According to our result, the Moho depth there exceeds 38 km in agreement with the finding of Makris et al. (1985). The comparison of our Moho model with the result for the Moroccan Meseta and the Rif Cordillera presented by Mancilla et al. (2012) shows that both results agree within ± 7 km in these regions. A generally better agreement between both results is found in the east part of the Rif Cordillera. According to our result, the minimum Moho depth there is roughly 35 km, while Mancilla et al. (2012) estimated a thinner crust with the Moho depth of only 27 km.

3.1.6.3 Study profiles

We selected four representative profiles at the study area to compare and interpret the gravity anomaly (free-air and Bouguer) variations with respect to the topography and the Moho depth. The locations of these four profiles are indicated in Fig.2. The gravity anomaly variations along the profiles are plotted in Fig.27, with the statistical summaries given in Table 5.

The AA' profile (Fig. 27a) trends NNW-SSE and crosses the Rif Cordillera and the High Atlas. This region is characterised by the deepest Moho, varying from 31 to 49 km, with the peak at the distance from 175 km and anti-correlation observed between the gravity anomaly trend and the Moho depth (section $80-300$ km). In the Rif

Cordillera region, values of the free-air and Bouguer gravity anomalies are in phase and negative with an isostatic imbalance characterised by the deepest Moho. Minima of the short-wavelength gravity spectrums reach almost −100 mGal, suggesting the presence of a very low-density structure at shallow levels. Both, the central High (35−36 km) and Middle (43−42.5 km) Atlas mountain ranges have more shallow sub-crustal depths than the Rif Cordillera (49 km) that spatially correlate with mountain hills along with the areas of the thinnest lithosphere.

The northern edge of the West African Craton has a shallower Moho depth, varying from 42 km in the Middle Atlas to 34 km in the High Atlas, confirming the observation done by Jessell et al. (2016).

The BB' profile (Fig. 27b) crosses Tunisia, from the Tunisian Atlas to Sahara. The Tunisian Atlas is characterised by the positive free-air gravity anomalies (up to 62 mGal) and the negative Bouguer gravity anomalies (to −45 mGal). The free-air gravity anomalies reflect a thick crust (39 km) beneath this region. At the distance of 360 km, the Moho depth decreases to 32 km, corresponding to an extension of the West African Craton into the northern segment of the Pan-African Trans-Saharan Belt, or the West African Mobile Zone present in the Saharan region. The free-air gravity anomalies remain negative. The Bouguer gravity anomalies exhibit a long-wavelength trend.

Table 5: Characteristics of the studied sections drawn on the Moho depth, the free-air and sediment-free Bouguer gravity maps.

Section	Distance (km)	Orientation	Borders
AA'	623	NNW−SSE	Rif−High Atlas
BB'	770	N−S	Tunisian Atlas−Sahara
CC'	865	NW−SE	Tell−Sahara
DD'	2050	WSW−ENE	High Atlas−Tunisian Atlas

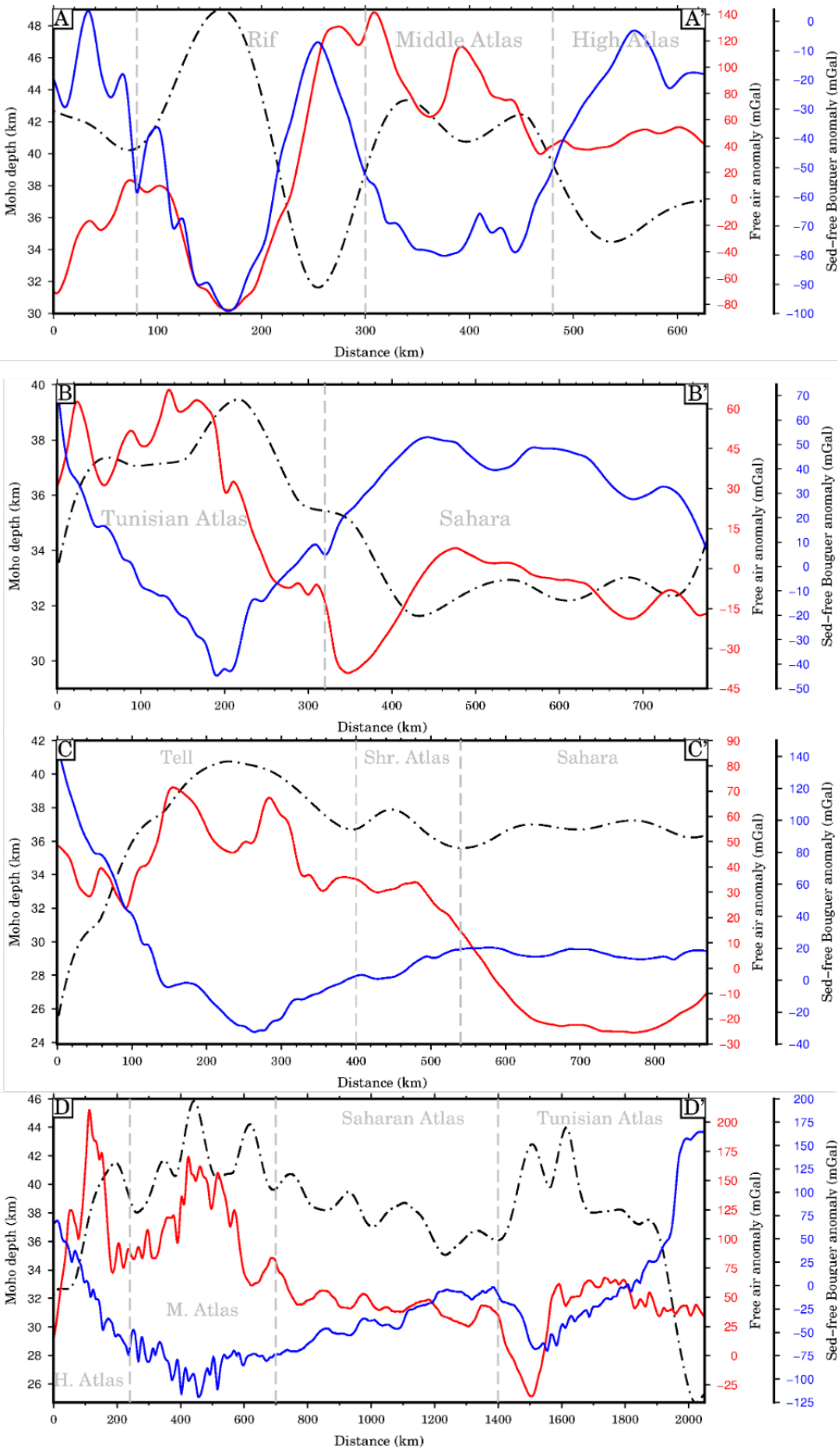

Figure 27: Study profiles for comparing values of the free-air and Bouguer gravity anomalies with the Moho depth and the topography across the Rif-Tell-Atlas orogenic region (see locations in Fig. 2b): AA' profile along the Morocco Atlas system, BB' profile along the Tunisia Atlas system, CC' profile along the Atlas system, and DD' profile through Morocco, Algeria, and Tunisia.

The CC' profile (Fig. 27c) crosses Algeria from the Tell Atlas to Sahara. Within this profile, the free-air gravity anomalies and the Moho depth undulations vary in a similar mode with a thicker crust beneath the Tell Atlas. Along the first part of the section (to 265 km), the Bouguer gravity anomalies decrease to −22 mGal, then slightly increase from the Saharan Atlas to Sahara. The isostatic compensation between the Tell and Sahara Atlas is apparent based on comparing gravity anomalies with the Moho depth. The Saharan Atlas is isostatically compensated, with the exception close to the Tunisian Atlas. Across Saharan section of this profile, the free-air gravity anomalies are mostly negative with a large amplitude, while the Bouguer gravity anomalies are negative. The crustal thickening in the Tell Atlas (40 km) weakens towards Sahara (38 km) through the Saharan Atlas (36 km), highlighting the sediments contribution (Palaeozoic, Mesozoic and Cenozoic) mainly occurring in the Pan-African Trans-Saharan Belt.

Along the DD' profile (Fig. 27d), the Moho depth merely correlates with the free-air gravity anomalies between the High Atlas and the Saharan Atlas. However, the Bouguer gravity anomalies are characterised by a short wavelength with the minimum of −125 mGal in the Middle Atlas. In contrast, a non-isostatic compensation likely occurs in the Tunisian Atlas, due to the short-wavelength minima (−25 mGal) observed in the free-air anomaly signal. A lack of correlation between the free-air and Bouguer gravity anomalies and the crustal thickness along the High, Middle, Saharan Atlas and the coastal border of the Tunisian Atlas reflects mainly a combined effect of the Cenozoic, Mesozoic and Palaeozoic to recent tectonic sediments. Along the north edge of the West African Craton, located between the High and Middle Atlas, maxima of the free-air anomalies ($150 - 205$ mGal) and of the Moho depth ($40 - 46$ km) indicate the presence of a very low-density material at shallow levels along the northern margin of the West African Craton.

3.1.7 Summary and concluding remarks

We have complied a new regional model of the Moho depth of the Atlas region (i.e. the Rif-Tell-Atlas orogenic region) and adjoining part of the West African Craton using gravity, topographic, bathymetric and sediment models constrained by seismic data by applying a regularized inversion based on the Gauss-Newton's formulation of the improved Bott's method with the regularization and tesseroid techniques involved. The Moho topography inferred by this method exhibits an all-inclusive remarkable consistency. Variations in the crustal thickness are heterogeneous in the east-west directions and closely related to the long-term Mesozoic to recent tectonic events of the Atlas orogenic formation. In the Western Atlas (comprising the Anti, High and Middle Atlas mountain ranges), the crustal thickness is roughly $35 - 44$ km, while the Central Atlas Massif exhibits a rather non-uniform Moho depth of 36 km in the Saharan Atlas and 32 km in the Aures Mountains system. A sharp crustal thickness transitions are observed between the Rif Cordillera to the Middle Atlas and around the Tell Atlas, where the Moho deepens to 55 km. In the Tunisian Atlas region, the Moho depth varies between 28 and 42 km, with a westward gradual deepening and maxima (42 km) under the Aures Mountains. Some inconsistencies identified between the Rif and Atlas Ranges cannot simply be explained under the assumption of isostatic compensation, while looking at the thickened crust of the Atlas Ranges with the Moho depth variations roughly within $36 - 42$ km.

The profile analysis revealed that the Atlas region is partially to fully compensated, with regions of possible overcompensation in the Saharan Atlas. The signature of the West African Craton in the Atlas is marked by a deep crustal geometry varying from 38 km in the Anti Atlas and from 40 to 44 km in the High and Middle Atlas. This crustal geometry of the West African Craton in the northern margin of the Atlas is supported by a high topography. The Pan-African Trans-Saharan Belt limited to the west by the West African Craton, to the east by the Sahara Meta-Craton and to the north by the Aures Mountains is mainly constituted by the Palaeozoic, Mesozoic and Cenozoic sediments. The presence of these sediments is cause of a shallow crust in

Sahara, the south Tunisia and in the south flank of the Aures Mountains. In the Tell Atlas, an average Moho depth between 30 and 35 km is detected in Tunisia. Thus, the NW-SE trending observed along the Atlas hills is associated with the thickest crust in north Africa. The Moho models from previous studies compiled using various methodologies in the Atlas region were used to check the reliability of our high-resolution crustal thickness estimate. The comparison of results revealed that our Moho model better agrees with seismic depth estimates than existing gravimetric Moho models (GEMMA, TUGUME13 and TEDLA11). This is particularly evident for the Rif Cordillera and the Atlas Mountains, where these models underestimate or even provide unrealistic Moho depth estimates.

3.2 Cameroon's crustal configuration from global gravity and topographic models and seismic data

3.2.1 Free-air gravity data

We used the EIGEN-6C4 global gravitational model (Förste et al., 2014) to generate the free-air gravity disturbances with a spectral resolution complete to the spherical harmonic degree of 2160. The free-air gravity disturbances computed on a $5' \times 5'$ geographic grid of points at the topographic surface are shown in Fig.28. Within the study area, these gravity data vary between -60 and 240 mGal, being typically positive inland over most of moderately elevated and mountainous regions, while negative offshore and over continental basins and lowlands.

Not surprisingly, more detailed pattern in the free-air gravity map is closely spatially correlated with the topography. Moreover, some larger regional features in this gravity map likely reflect the lithospheric density heterogeneities. In particular, negative values of the free-air gravity disturbances often refer to the over compensated topography, which might possibly indicate a considerable Moho deepening due to compressional tectonism. Positive values, on the other hand, typically originate from the under compensated topography with a decrease in crustal thickness.

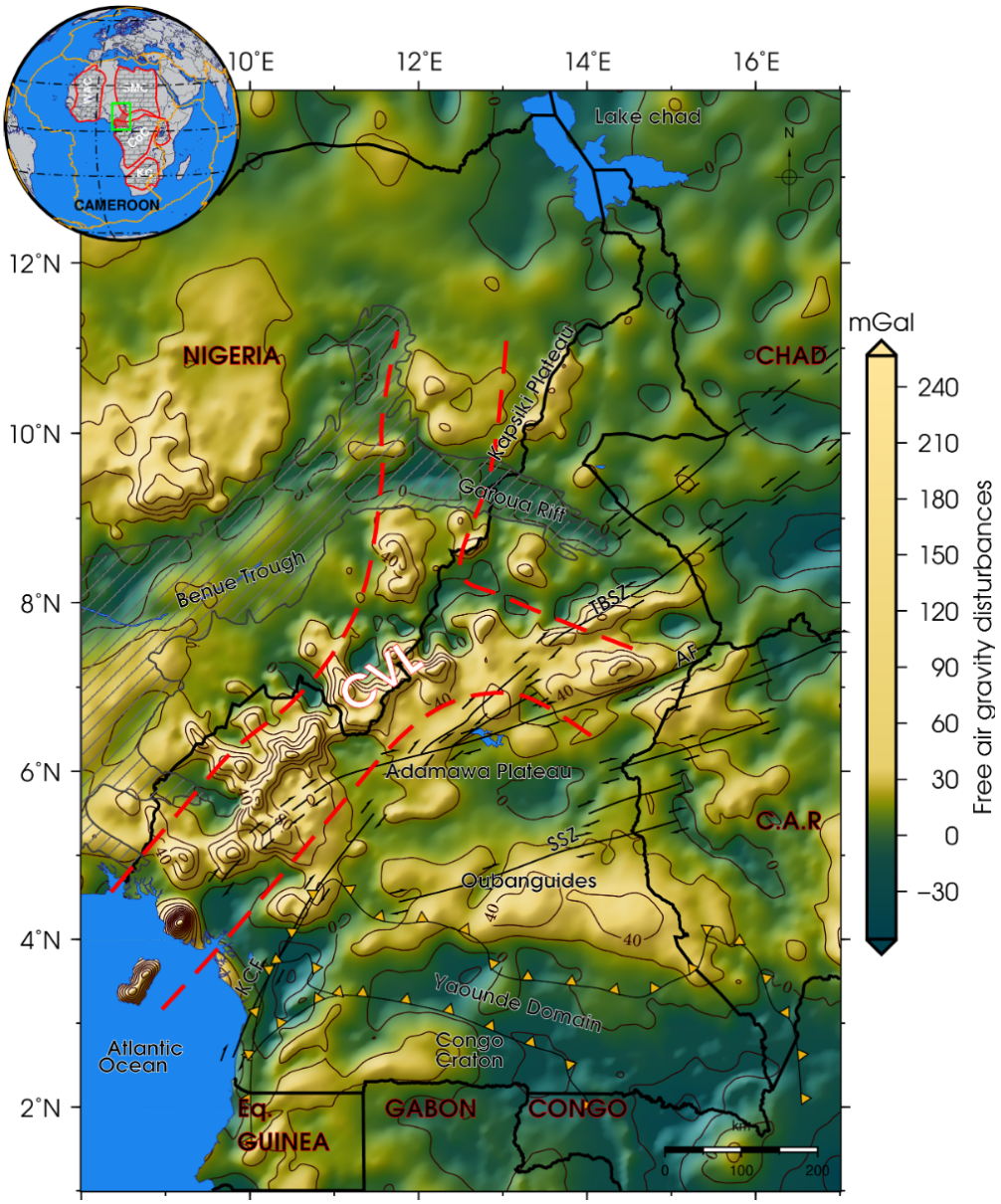

Figure 28: Regional map of the free-air gravity disturbances computed from the EIGEN-6C4 on a $5' \times 5'$ geographical grid.

The regional maxima of the free-air gravity disturbances are detected along the highest mountain ranges of the Cameroon Volcanic Line that extends from the Atlantic Ocean to the Adamawa Plateau. In the high mountain regions, the free-air gravity disturbances reaches roughly 150 mGal. Small values of the free-air gravity disturbances are over the Congo Craton in the southern Cameroon mostly along the Yaoundé domain.

3.2.2 Bouguer gravity data

The ETOPO1 topographic and bathymetric datasets (Amante and Eakins, 2009) were used to perform topographic and bathymetric gravity corrections. These two gravity corrections were made using the tesseroid method. The reader is referred to the study conducted by (Uieda et al., 2016) for a detailed description of this method. The topographic gravity correction was calculated for a homogeneous density distribution. More specifically, we used the density value of 2670 kg.m^{-3} which is generally adopted to represent the density of the upper continental crust (Hinze, 2003). The bathymetric gravity correction was calculated using the depth-dependent seawater density model developed by Gladkikh and Tenzer (2011).

The combined topographic and bathymetric gravity correction is shown in Figure 29a. For regions with a well known geological stratigraphy, further gravity corrections could be applied to model and subtract the gravity signature of sediments and other lithospheric density disturbances (Tenzer et al., 2009; Tenzer and Gladkikh, 2014; Tenzer et al., 2014). In our study we used the sediment and consolidated crust information from CRUST1.0 (Laske et al., 2013) to calculate the gravity correction of the total sediment and consolidated crust. This combined gravity correction is shown in Figure 29b.

We applied these gravity corrections to the free-air gravity disturbances. The resulting Bouguer gravity map is shown in Fig. 30. The Bouguer gravity disturbances vary mostly within the interval from -100 to 240 mGal. Negative values prevail over the Adamawa Plateau, the Yaoundé domain and the Congo Craton, while small posi-

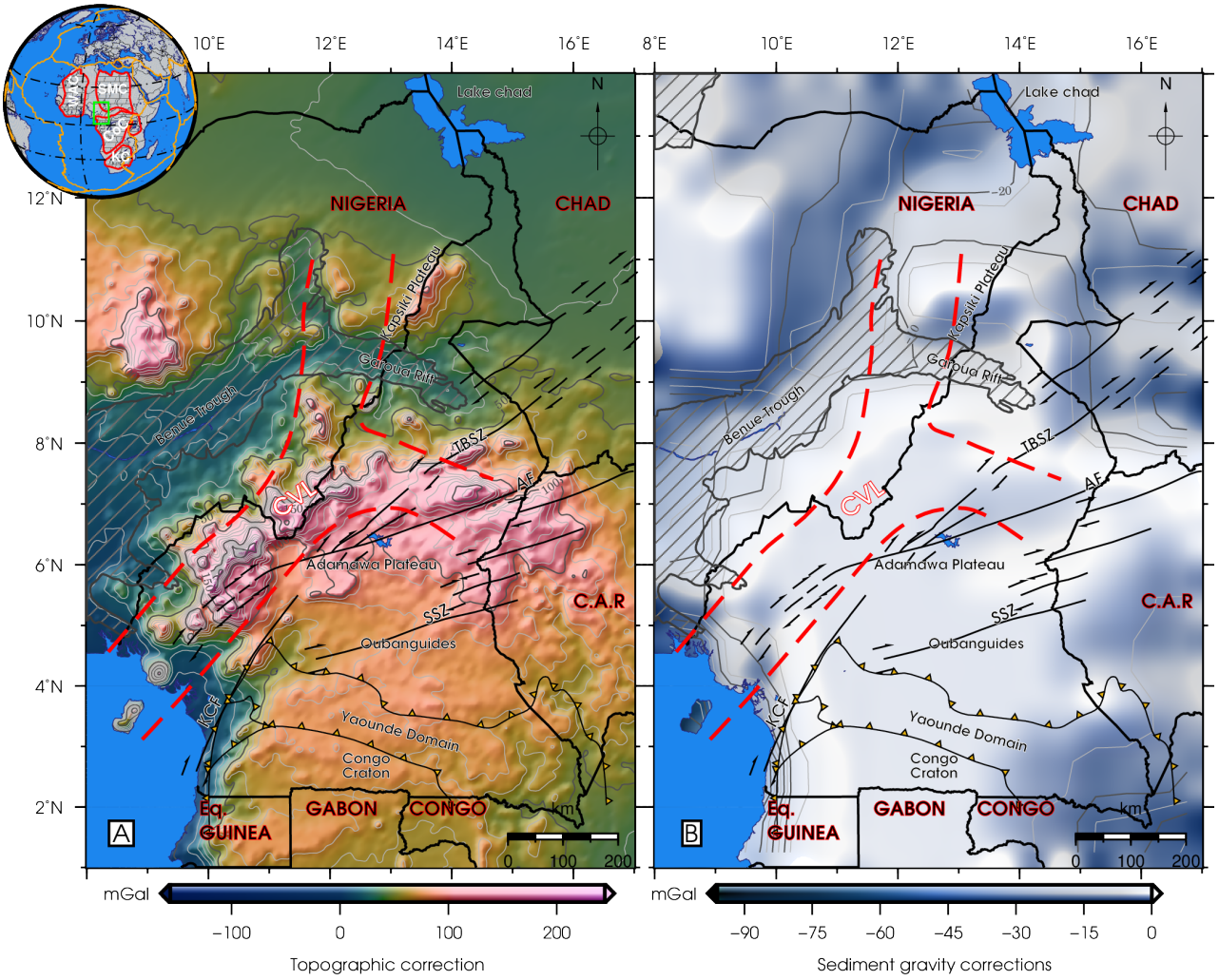

Figure 29: Regional map of: (a) the topographic-bathymetric and (b) sediment gravity corrections computed on a $5' \times 5'$ grid of surface points.

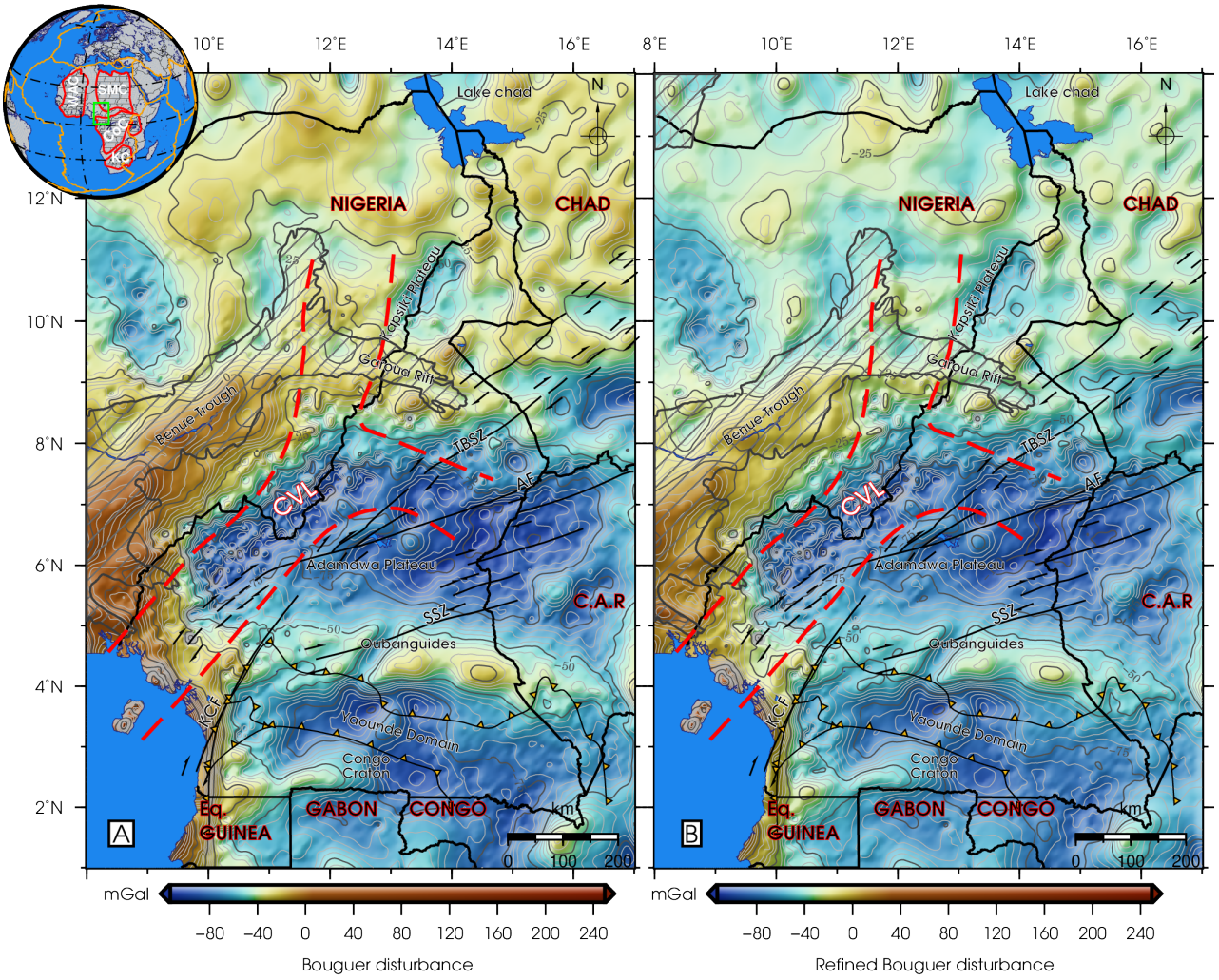

Figure 30: Regional maps of the Bouguer gravity anomalies: (a) before and (b) after applying the sediment gravity correction computed on a $5' \times 5'$ grid of surface points.

tive values are over basins and platforms. The Bouguer gravity disturbances are highly spatially correlated with the crust thickness variations as well as deeper lithospheric structures. The Bouguer gravity lows reflect either some granite batholiths and/or the regional Moho deepening due to the isostatic compensation of major topographic features.

Overall, the Bouguer gravity map exhibits a noticeable E−W trending, with sections of gravity highs along the Oubanguides Belt. These gravity highs likely reflect sources of a dense material beneath this region. Ngalamo et al. (2018) suggested that the presence of a denser material beneath the Oubanguides Belt was possibly due to the densification of an under-thrust portion of the Congo Craton, which might be modified by the ascendance of asthenospheric material and slab detachment during the Neoproterozoic Pan-African orogenic event. These gravity highs are coupled by gravity lows to the north over the Adamawa Plateau as well as to the south over the Yadé domain, extending further in the southernmost area. These areas are characterized by intrusive bodies, fault blocks, graben, and masses extending vertically and horizontally as geological units. To the west of Cameroon, the Benue Trough is delineated by the existence of an NE−SW elongated high positive values of the Bouguer gravity disturbances that likely manifest a combination of mafic bodies and an elevated asthenosphere.

3.2.3 Seismic data

The Moho depth at the 32 CBSE (Cameroon Broadband Seismic Experiment) sites estimated from passive and active seismic sources (Tokam et al., 2010; Gallacher and Bastow, 2012) is presented in Fig. 31 (see Section 2.1.3). As seen, the thinned crust ($\backsim$ 25 km) is imaged beneath the Garoua Rift, while the transition from the Cameroon Volcanic Line to the Congo Craton is heralded by a transition in the Moho depth from roughly 36 km to $43 - 48$ km depth (Tokam et al., 2010; Gallacher and Bastow, 2012).

We used these seismic Moho estimates to inspect the expected trend in the Bouguer

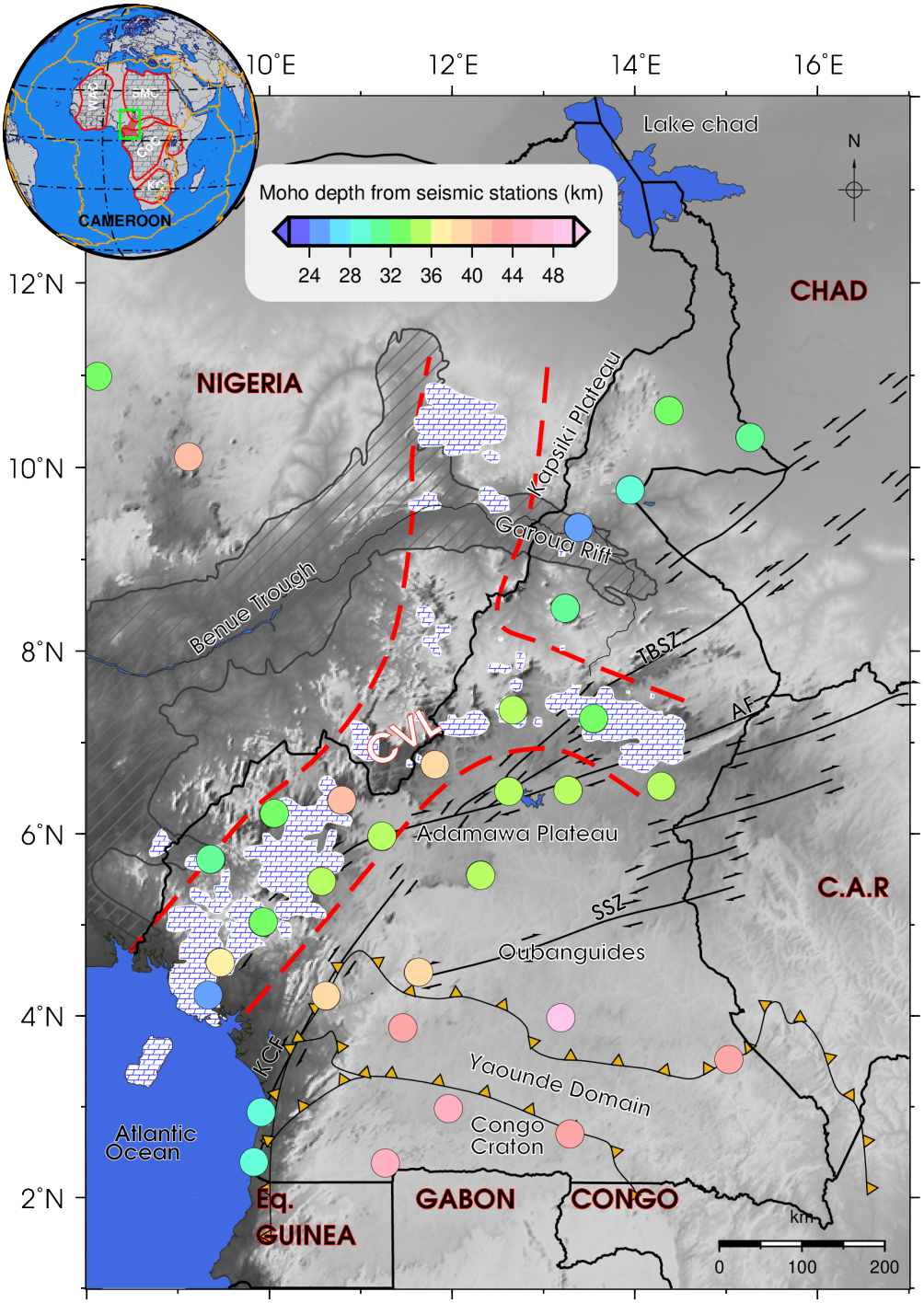

Figure 31: Seismic Moho depth estimates from CBSE seismograph stations (circles) including 2 sites in Nigeria, superimposed on a regional shaded topography.

gravity map (Fig.30b). We observe a typical negative correlation between large negative values of the Bouguer gravity disturbances with the elevated topography in the West Cameroon Domain, the Garoua Rift and along the Adamawa Plateau that is consistent with the Airy's isostatic hypothesis. This finding also agrees with the observation of Marcel et al. (2018). Assuming that volcanic activities arising in this region seems to be associated with the upward pressure exerted by the asthenosphere on the basis of the lithosphere. Volcanic activities could therefore be the consequence of the upward flow of mantle material from depths to restore the isostatic equilibrium.

3.2.4 Results

The Bouguer gravity data described in previously were used as input to estimate the Moho depth according to a numerical procedure. We applied a regularized non-linear gravity inversion to estimate the Moho depth from the Bouguer gravity disturbances. In principle, this method comprises two numerical steps. Firstly, we determined the regularization parameters by using the predefined set of initial values for mean values of the Moho depth and density contrast. In the second step, we carried out the gravimetric inversions for different values of the Moho density contrast as well as the mean Moho depth. The final gravimetric solution was selected based on the principle of minimizing the mean square error (MSE) of Moho depth differences between gravimetric and seismic results. The Moho solution obtained based on solving the regularized non-linear gravity inversion is presented next.

3.2.4.1 Moho depth from gravity inversion

The method applied here for the gravimetric Moho inversion is based on finding the gravimetric Moho solution that closely agrees with seismic Moho depth by means of minimizing the MSE between gravimetric and seismic solutions. The choice of optimal gravimetric solution depends on two input parameters that represent the mean Moho depth and density contrast. For selected values, the optimal gravimetric solution was obtained for the mean Moho depth of 32.5 km and the Moho density contrast of 500 $kg.m^{-3}$ (Fig. 32). We note that both these parameters realistically represent the

Moho geometry beneath Cameroon's crustal structures.

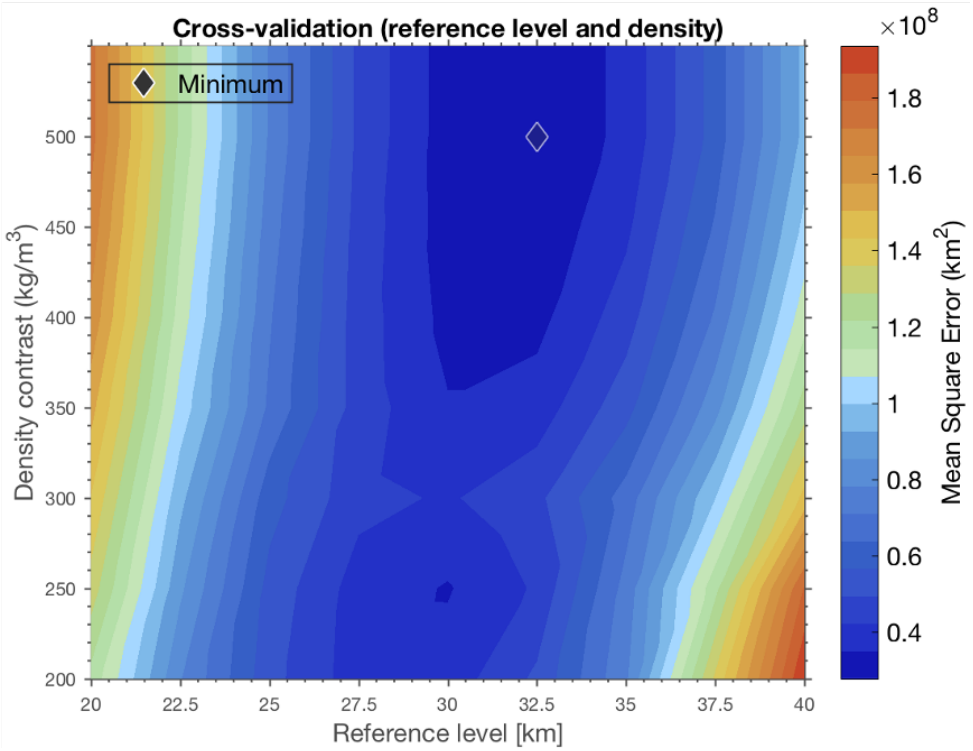

Figure 32: Validation steps exploited to determine the Moho reference level and the density contrast. The colour scale represents the Mean Square Error. The best-fit model is marked by the grey rectangular, which indicates a density contrast of 500 kg.m^{-3} and a Moho reference depth of 32.5 km.

We further used the Moho density contrast interface for the forward modelling of the Bouguer gravity disturbances. As seen from the predicted values of the Bouguer gravity disturbances shown in Fig. 33a, the values relatively closely agree with the Bouguer gravity disturbances (Fig. 30). Nevertheless, some localized differences in the spatial pattern and intensity of the Bouguer gravity disturbances could also be recognized. An average misfit between the predicted and observed Bouguer gravity disturbances has a correlation coefficient of 0.90, which is a plausible value for a regional gravity field modelling. The Bouguer gravity residuals obtained after subtracting the predicted values from observed ones are shown in Fig. 33b. The Bouguer gravity residuals (Fig. 33b) reach large values up to more than 10% of the signal, mainly at higher frequencies; thus possibly reflecting the (small) superficial density anomalies within the crust. This correlation coefficient points out that density reduction in the mantle beneath the crust may be related to an increase in temperature with depth, thus reflecting the geodynamic features of the Cameroon Volcanic Line.

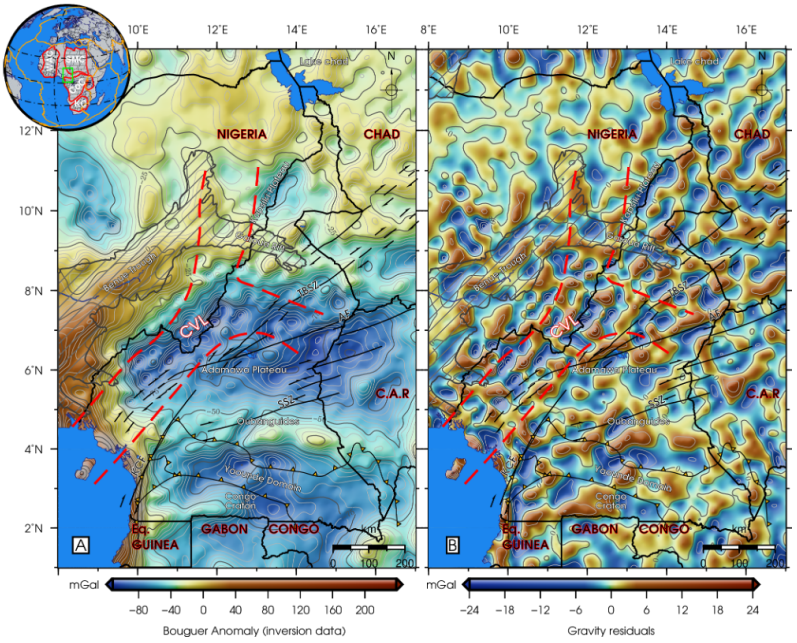

Figure 33: Bouguer gravity residuals (left panel) between the observed data (in Fig. 30a) and the predicted data (right panel) that were computed based on solving the gravimetric inversion method.

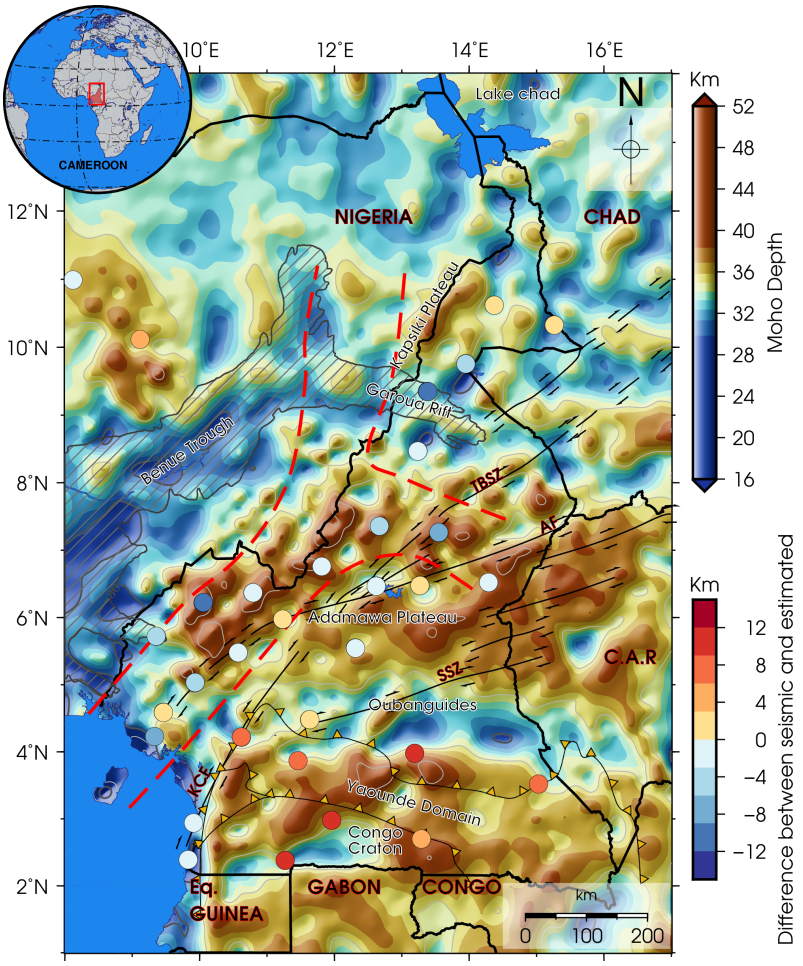

Figure 34: Regional map of the Moho depth estimated based on a regularized non-linear inversion of the Bouguer gravity data. The map also shows the Moho depth differences between the seismic and gravimetric estimates at the CBSE sites (plus 2 sites in Nigeria).

The final result of a regional Moho recovery from the Bouguer gravity disturbances (for the selected best-fitting parameters of the Moho density contrast 500 kg.m^{-3} and a Moho reference depth 32.5 km) is shown in Fig. 32. The positive anomaly near the Atlantic Ocean characterizes the progressive change in from the continental structure to the ocean one as shown on the 3-D representation in Figure 35. To validate this result, we also plotted (in Fig. 34) the Moho depth differences between the seismic and gravimetric estimates. These differences are discussed next.

3.2.4.2 Validation of result

As stated above, the best fit by means of minimizing of MSE of the Moho depth differences was attained for the mean Moho depth of 32.5 km and the Moho density contrast of 500 kg.m^{-3}. The MSE values with respect to the seismic Moho depth at the CBSE sites (and 2 sites in Nigeria) are plotted in Fig. 36. As seen, most of these differences are distributed within $\pm$10 km, with a mean of 0.5 km and STD of 5.3 km.

3.2.5 Discussion of results

3.2.5.1 Gravity maps

The gravity maps (in Figs. 29 and 30) closely mimics a regional configuration of major known tectonic and regional geological features (Fig. 3). The Central African Shear Zone on the Oubanguides Belt (formed by the Neopetrozoic rocks) is characterized by high values of the free-air gravity disturbances and low values of the Bouguer gravity disturbances. This cratonic formation consists of a large number of young volcanic eruptions aligned along the suture (weak) zone. The gravity pattern there supports the presence of a thick crust or an under-plating below this craton. Furthermore, it implies that the Central African Shear Zone must have localized these phenomena and added high-density rocks at the mantle level.

Along the 4°N parallel, we observe a linear trend of the positive Bouguer gravity disturbances that coincides with a zero-topography line. This suggests the presence

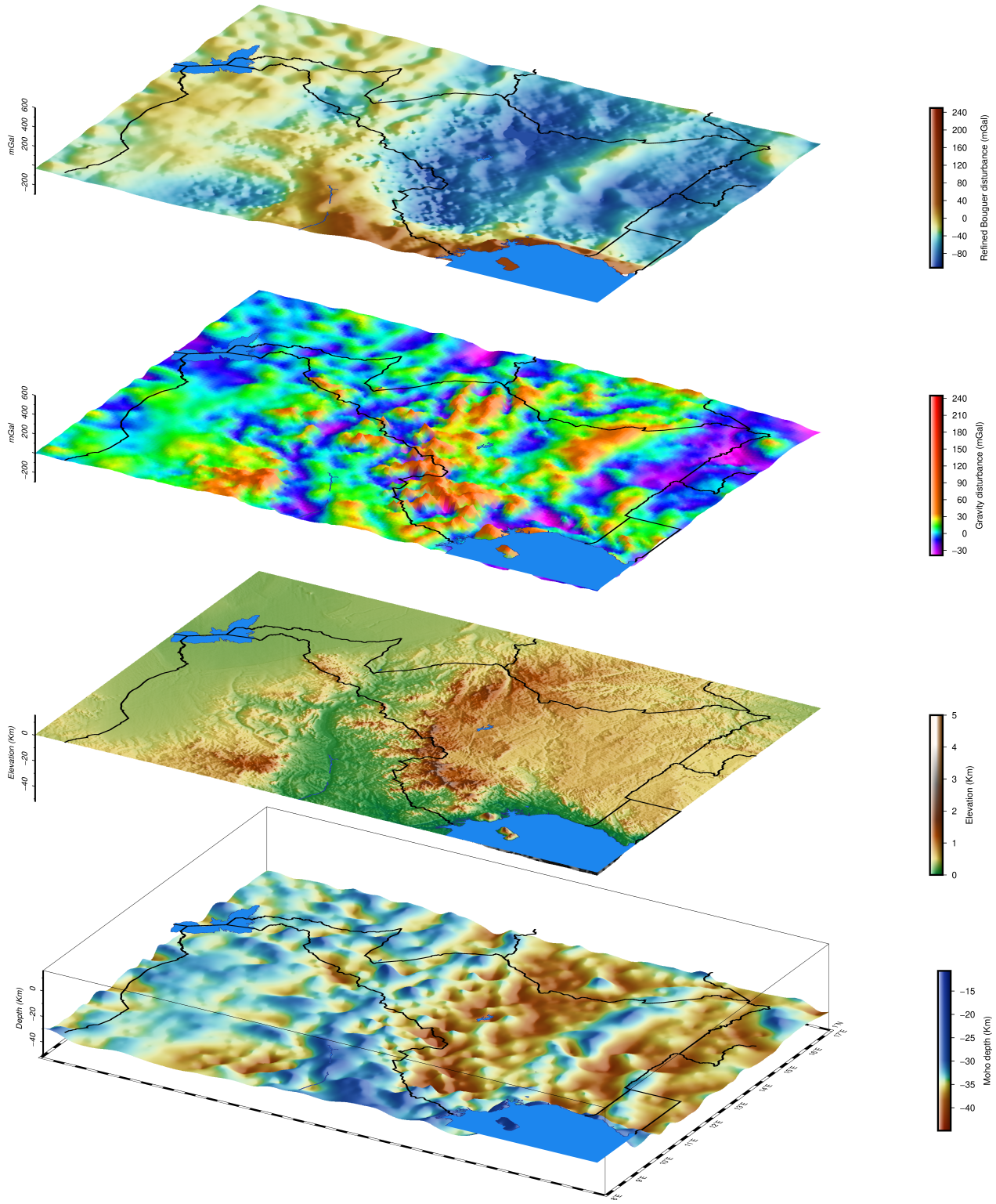

Figure 35: Relation between the refined Bouguer gravity disturbance (uppermost), and (downwards) Gravity disturbance, Elevation, Moho. Note the relation between the Benue through and the CVL path, which can be delineated in all the signals.

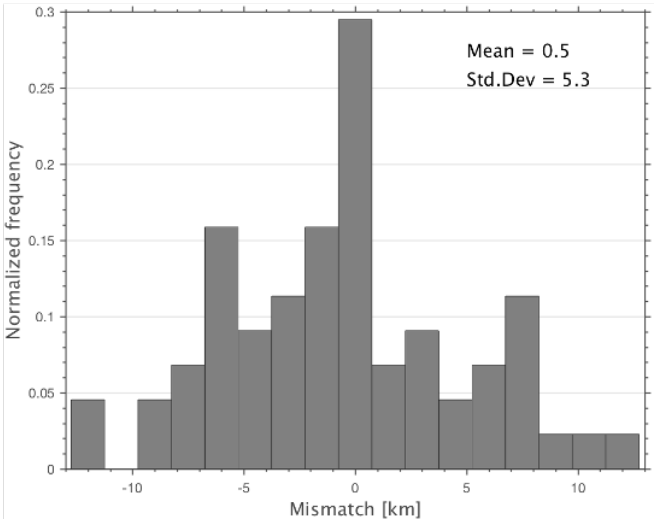

Figure 36: Histogram of the Moho depth differences between the seismic and gravimetric estimates at the CBSE sites in Cameroon and 2 sites in Nigeria.

of a high-density material originated from the uplifting of the mantle to a shallow depth. The entire part of the Yaoundé domain, the Congo Craton and the northern part of the Adamawa Plateau are characterized by negative values of the Bouguer gravity disturbances. This gravity low in the Bouguer gravity map likely reflects the character of outcropping crystalline basement rocks that form the Congo Craton as well as the Yaoundé domain. These crystalline basement rocks are formed mainly by low-density lithologies, particularly syntectonic granites, felsic gneisses and metasedimentary rocks. The extension of the Bouguer gravity lows towards north of the Adamawa Plateau might be explained by the existence of large granitoids in the crust.

3.2.5.2 Bouguer gravity images at different elevations

We compiled the Bouguer gravity maps at constant elevations of 20, 40, 60, 80, 100 and 120 km above sea level in order to suppress a gravitational signal from shallow sources (Jacobsen, 1987; Leonov, 2011). By analogy with the computation of the Bouguer gravity disturbances at the topographic surface, this procedure was practically realized by computing the free-air gravity disturbances and the gravity corrections at these elevations. The gravity corrections were then applied to the free-air gravity disturbances in order to obtain the Bouguer gravity disturbances.

In this way, we could enhance a gravitational signal from deeper regional geological structures. The individual Bouguer gravity maps are presented in Fig. 37.

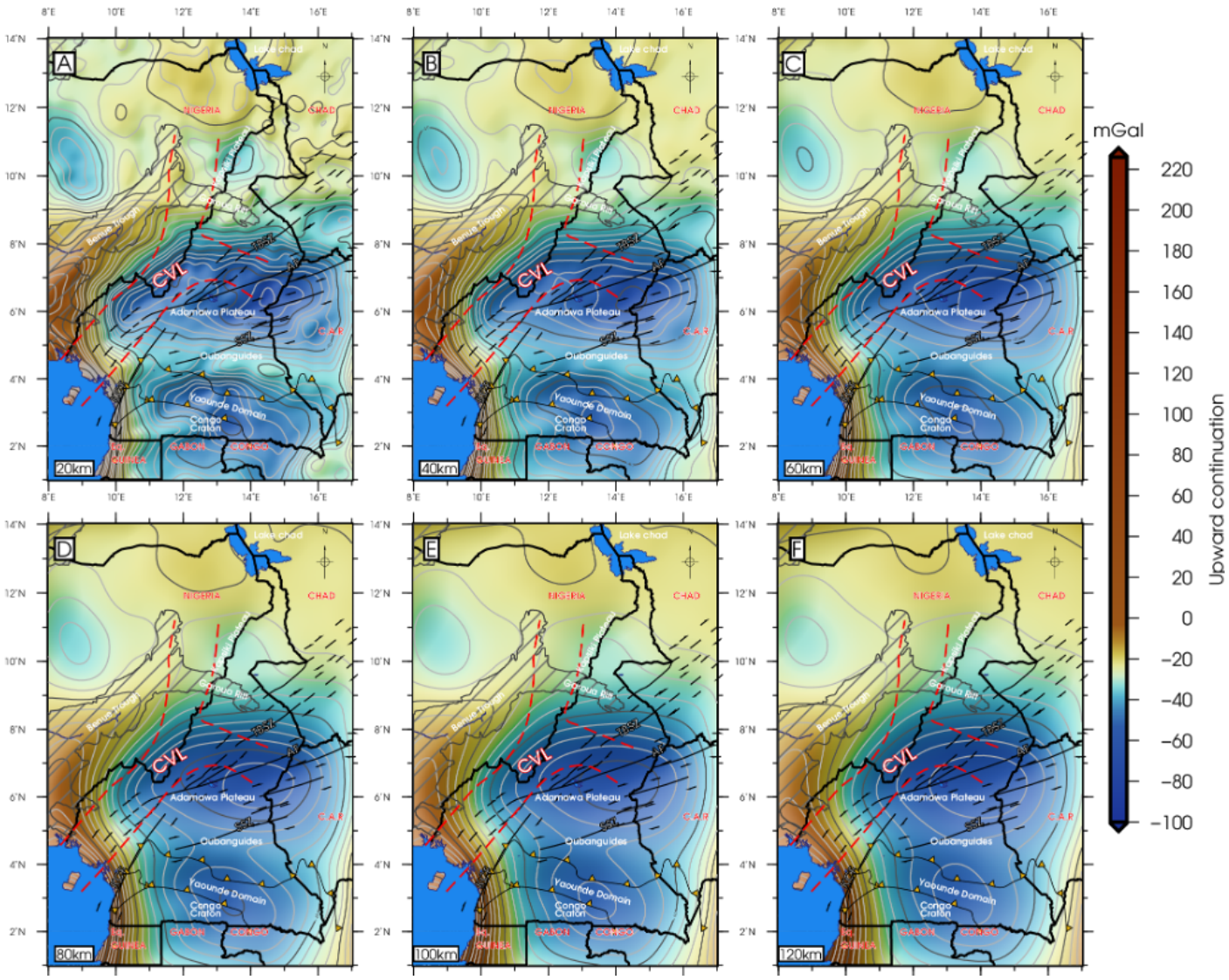

Figure 37: Regional maps of the Bouguer gravity disturbances continued upward at the constant elevations of: (a) 20 km, (b) 40 km, (c) 60 km, (d) 80 km, (e) 100 km, and (f) 120 km above the sea level.

The range of Bouguer gravity disturbances computed at different altitudes is mostly within the range from −100 to 220 mGal (Fig. 37). Along the coast, we observe positive values while negative elsewhere. The study area presents a regional structure that is very well recognized in the long-wavelength pattern of negative values centred at the Adamawa Plateau and the Congo Craton domain (Figs. 37c, d). This gravity low is oriented NE−SW near the coast following the volcanic massifs of the Cameroon Volcanic Line, and it becomes E−W trended in the Adamawa re-

gion. The long-wavelength negative values of the Bouguer gravity disturbances are commonly interpreted as the manifestation of a low-density body in the upper mantle (Okereke, 1988; Poudjom et al., 1995). Located at the western margin of the Cameroon Volcanic Line, the Benue Trough is characterized by NE−SW relative positive disturbances with the amplitude of 80 mGal. This gravity feature indicates a transition zone between the continental and oceanic lithosphere due to the fact that sediments usually have a lower density than the underlying metamorphic or igneous rocks.

Around the Benue Trough, on the other hand, the steep gradient in the Bouguer gravity disturbances underlain by the Oubanguides (Pan-African) Belt is still visible in the Bouguer gravity map even at the elevation of 60 km, while disappears at elevations from 80 km. This limit is marked by a long and regular vertical gradient about 1 mGal/km (Tadjou et al., 2009; Ngalamo et al., 2018) that reflects a change in the density of crustal rocks from the north to the south. The E−W orientation of the negative Bouguer gravity disturbances in the Adamawa Plateau is in agreement with known geology. Overall, The Bouguer gravity maps are consistent with the known tectonics and geological settings of the study area. According to results presented by Ngalamo et al. (2018), the Moho and the lithosphere-asthenosphere boundary (LAB) beneath the Congo Craton and the Yaoundé domain are reaching depths down to about 50 km and below 120 km, respectively. Beneath the Central African Shear Zone, the Adamawa Plateau and the Benue Trough, the shallower Moho and LAB depths reach typically 30 km and 70 km respectively. These large Moho and lithospheric thickness modifications beneath the Central African Shear Zone might be due to several geotectonic events that occurred during the Precambrian.

3.2.5.3 Moho models

The final gravimetric Moho model (shown in Fig. 34) relatively closely mimics major known geological features. According to our estimate, the Moho depth within the study area varies from 16 and 52 km. Overall, the largest spatial changes in the Moho geometry coincide with major tectonic margins, with a regional crustal

thickening under the Congo Craton, the Yaoundé domain, including southeast of the Adamawa Plateau where the Moho locally deepens to about 45 km. In contrast, thinner crustal structure is detected in the central and northern part of the Adamawa-Yade domain, with a shallow Moho depth locally reaching only 34 km beneath the northern Adamawa Plateau. Even shallower Moho was found beneath the Kribi Campo Fault, with minima of only 18 km in agreement with Angue et al. (2011). Beneath the Cameroon Volcanic Line and in the central segment of the Oubanguides Belt located to the south of the Cameroon Volcanic Line, the Moho depth varies between 35 and 39 km. Interestingly, however, the Moho under the Mount Cameroon deepens to only about 30 km. Beneath the Yaoundé domain and the Congo Craton, the Moho deepens to roughly 50 km (Tokam et al., 2010; Guidarelli and Aoudia, 2016; Ngalamo et al., 2018). Despite a relatively limited validation due to a lack of seismic data in the investigated area, the Moho depth estimated relatively closely agrees with the values obtained from passive seismic receiver functions. Around the Cameroon Volcanic Line, the West Cameroon domain, the Garoua Rift and coastal plains, the gravimetric solution very closely coincides with the seismic results, with differences less than ± 2 km. The gravimetric result, on the other hand, likely slightly overestimates the Moho depth beneath the Yaoundé domain and the Congo Craton, with differences there locally reaching 8 to 12 km. According to Knapmeyer-Endrun et al. (2014) differences between the gravimetric and seismic solutions are roughly within the limit of tolerance (Table 6).

Table 6: Summary of the Cameroon's crustal structure by geological terrain compare between Moho depth estimates obtained.

Terrain	Station	Latitude	Longitude	Gravity	Ngalamo et al. (2018)	Tokam et al. (2010)	Gallacher and Bastow (2012)	Mine-Ngalamo et al. (2018)	Mine-Tokam et al. (2010)	Mine-Gallacher and Bastow (2012)
Coastal plain	1	2,39	9,83	27,02	42	28	37,6	-14,98	-0,98	-10,58
	5	2,94	9,91	28,4	43	28	37,4	-14,6	0,4	-9
Congo Craton	2	2,7	13,29	43,21	43	43	44,6	0,21	0,21	-1,39
	4	2,98	11,96	35,34	39	45	47,5	-3,66	-9,66	-12,16
	6	2,39	11,27	30,51	42	45	41,8	-11,49	-14,49	-11,29
	7	3,87	11,46	36,47	37	43	41,8	-0,53	-6,53	-5,33
	11	3,98	13,19	40,34	44	48	43,3	-3,66	-7,66	-2,96
Oubanguides	3	3,52	15,03	39,96	41	43	44,6	-1,04	-3,04	-4,64
	10	4,22	10,62	37,42	37	38	35,8	0,42	-0,58	1,62
	12	4,48	11,63	34,33	37	38	37,8	-2,67	-3,67	-3,47
	17	5,55	12,31	36,41	37	35,5	37,8	-0,59	0,91	-1,39
Southern CVL	9	4,23	9,33	34,24	30			4,24		
	15	5,03	9,93	34,99	40	33		-5,01	1,99	
	16	5,48	10,57	40,3	40	35,5	34,1	0,3	4,8	6,2
	19	5,98	11,23	31,53	38	35,5		-6,47	-3,97	
	20	6,23	10,05	37,75	36	33	33,7	1,75	4,75	4,05
	23	6,37	10,79	40,02	37	40,5	38,3	3,02	-0,48	1,72
	13	4,59	9,46	32,28	44	28	36,5	-11,72	4,28	-4,22
	18	5,72	9,36	36,15	39	30,5		-2,85	5,65	
Adamawa Plateau (northeast CVL)	21	6,47	12,62	39,31	34	35,5	34,1	5,31	3,81	5,21
	22	6,48	13,27	35,27	33	35,5	35,8	2,27	-0,23	-0,53
	24	6,52	14,29	38,93	35	35,5	38,2	3,93	3,43	0,73
	25	6,76	11,81	34,12	39	38	38,2	-4,88	-3,88	-4,08
	26	7,27	13,55	37,8	37	33	34,9	0,8	4,8	2,9
	27	7,36	12,67	37,43	34	35,5	39	3,43	1,93	-1,57
Garoua rift	28	8,47	13,24	38,44	38	30,5		0,44	7,94	
	29	9,35	13,39	32,1	26	25,5	25,3	6,1	6,6	6,8
	30	9,76	13,95	34,43	29	28	26,5	5,43	6,43	7,93
	31	10,33	15,26	31,3	35	30,5		-3,7	0,8	
	32	10,62	14.37	32,8	34	33	33,3	-1,2	-0,2	-0,5

3.2.5.4 Cross comparisons of Moho models

We compared our Moho depth estimate with two gravity-based models, namely, the Veining Meinesz's (VMM) model (Bagherbandi et al., 2013) and the GOCE Exploitation for Moho Modelling and Applications (GEMMA) model (Reguzzoni and Sampietro, 2015); see Fig. 38. The VMM model (Bagherbandi et al., 2013) was compiled based on generating the isostatic gravity disturbances with a global resolution of $1° \times 1°$. The GEMMA model was compiled globally on a $0.5° \times 0.5°$ grid based on combining gravity and seismic data. The corresponding Moho depth differences are plotted in Fig. 39, with the statistics summarized in Table 7. Interestingly, we see a relatively deep Moho (32 to 48 km) beneath the Congo Craton and the Adamawa Plateau in both solutions.

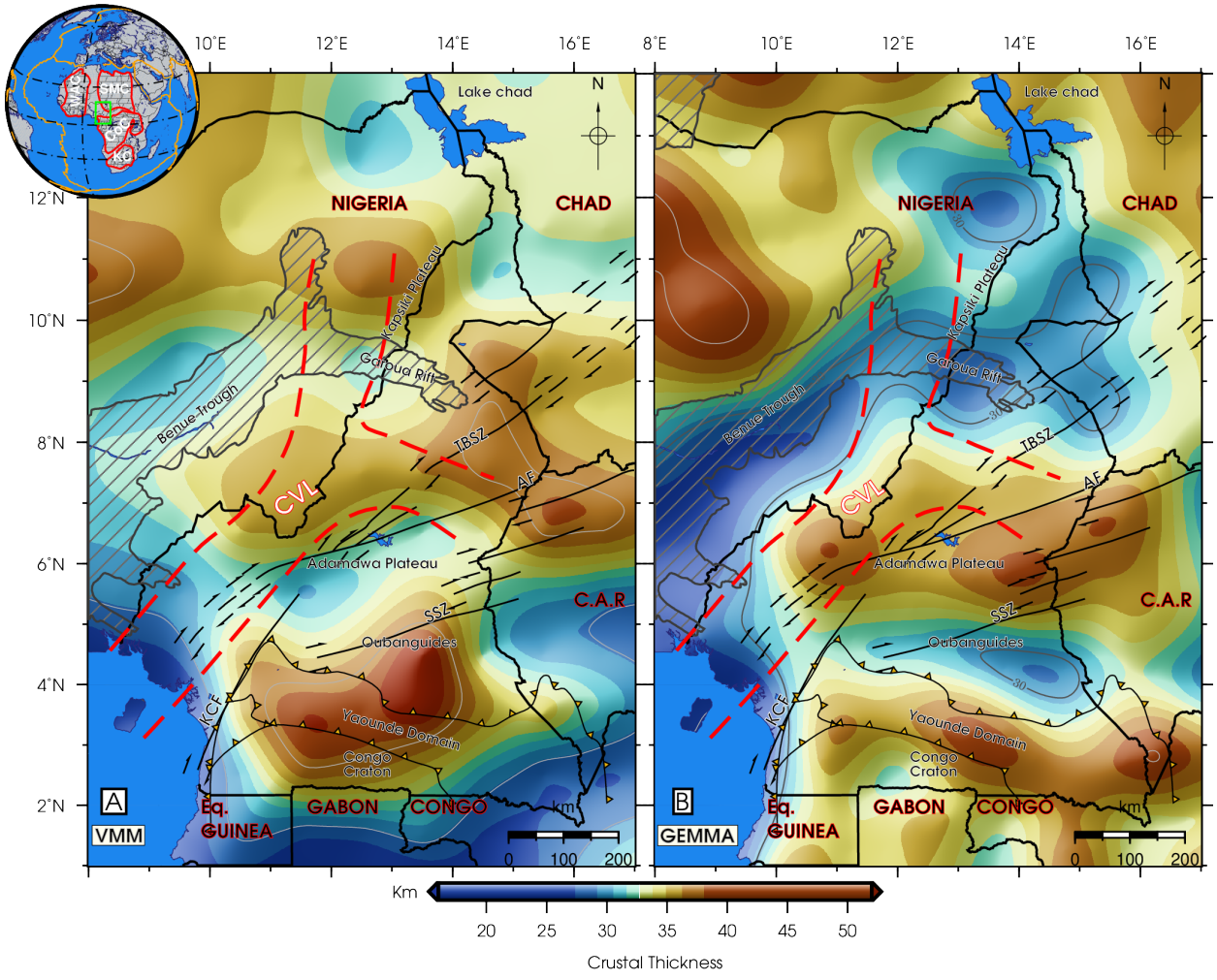

Figure 38: The juxtaposition of existing crustal models for the Cameroon region. The gravity-based models are VMM (Bagherbandi et al., 2013) and GEMMA (Reguzzoni and Sampietro, 2015).

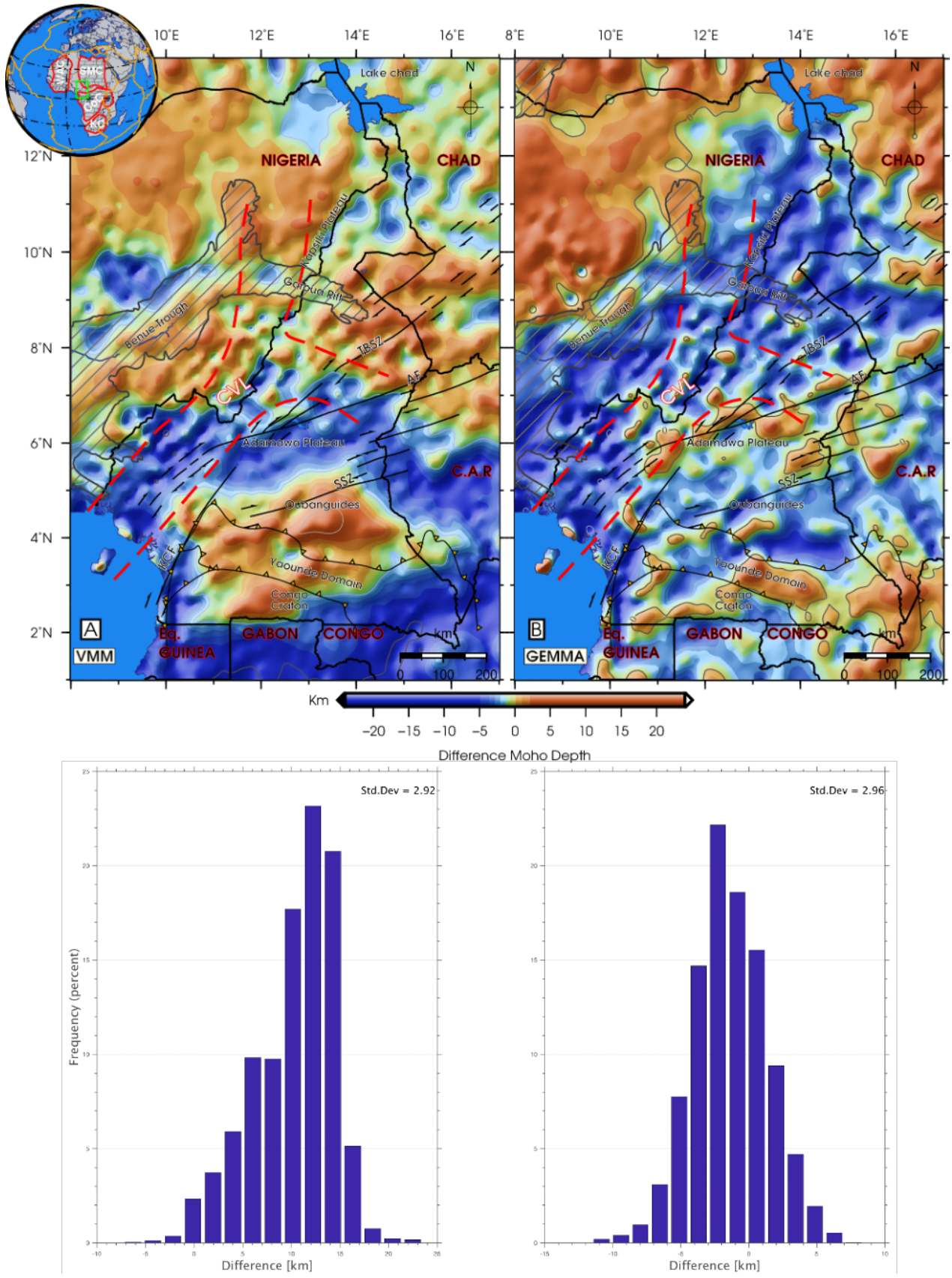

Figure 39: Comparison of our model with (a) VMM model by (Bagherbandi et al., 2013), and (b) GEMMA model by (Reguzzoni and Sampietro, 2015).

They also predicted the shallow Moho depth of roughly 24 to 32 km beneath the Benue Through and the Garoua Rift. Nevertheless, the VMM model forecast a marked regional Moho deepening beneath the centre of the basin of the Oubanguides and the Yaoundé Domain that causes maximum Moho depth differences 23.5 km between these two models (Table 7). Moreover, the VMM model contradicts the Moho geometry exhibited in the GEMMA model mainly in the Adamawa Plateau, the Oubanguides, the Yaoundè Domain, and the Congo Craton. The GEMMA model agrees better with our model than the VMM model. Nevertheless, both models have a very similar standard deviation of differences with respect to our model. A good agreement of the GEMMA model with our is explained by using in both cases global gravity models constrained by 32 seismic data of the CBSE.

Table 7: Cameroon's statistical comparison between VMM, GEMMA and the Referenced Crustal Models

Differences	**Min (Km)**	**Max (Km)**	**Mean (Km)**	**STD (Km)**	**RMSE**	**Correlation**
VMM	-7,31	23,50	10,31	2,93	11,11	0,59
GEMMA	-11,53	9,85	1,37	2,96	3,05	0,76

3.2.6 Summary and concluding remarks

The computation of gravity values at increasing elevations accentuates the effect of deep gravity sources, while attenuates or even removes the influence of the superficial ones. We applied this procedure to compile Bouguer gravity maps at constant elevations above sea level from 20 up to 120 km with a step of 20 km. In this way, the low-pass filter transforms and smooths gradually the initial uneven Bouguer gravity disturbances, while highlighting a gravitational signature of deeper crustal and lithospheric features.

The Bouguer gravity maps revealed that from 80 km up, the Adamawa-Yadé and the Congo Craton cores could be observed. The core of the Adamawa-Yadé Craton

has a stronger signature than the Congo Craton. The presence of these two structures revealed many similarities between the Congo Craton and the Adamawa-Yadé domain. This finding supports the extensional processes of both domains during the Neoproterozoic era that was a unique structure in the past (Toteu et al., 2001). Similarly, (Nkoumbou et al., 2014) suggested that the Adamawa-Yadé domain was the Archean-Paleoproterozoic micro-continent that formed the part of the Congo Craton (characterized by the same Palaeoproterozoic and the Archaean crust reworking), while being separated from it in the early Neoproterozoic. An alternative hypothesis suggests that the sedimentary budget of the Yaoundé domain has been imparted by the northern part of the Congo Craton, together with the Adamawa-Yadé domain (Nkoumbou et al., 2014). Thus, suggesting that the crustal manifestation of the suture zone between the Congo Craton and the Adamawa-Yadé domain is depicted by the Yaoundé domain.

Our result generally supports the statement that this micro-continent was sutured back with the Congo Craton as a result of the collision between these two tectonic entities after the consumption of the oceanic basin separating them and the formation of a continental arc. Moreover, we propose that the Congo Craton acted as a single and stable cratonic block, while the Adamawa-Yadé structure acted as a micro-craton due to the remobilization by granitoid emplacement as the result of the sub-continental lithospheric mantle delamination that accompanied the collision with the Congo Craton. We denote that, the delamination occurs when the lower continental crust and mantle lithosphere break away from the upper continental crust.

Large values of the Bouguer gravity disturbances observed in Figs. 37a, b) within the northwest margin of the Adamawa-Yadé domain with the NE-SW trend could be caused by underplating of magmatic bodies beneath the Benue Trough and the Chad basin, that leads to a favourable factor for melting and/or delamination processes at the base of the crust and within the uppermost mantle. The Cameroon Volcanic Line is, on the other hand, characterized by the Bouguer gravity anomaly lows that could possibly be associated with the melt at the base of the crust and the uppermost mantle

(Ngalamo et al., 2018). These observations support the proposed ideas of Poudjom et al. (1997) as well as Ngalamo et al. (2018). We have applied the regularized non-linear gravity inversion based on Uieda and Barbosa (2016) to estimate the Moho depth, and compared our gravimetric solution with the seismic results obtained at 32 (30 in Cameroon and 2 from Nigeria) passive seismic stations. Along coastal plains, the result obtained from the regularized non-linear gravity inversion closely agrees with the result of (Tokam et al., 2010) as well as from the regional investigation conducted by Angue et al. (2011). Our results beneath the Congo Craton are in a good agreement with the results of previous studies done by Poudjom et al. (1995) and Guidarelli and Aoudia (2016). These results indicate that the Moho depth beneath the Congo Craton varies between 41 and 50 km. However, for the stations 4 and 6 (Table 6), the Moho depth differences between our and their results exceed even 10 km. Our result thus likely underestimates the Moho depth under this cratonic structure. A similar disagreement (up to 12 km) was found with seismic results. This finding might be explained by the presence of a mass excess in the crust or in the uppermost mantle. A body with a positive density contrast whose gravitational effect was not subtracted from data during processing amplifies the observed gravity disturbances.

Consequently, the gravimetric inversion yields a shallower Moho. Such inconsistencies between the gravimetric and seismic Moho solutions were emphasized, for instance, in studies of the Egyptian crust by Sobh et al. (2019), the South American crust by Uieda and Barbosa (2016), the crust thickness under the Paraná Basin by Mariani et al. (2013), or the crust thickness beneath the Amazon Basin by Nunn and Aires (1988). Differences between gravimetric and seismic Moho depth estimates in certain regions could also be attributed to various considerations, relevant to the applied corrections, constraining seismological data, the resolution of topographic model, or the contribution of sediment thickness and igneous intrusions. Additionally, the topographic gravity correction computed while considering only a uniform topographic density, would be partly responsible for errors in the Moho depth esti-

mates.

We used the VMM and GEMMA model to check the reliability of our (high-resolution) Moho model. The validation revealed a better agreement of our model with GEMMA, this was explained by the fact that both solutions were obtained from global gravity models constrained by the CBSE seismic data. Nevertheless, our model better agrees with the CBSE seismic results. According to our result, a greater confidence in our Moho depth estimates are well established in the entire region. Moreover, our model seems to be very accurate along the Cameroon Volcanic Line, coastal plains and the Garoua Rift. We see that there our model fits (with an uncertainty about ± 4 km) both the seismological data as well as results published by Ngalamo et al. (2018), Tokam et al. (2010) and Gallacher and Bastow (2012). The Moho depth varies from 31 km in the Garoua Rift to 43 km in the Congo Craton with estimated uncertainty of ± 12 km in the Congo Craton. Along the Adamawa plateau, the Cameroon Volcanic Line, the Oubanguides Belt and the Coastal Plain, the Moho varies from 27 to 39 km. Our Moho model merely correlates with seismic data along Y-shape of the Cameroon Volcanic Line, the Garoua Rift, and the Adamawa Plateau. According to previous studies, minor discrepancies are observed mainly between Ngalamo et al. (2018) and Tokam et al. (2010). However, for stations 4, 6, 7 along the Congo Craton our Moho model has fewer estimates with a discrepancy greater than 10 km. We attribute these errors to a different methodology and data quality. A good correlation observed in the Adamawa Plateau between our model and seismic data, lead us to check the relationship between the Moho and the topography. As stated by Eyike and Ebbing (2015), the relationship between these two parameters likely indicate structures formed during a compressional regime, while the opposite relationship observed in the Garoua Rift may depict structures formed during an extensional regime.

3.3 Equatorial east African crustal configuration from gravity and seismic data analysis

In this section, we briefly summarize input data and models used to compile gravity maps. We interpret these gravity maps in the context of geological and tectonic configuration and topographic relief. We also summarize available seismic data used in this study for a joint gravimetric and seismic data analysis.

3.3.1 Free-air gravity data

The free-air gravity disturbances computed on a $5' \times 5'$ geographic grid of surface points are shown in Fig. 40. Within the study area, the free-air gravity disturbances range roughly between -100 and 150 mGal. This observation agrees with the spatial correlation between topography and gravity, except for the Rwenzori Belt.

3.3.2 Bouguer gravity data

The combined topographic-bathymetric gravity effect computed on a $5' \times 5'$ geographic grid of surface points is shown in Fig. 41a. This combined gravity effect is highly spatially correlated with the topography. Within the study area, the correction roughly varies between -150 to 300 mGal. Large positive values are mainly in the southwest Kenya (300 mGal) between the Mount Elgon and the Mount Kenya along the East Rift and along the West Rift around Rwanda-Burundi west boundaries (300 mGal). The sediment gravity correction is shown in Fig. 41b. This correction reaches the largest negative values ($\backsim -100$ mGal) along the coast of the Indian Ocean.

We applied the topographic-bathymetric gravity correction to the free-air gravity disturbances. The resulting Bouguer gravity map is shown in Fig. 42a. Subsequently, we applied the sediment gravity correction to the Bouguer gravity disturbances. The refined Bouguer gravity disturbances are shown in Fig. 42b. From Figs. 40 and 42a, we see that the application of the combined topographic-bathymetric gravity correction significantly modified the free-air gravity pattern. Additional, but much

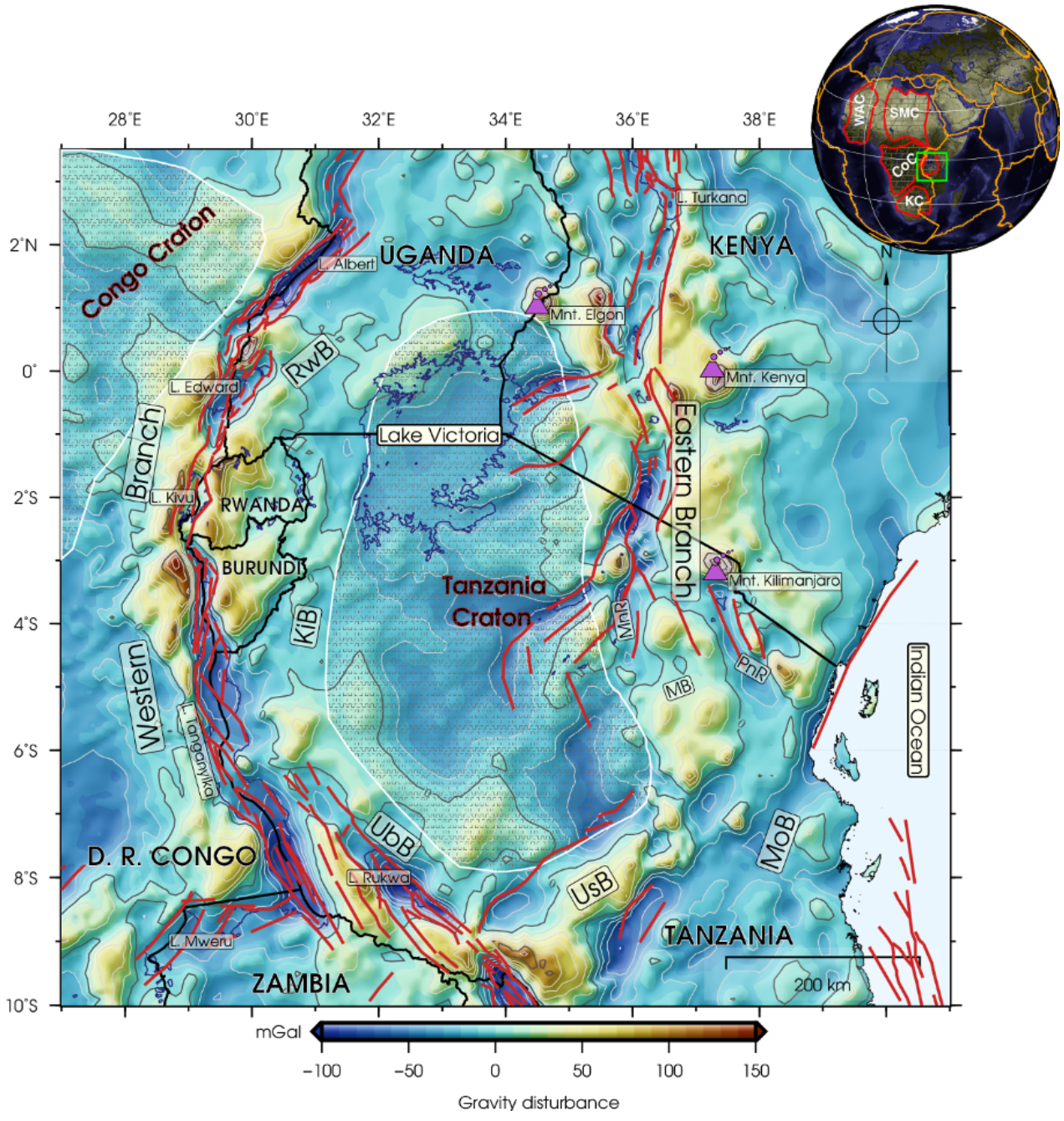

Figure 40: EARS regional map of the free-air gravity disturbances.

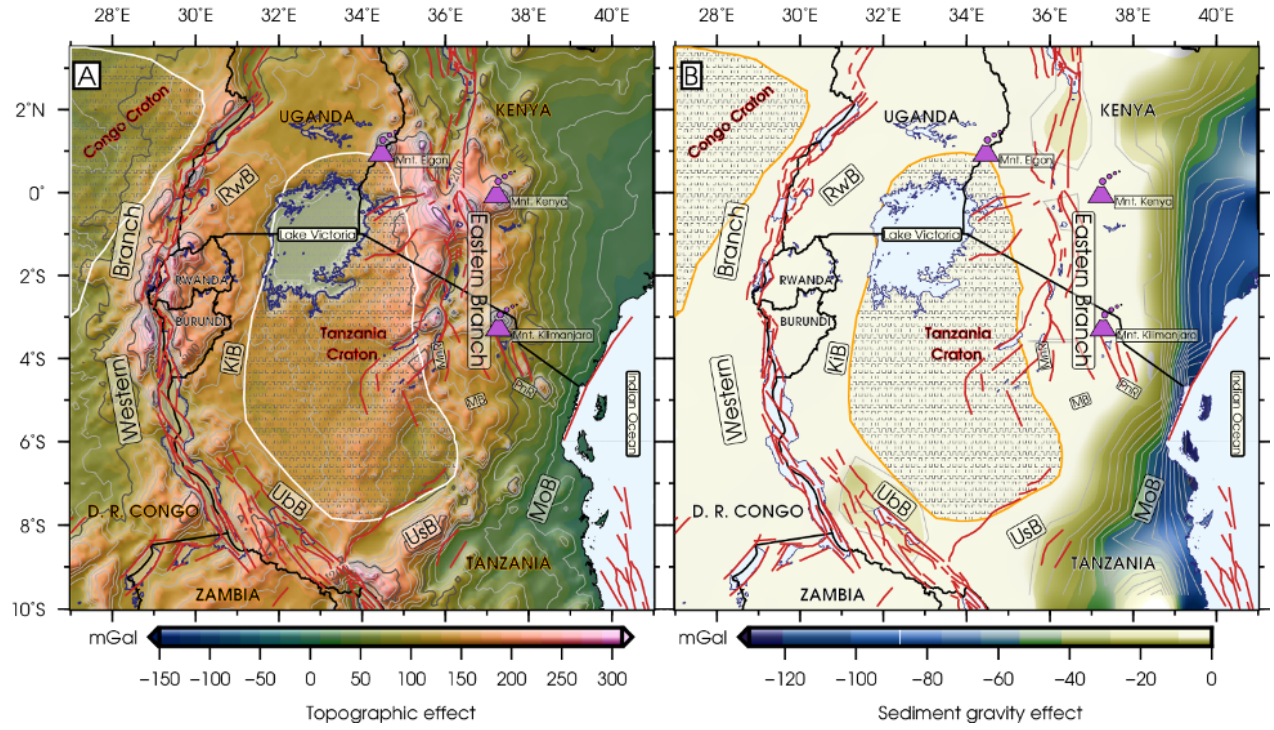

Figure 41: Regional maps of: (a) the topographic-bathymetric and (b) sediment gravity effects.

less prominent changes in the Bouguer gravity map are also recognized after applying the sediment gravity correction.

As seen in Fig, 42b, the refined Bouguer disturbances vary roughly between −350 and 225 mGal. Coastal areas along the Indian Ocean are characterized by large spatial gravity variations with increasing values towards the east. This prevailing trend is attributed to a crustal thinning of continental margins. The area to the west of Lake Tanganyika and Lake Edward in Congo is characterized by average (refined) Bouguer gravity values of ∽−100 mGal and with values decreasing eastwards and reaching broad lows and highs related to the Congo River basin and the Kibaran mobile belt. The NNW trend observed along Lake Tanganyika coincides with the Tanganyika-Rukwa-Malawi lineament that is interpreted as an intra-continental transform fault zone (Delvaux, 2001).

Around the Rwenzori Belt, the Bouguer gravity disturbances are ∽−75 mGal. The Kenya Rift is characterized by large negative values of about −225 mGal and ∽−50 mGal towards Lake Turkana that are explained by crustal thinning (negative anomaly) and related to the late Cenozoic rifting. However, multiple rifting episodes occurred in the Lake Turkana area. Consequently, the gravity pattern in that region

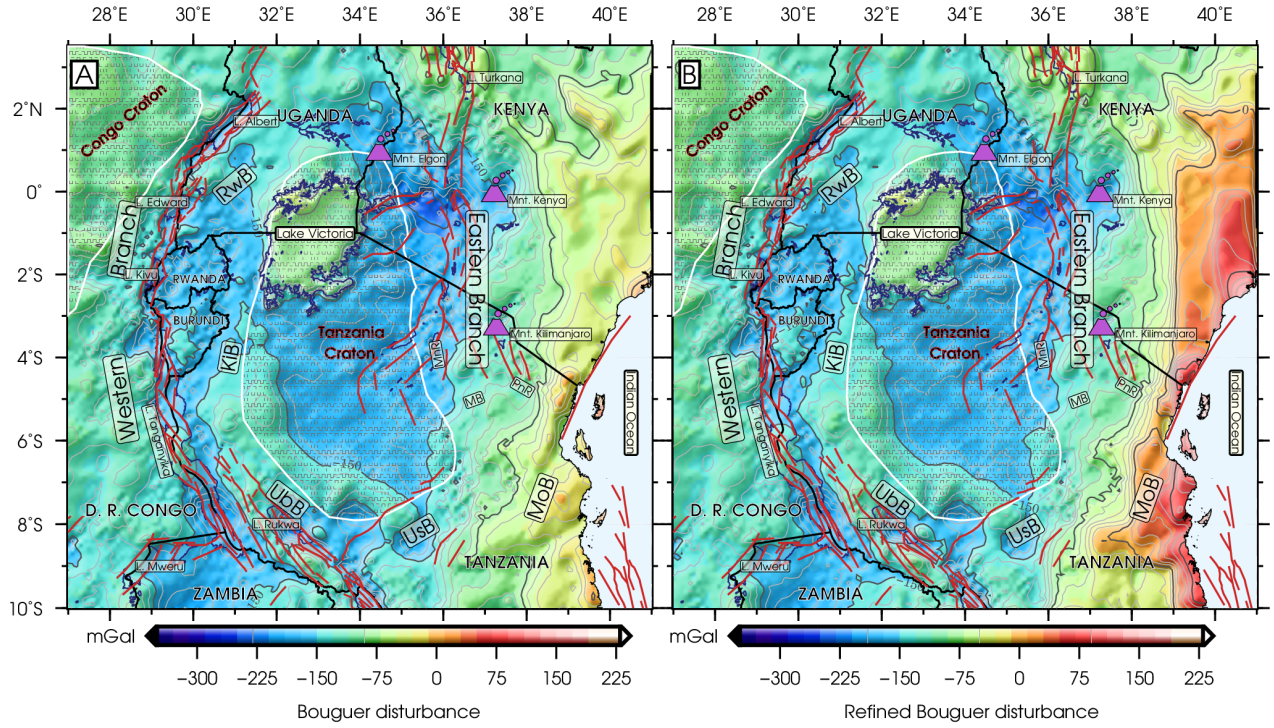

Figure 42: Regional maps of the Bouguer gravity disturbances: (a) before and (b) after applying the sediment gravity correction.

appears to partially reflect these older episodes of rifting (Chorowicz, 2005). Along the central and southern segments of the Kenya Rift, the regional Bouguer gravity pattern indicates that over all major volcanic centres gravity highs are superimposed on regional gravity lows. The southern segment of the Kenya Rift is characterized by a broad gravity low associated with the Kenyan Dome. These short-wavelength gravity features observed along the Kenyan Dome may result from structures in the crust, while the long-wavelength gravity minima are likely attributed to the mantle structure. Gravity highs along the eastern branch are likely due to mafic bodies of main volcanic centres, the densification of the upper crust due to diking, and horst blocks where the Precambrian basement has been brought to or near the surface. Negative (refined) Bouguer gravity disturbances spread over the entire extent of the West and East Rifts. Minima are centred along the East African Rift System close to the equator. Regions with negative values suggest an isostatic equilibrium within the region (McCall, 1957), considered to be produced either by low density of surficial volcanism (Fairhead, 1976) or by perceived asthenospheric intrusions (Chorowicz, 2005).

The long-wavelength pattern in the Bouguer gravity map has two minima, one situated over the Archean craton-mobile belt boundary between Ubendian System to the southwest and Usagaran System to the east and southeast and the other one over the rift valley. We can delineate a long-wavelength gravity pattern in west Kenya (−225 mGal) and northeast Tanzania (−180 mGal). Bouguer gravity lows roughly of −120 mGal are delineated over the boundary between the Mozambique Belt and the Tanzanian Craton suture zone. This low intermediate-wavelength gravity pattern is observed over the Kenya Rift that extends up to 7°S. This gravity pattern is attributed to a thickened crust of the suture along the Late Proterozoic Orogeny of the Mozambique Belt and the Tanzanian Craton (Nyblade and Pollack, 1992).

3.3.3 Upward gravity continuation

To decipher the long-wavelength trend attributed to deeper lithospheric structures, we smoothed the refined Bouguer gravity disturbances by applying the upward continuation. In this way, the short-wavelength gravity pattern reflecting shallow sources was filtered out, while revealing a medium-wavelength signal from deeper sources. According to (Meng et al., 2009), the field resulting in a certain elevation H exhibits sources situated at a maximum depth of $D_0 = 1/2H$. We continued upward the refined Bouguer gravity disturbances to 20, 40, 60, 80, 100, and 120 km elevations. Individual results are plotted in Fig. 43. According to (Jacobsen, 1987), this process allows paying attention to the underground response by accentuating the effect of deeper gravity sources and even removing/attenuating the influence of superficial ones. Thus, this low-pass filter smooths the regional gravity field (Fig. 42b) or certain wavelengths or predetermined trend into gravity field that highlights broader regional crustal features. As seen in Fig. 43, the upward-continued (refined) Bouguer gravity disturbances range roughly from −250 to 100 mGal. The main gravity lows (Fig.43a), located mainly over the Tanzanian Craton and west Kenya, are still apparent in gravity pattern even at elevations up to 80 km, while remain almost unchanged from 100 to 120 km.

Consequently, its origin is possibly located deeper in the lithosphere. The gravity pattern generally trends N-S, but as the wavelengths increase the gravity pattern takes on a more NNE-SSW trend (Figs. 43d, 43e). The N-S gravity low trend extends along the 38°E meridian from about 3°S to 6°S. This could be explained by a deep-seated structural grain, which predates the late Cenozoic rifting. The Kenya Dome and the south segment of the East Rift and regions around Lakes Edward and Kivu are marked by distinctive gravity lows (Fig 43a,b). As the elevation increases, these gravity lows expand and eventually merge into a one broad gravity low tip of which is centred on Lake Victoria mostly on its eastern flank (Fig. 43e,f). This suggests that there is a deep mantle anomaly centred beneath the north part of the Tanzanian Craton and Lake Victoria which is associated with a low density material.

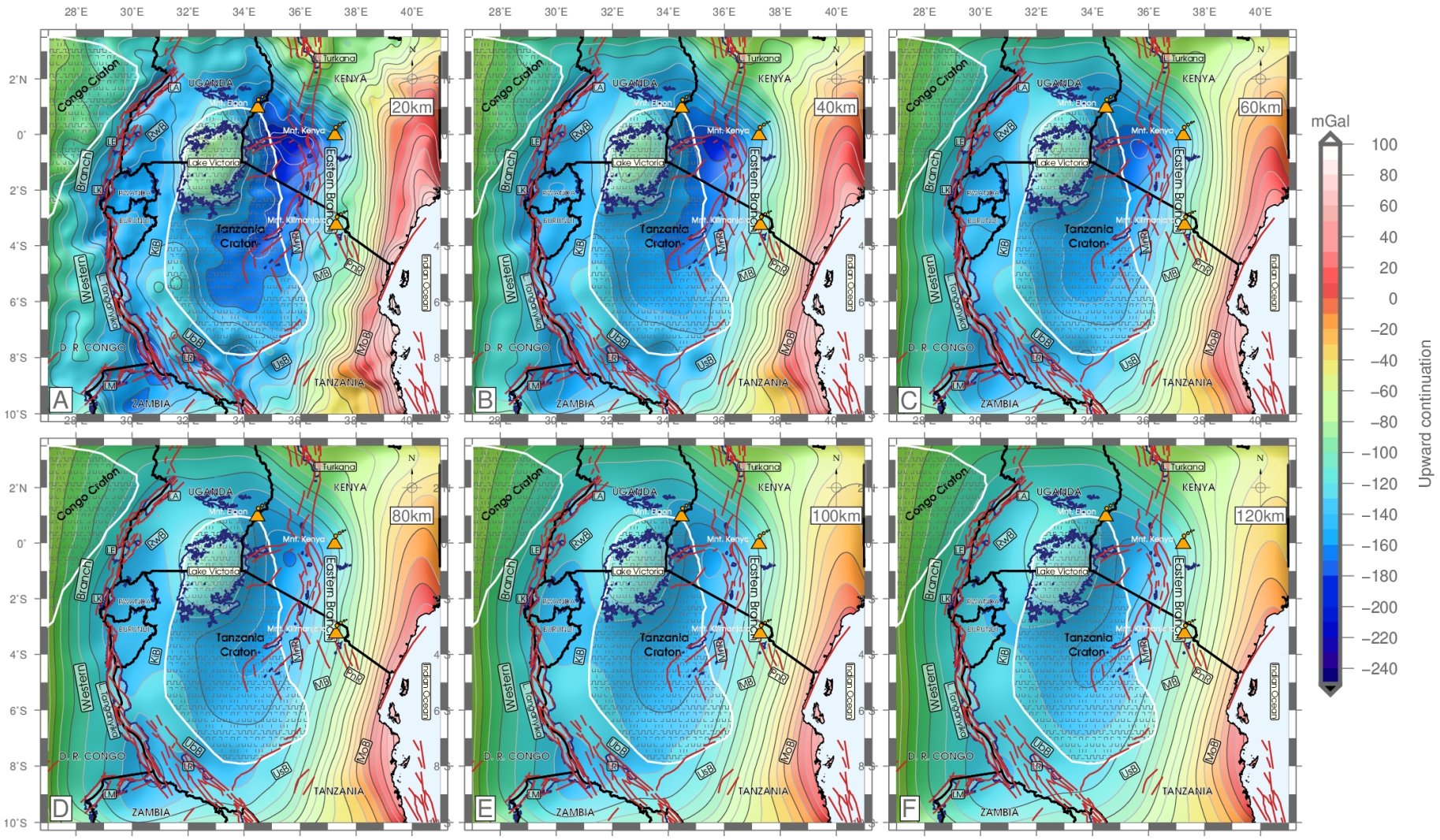

Figure 43: Maps of the refined Bouguer gravity disturbances at elevations of: 20 (a), 40 (b), 60 (c), 80 (d), 100 (e), and 120 (f) km.

The low-pass filter has largely removed a gravity signal from shallow structures such as grabens associated with the Mesozoic rifting. This map, therefore, shows that gravity highs are primarily due to deeper features in the lower crust or eventually in the uppermost mantle. Intermediate-wavelengths of the Bouguer gravity lows over west Kenya have minima over the Archean-Proterozoic suture and extend into northeast Tanzania (Figs. 43b-e).

This feature is assigned to a broad zone of a low-density material in a very thin lithospheric mantle, not only beneath the axis of the Kenya Rift, but further extending far to the west beyond the Cenozoic rift structures (Fairhead, 1976). Two shorter-wavelength components can be distinguished from this anomalous feature, namely the contribution of a rift structure and the manifestation of crustal roots along the Proterozoic-Archean boundary suture and a high-density crust in the Mozambique Belt beyond the crustal roots. NNW-SSE and NW trending regional gravity highs observed around the Lakes Turkana and Ubendian Belt respectively are prominent in gravity maps at elevations from 20 to 60 km (Figs. 43a-c). Ebinger et al. (1997) suggested that these basins were developed during the Mesozoic rifting which left imprints on the lithospheric structure.

3.3.4 Seismic data

Over the last four decades, large number of joint international collaborative large-scale seismic projects have been conducted in east Africa to better understand the lithospheric structure and to search for source regions and reason for the wide-spread earthquake activity using methods, such as seismic refraction profiles or regional broadband seismic networks operated in Tanzania, Kenya, and Ethiopia (Fig. 44).

The first reconnaissance experiment has been conducted through the Kenya Rift International Seismic Project (KRISP) programs during 1985, $1989-1990$, and $1993-1995$ networks (KRISP, 1987; Henry et al., 1990; Prodehl et al., 1994). In $1994-1995$, 20 stations were deployed along with linear arrays crossing Tanzania during the Tanzania Broadband Seismic Experiment program (Nyblade et al., 1996). Fol-

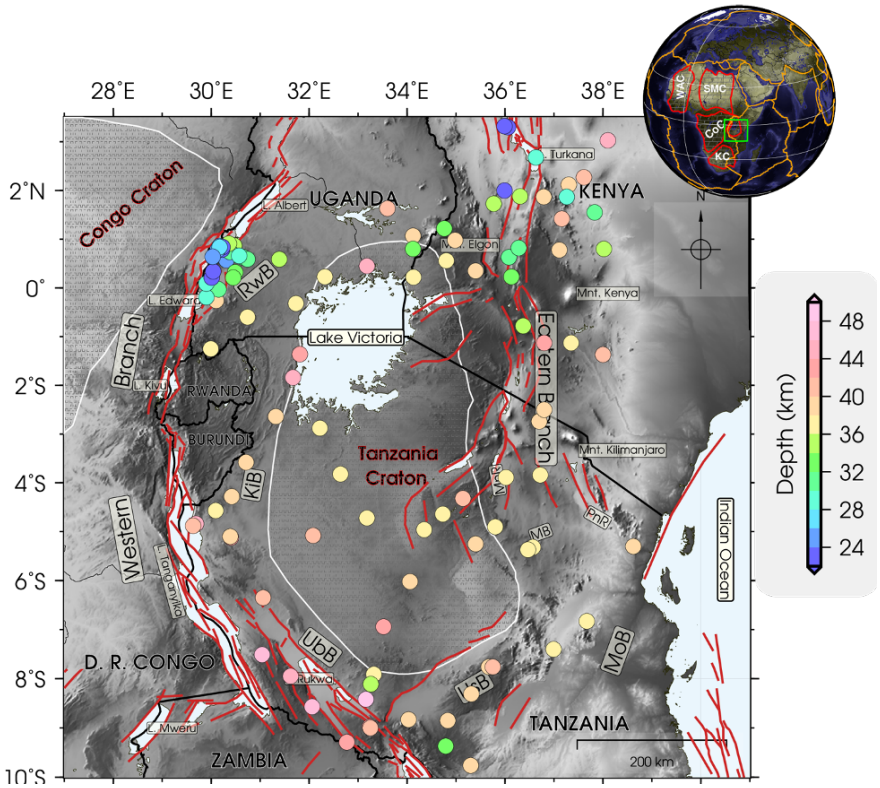

Figure 44: Seismic Moho depth estimates from receiver functions analysis at seismograph stations (circles), superimposed on a regional shaded topography.

lowing these records, 10 stations spanning from south to central Kenya were installed by the Kenya Broadband Seismic Experiment networks between 2000 − 2002. In addition to these activities, the International Ethiopia Afar Geoscientific Lithosphere Experiment project was launched between 2001−2003 (Bastow et al., 2005) together with the permanent Geoscope stations and Global Seismic Network in east Africa. More recently, the Africa Array Eastern Africa Broadband Seismic Experiment (AAEASE) and the Africa Array Tanzania Basin Seismic Experiment (AATBSE) deployed in total 28 stations from January 2009 to July 2011 in southeast and southwest Tanzania and along the coast. According to the analyses of these seismic surveys, the Moho depth in south Kenya along the axis of the rift appears to shallows from 35 km to only ∽ 20 km beneath its northern part. Beneath the Mozambique Belt (Novak et al., 1997), the Moho deepens to ∽ 38 km, and to 37 km beneath the Tanzanian Craton (Fuchs, 1997). From the Rayleigh wave dispersion and teleseismic receiver functions, (Last et al., 1997) found that the Moho deepens to ∽ 43 km beneath the Paleoproterozoic Ubendian Belt. They also obtained almost an identical Moho image of ∽ 38

and $\backsim$ 40 km for the Mozambique Belt and the Tanzanian Craton respectively. Under the Cenozoic rift valleys, the Moho depth shallows to $20 - 32$ km and estimates beneath the unrifted crust vary from 40 to 48 km. Receiver functions calculated for datasets conducted by the Kenya Broadband Seismic Experiments indicate that the Moho depth on average varies from 39 to 42 km in the Kenya Rift, while from 35 km beneath the south part in the Kenya Dome to 40 km in the north part of the Turkana depression along the Kenya Rift (Dugda, 2005). Along the West Rift, a thinner crust with a Moho depth within $21 - 28$ km in the Rwenzori Mountains was observed, whereas the surrounding Neoproterozoic Mozambique ($38 - 40$ km) and the Ubendian Belts (> 40 km) and the adjoining Tanzanian Craton ($\backsim$ 40 km) are possibly underlined by a thick crust (Dugda, 2005; Wölbern et al., 2010; Tugume et al., 2013).

3.3.5 Results

The refined Bouguer gravity data described in Section 3.3.1 were used to estimate the Moho depth according to the procedure described in Section 2.3. The result of the gravimetric Moho inversion constrained on seismic data is presented and then compared with seismic results and existing gravimetric studies next.

3.3.5.1 Optimal regularization parameters constraints

In order to provide physical consistency to output results, seismic constraints from previous regional and local seismic studies (Fig. 44) were applied to validate the reference Moho model and density contrast. Using the hold-out method defined by Kim (2009), the regularization parameter, reference (mean) Moho depth and Moho density contrast were obtained that are required as input parameters for the regularized Bott method.

We first set the reference Moho depth and Moho density contrast at 30 km and 400 kg/m^3 respectively. These both values have no influence on a regularization parameter (Uieda and Barbosa, 2016). The optimal regularization parameter was found to be 10^{-5}. This value corresponds to the one that best predicts testing data from the 16

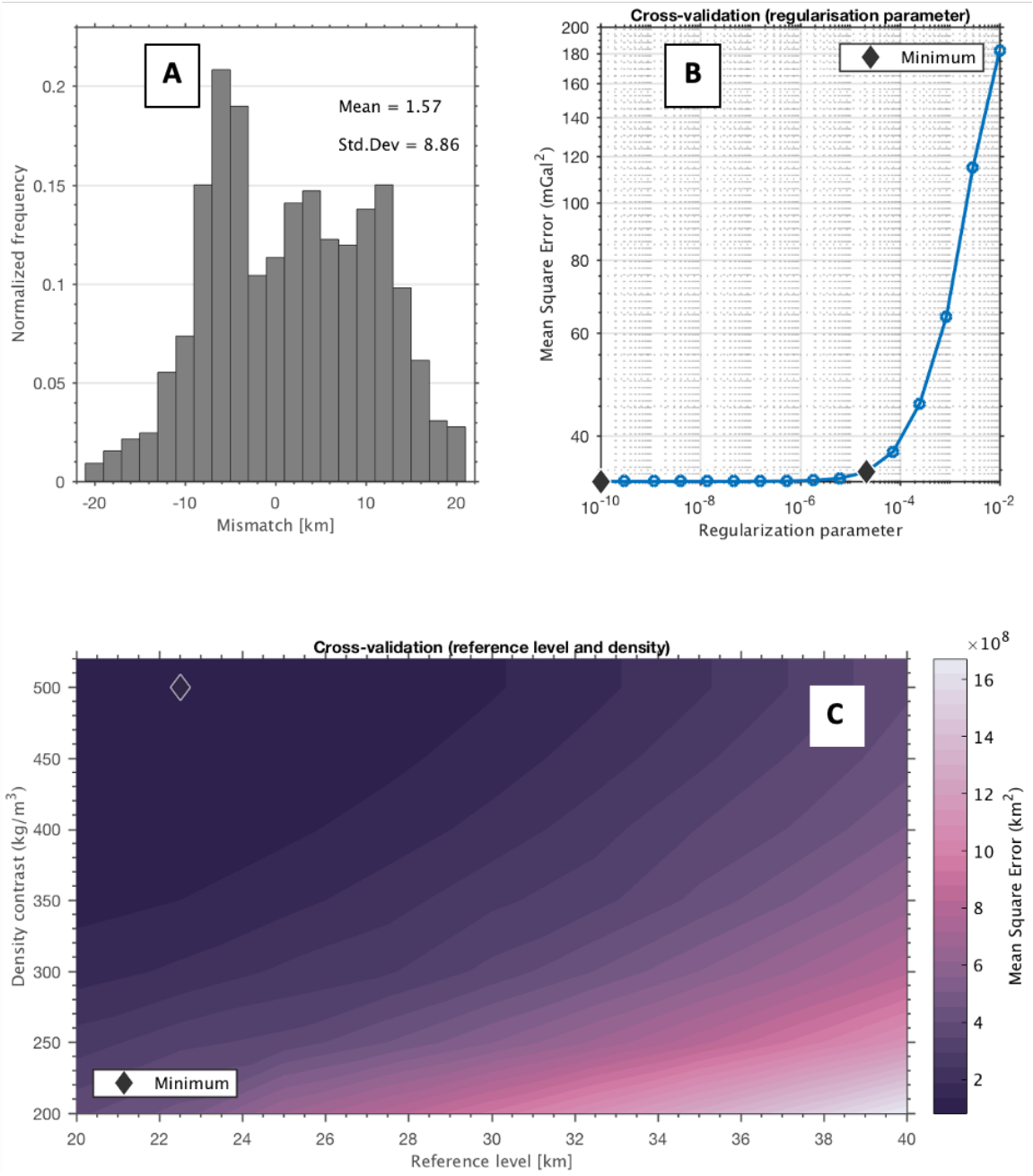

Figure 45: Parameter estimation results. Black diamonds represent (optimal) values; (a) Gravity residuals; (b) estimated regularization parameter. The numbers are the regularization parameters (μ). The best μ in this model is regarded as 10^{-5} which is the inflection point of the curve; (c) estimated reference Moho depth and density contrast based on seismic constraints.

values indicated by the diamond box in Fig. 45b. In the second step we carried out a gravimetric inversion for different values of the Moho density contrast as well as the mean Moho depth. The Moho reference depth ranged from 20 to 40 km with a 0.5 km incremental step, and for the Moho density contrast between 200 and 500 kg.m^{-3} with 50 kg.m^{-3} interval. The best fit was attained for the values of 22.5 km and 500 kg.m^{-3} of the mean Moho depth and the Moho density contrast respectively (Fig. 45c).

The final gravimetric solution was then selected based on the principle of minimizing the mean square error (MSE) of the Moho depth differences between gravimetric and seismic results. The histogram of the Moho depth differences between seismic and gravimetric estimates is plotted in Fig. 45a. The systematic bias between the gravimetric and seismic solutions is 1.6 km and the STD is 8.9 km. The Moho depth differences are roughly within ±19 km.

3.3.5.2 Moho model

As stated above, the method applied here for the gravimetric inversion was based on finding the Moho solution that closely agrees with the seismic Moho depths by means of minimizing the MSE between gravimetric and seismic results. The choice of optimal gravimetric solution depends on two input parameters that represent the initial Moho depth and the Moho density contrast. The available data from the KRISP broadband seismic experiment were used to validate results by examining all possible combinations for the Moho mean depth. The final Moho solution is shown in Fig. 46. This model highlights more realistically some regional tectonic features. The gravimetric Moho model relatively closely agrees with seismic results derived from receiver function analysis at EARS sites. We see that the Moho depth variations at these sites are between 8 and 47 km, and more specifically between 22 and 47 km in lowlands.

The deepest Moho is observed in southern Kenya beneath the East of the Archean Tanzanian Craton, with depths there exceeding 40 km in north Zambia and reaching maxima of 47 km in southwest Kenya. The Moho depth shallows substantially

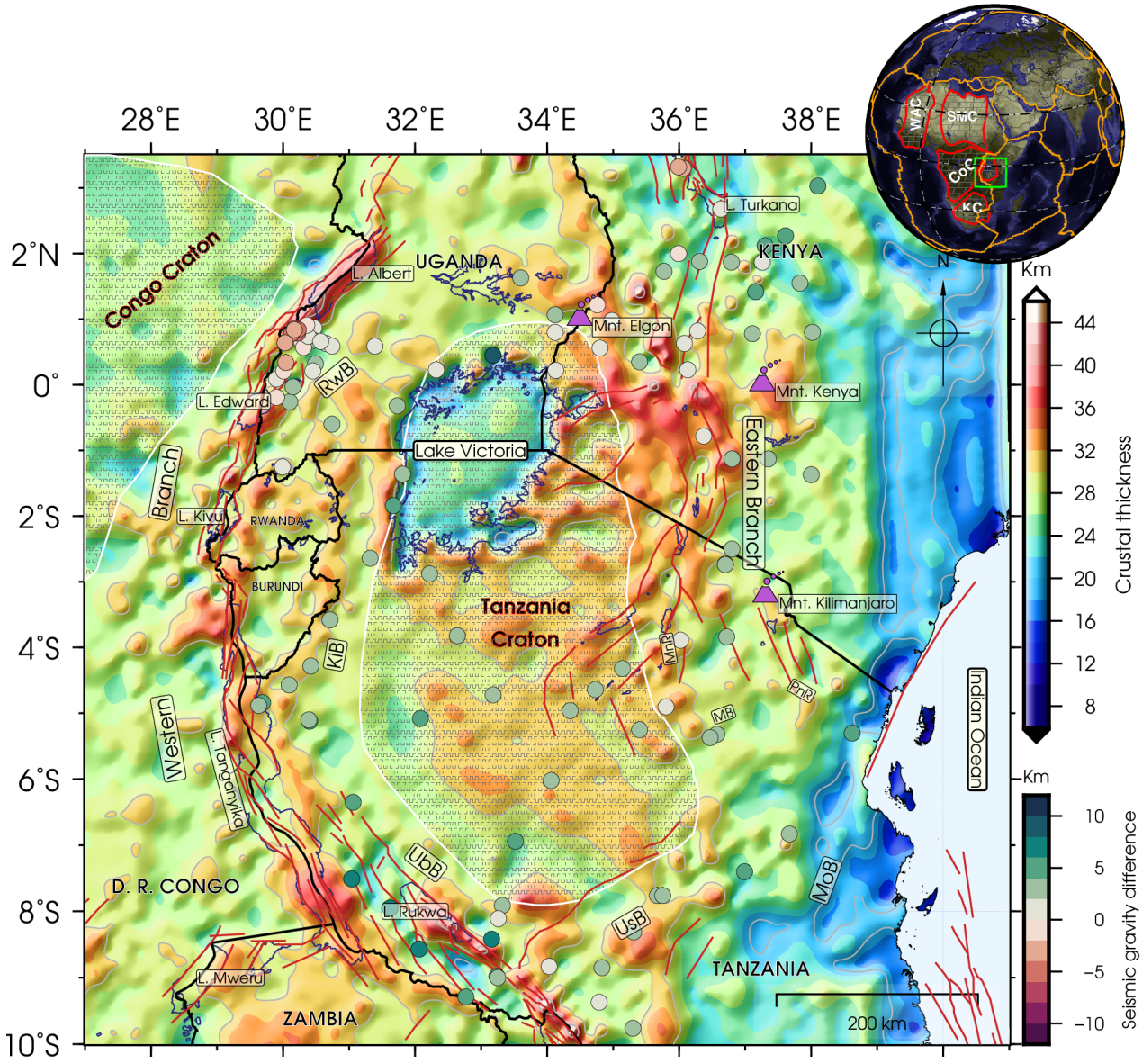

Figure 46: EARS Regional Moho model. Figure also indicates differences between the gravimetric and seismic estimates of the Moho depth at 41 seismic sites (circles).

eastwards from the continent towards continental margins along the Indian Ocean shorelines. Along the Proterozoic terranes, the Moho depth varies from 40 to 45 km, and in the Tanzanian Craton in average from 39.5 km (with the range from 37 km to 42 km) in the south to 44.5 km (with the range from 42.5 to 46.5 km) in the north. Some differences were identified, while comparing the Moho depth in the Proterozoic and Tanzanian Archean Craton terranes at EARS sites. According to studies conducted by (Novak et al., 1997), the Moho depth under the south-eastern and north-western Chyulu Hills reaches 42 and 40 km respectively.

Along the Rwenzori Belt, the Moho depth varies between 34 and 40 km with an average depth of $\backsim$ 37 km. This result is consistent with that reported by Wallner and Schmeling (2011). In the vicinity of the Rwenzori Mountains, within the rift, Moho appears less than 30 km deep. We observe that the Moho depth varies from 27 to 29 km below the northern part of the Rwenzori group, that is slightly thinner than crust under its southern part. A depth of 34 km is under Lake Edward basins, between the eastern part of the rift and the southern part of the Rwenzori Mountains (Wölbern et al., 2010). Beneath the Rwenzori Mountains, Ring (2008) established that the earthquakes extended to the upper mantle at a depth of $35-40$ km, meaning that the lower crust must be very solid and the uplift may have been compensated by the mantle. Within the east branch of the Albertine Rift in Uganda, our result shows that the Moho depth is 30 km. For the Kibaran Belt, the Moho depth is $\backsim$ 39 km. We observe a large crustal thickness variability in this terrane with a significant Moho deepening to about 43 km beneath the southwest margin of Lake Victoria, while a thinner crust in Burundi is characterized by the Moho depth of $\backsim$ 28 km. Along the Ubendian mobile belt, the Moho depth is roughly 42 km. The Moho depth along the Usagaran mobile belt is $\backsim$ 39 km. In the Mozambique Belt, the Moho deepens nearly everywhere less than 28 km. These results are in agreement with findings by Last et al. (1997), Dugda (2005) and Wölbern et al. (2010).

Our spatial variations in Moho depth model indicates a fairly homogeneous thickness under the Rukwa and Tanganyika Rifts with the Moho depth $35-42$ km. This

finding agrees with the result by Tugume et al. (2012). Beneath the Tanganyika rift the Moho depth is gradually increasing towards the south. This variation in the crustal thickness along the rift corresponds to the overlapping of the southern Tanganyika Rift and the northern Rukwa Rift (Hodgson et al., 2017). A Moho depth of 28 km is observed beneath Lake Victoria.

Interestingly, along the East Rift, the Moho depth decreases from 24 km near the coast to 44 km north of Kilimanjaro. To the north, along the rift axis from the Kenya domal uplift towards Lake Turkana, the Moho depth decreases abruptly to $\backsim$ 20 km. The elevation of rift floor there is at its lowest while the amount of extension is higher. This would suggest that the isostatic compensation of the topographic dome of Kenya tends to be obtained by a crustal thickening in addition to a low-density upper mantle material. The observed Moho depth variations can be considered as a function of rift development. The further the rifting process has progressed, the thinner the crust becomes. This result supports the finding of Mechie et al. (1997). They identified a possible presence of a hot mantle material beneath the Kenya Dome (onset of volcanism $15 - 20$ Ma ago) that is compatible with the abrupt change at the rift boundaries.

We have observed some uncertainties due to a fixed value of the Moho density contrast. As expected, the gravitational inversion of a simple two-layer model with a fixed density contrast at the Moho interface introduces uncertainties in estimated Moho depth. Along the edge of the Congo Craton and Lake Victoria, our model underestimates the Moho depth. On the other hand, our model overestimates the Moho depths in the most active and presumably hottest volcanic zone of the Kenya Rift. Particularly along Lake Albert, where our model predicts a Moho depth of about 40 km, and where we observe that differences with seismic estimates can reach or exceed 10 km. This may indicate that the attenuation of the regularization should not be applied unilaterally to the whole model, with the consequence that the model cannot reproduce realistically the Moho depth as indicated by Uieda et al. (2016). Another cause of these disparities may also be the presence of mantle and crustal density

anomalies whose gravitational effects have not been eliminated during gravity data processing. Beneath the Manyara Rift and the Masai Block, our Moho depth model is consistent with gravitric results, but significantly differs from seismic estimates. Chisenga and Yan (2019) and Ghomsi et al. (2019, 2020) have linked these limits to large lateral density variations within the lower crust and uppermost mantle that contributes to the Moho depth estimates from seismic and gravity data.

3.3.6 Discussion of results

The Moho result presented in the preceding section was validated against published results. We also assessed expected uncertainties in our Moho model.

3.3.6.1 Cross comparisons of Moho models

We compared our regional Moho model (shown in Fig. 46) with the global combined gravimetric-seismic model GEMMA (Reguzzoni and Sampietro, 2015) and with two continental-scale models. The Tedla11 model (Tedla et al., 2011) compiled based on gravity modelling was obtained using 3D Euler deconvolution with an output resolution of 0.225°. The Tugume13 model (Tugume et al., 2013) was compiled by applying the Parker-Oldenburg method with a resolution of 0.25°. The comparison of these models revealed remarkable Moho depth differences along the Mozambique Belt, but a close agreement in the south part of the Tanzanian Craton (Figs. 47a-c).

The Moho depth differences between investigated models range within ±5 km over most of regions characterized by a thick continental crust. We observe an anti-correlation between the Tedla11 model and other two models (GEMMA and Tugume13) mainly along margins of the Congo Craton and in the central part of the Tanzanian Craton. These discrepancies have been notified already by Reid et al. (2012). They stated that the Moho model derived by Tedla et al. (2011) based on applying Euler deconvolution produces some misleading results, particularly in the Kaapvaal Craton. A possible reason is that they did not consider geodynamics of the continental evolution, and even more importantly the topographic correction. Thus, their model is not sufficient to capture realistically the Moho depth, but rather den-

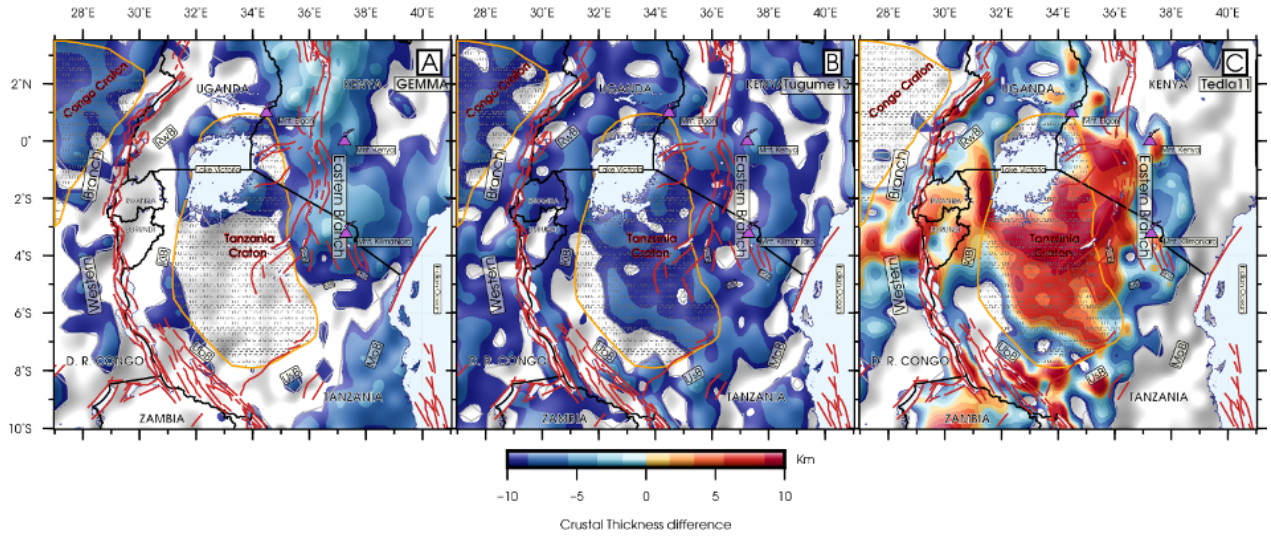

Figure 47: Comparison of our model with the published results: (a) GEMMA (Reguzzoni and Sampietro, 2015), (b) Tegume13 (Tugume et al., 2013), and (c) Tedla11 (Tedla et al., 2011).

sity heterogeneities within the crust and possibly also within the uppermost mantle. Tugume et al. (2013) suggested that these misfits are due to an overestimation of the crustal model by Tedla et al. (2011) caused by considering only a few point constraints on the crustal thickness in Africa.

The Moho variations were correlated with major geologic boundaries. As stated previously, the Mozambique Belt, which consists of the Archaean and Paleoproterozoic gneisses, has been affected by multiple collisional events $450 - 1200$ Myr ago (Walker et al., 2004). Walker et al. (2004) stated that uncertainties in the estimated Moho depth might be due to constant geodynamic modifications of the uppermost mantle, which is restricted along the Kenya Rift. Macheyeki et al. (2008) presented some uncertainties of the crustal root ($2 - 5$ km) between the Tanzanian Craton and the Mozambique Belt and assigned this suture-thickened crust to a localized rifting. The residual maps highlight dissimilarities in spatial variations of rifted orogenic belts (Fig. 46a-c). These features point out the effect of non-collisional events in the West Rift. Along the Albertine Rift developed in the Proterozoic felsic and the western side of the Rwenzori Mountains, we observe good correlation between our and GEMMA models. Attesting that both models are consistent with density heterogeneities within the crust. It is important to state that small differences observed along the West Rift are consistent with the eastern dissection part of the African lithosphere, thereby

separating the study area into the Nubian plate to the west and the Somalian plate to the east (Nyblade, 2002; Calais et al., 2006). Ring (2008) proposed that the uplift of the Rwenzori Mountains is possibly due to the motion of the Archean Tanzanian Craton independently from the plate boundary zone (Somalian and Nubian) situated between both rift branches. This plate boundary zone is being interpreted as a vast zone of a uniformly distributed deformation (Calais et al., 2006). Results of topographic geochronology of the central part of the Rwenzori Mountains indicate their formation between the Pliocene and the Pleistocene, reasoning that its formation has not been due to the Gondwana expansion and pointing out independent stress fields that link the presence of distinct and smaller blocks.

3.3.6.2 Model performances

The Taylor (2001) diagram is a polar coordinate diagram used to highlight similarities or existing differences between observed and simulated datasets. We produced this diagram (Fig. 48) to demonstrate statistical parameters of three Moho models used for the validation of our result on the same grid. The distance between individual foci and the reference field (black circles) refers to the root-mean-square (RMS) difference. Radial black lines exhibit correlation coefficients between modelled and observed fields. The normalized standard deviations are shown by black dashed circles. The Taylor diagram reveals the performance of the Moho models, with the statistical summary in Table 8. We see that TUGUME13 and GEMMA models are clustered and closer to our model than Tedla11. We observe that the Tedla11 model has a good standard deviation that is close to our model. However, it has a lower correlation highlighting its weakness to represent efficiently pattern structures. In general, a higher RMSE is worse than a lower one, as it is the case for Tedla11 model. Thus, GEMMA is more consistent and reliable than Tedla11. Nevertheless, Tugume13 model could also be taken into consideration when looking at its performance. A good agreement between GEMMA and our models are due to applying estimations from satellite gravity data constrained by seismic data at EARS sites.

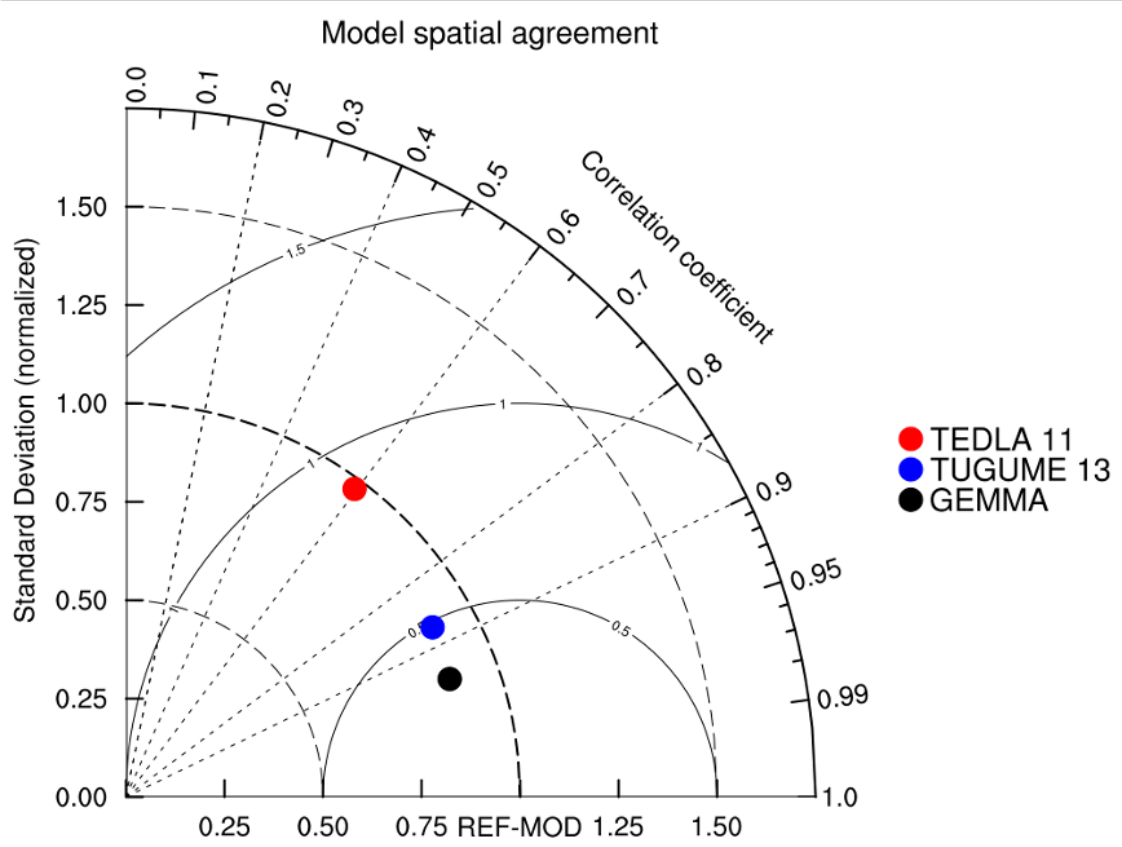

Figure 48: Taylor diagram displaying statistics of comparison of our Moho model with GEMMA, Tegume13, and Tedla11.

Table 8: Statistical comparison between GEMMA, Tugume13, Tedla11 and the Referenced Crustal Models based on Taylor diagram.

Models	Correlation	STD	RMSE
GEMMA	0.93	0.8	0.3
Tugume13	0.87	0.85	0.49
Tedla11	0.6	0.98	0.8

3.3.6.3 Study profile

The profile A-A', which is about 1,333 km long (Figs. 5 and 49), extends along latitude 3.5°S between 27.5°E to 39.5°E longitudes. This W-E profile samples the topographic relief across the West Rift near the northernmost Lake Tanganyika, the Tanzanian Craton, and the East Rift until the Mozambique Belt as well as significant changes in the crustal and upper mantle structures.

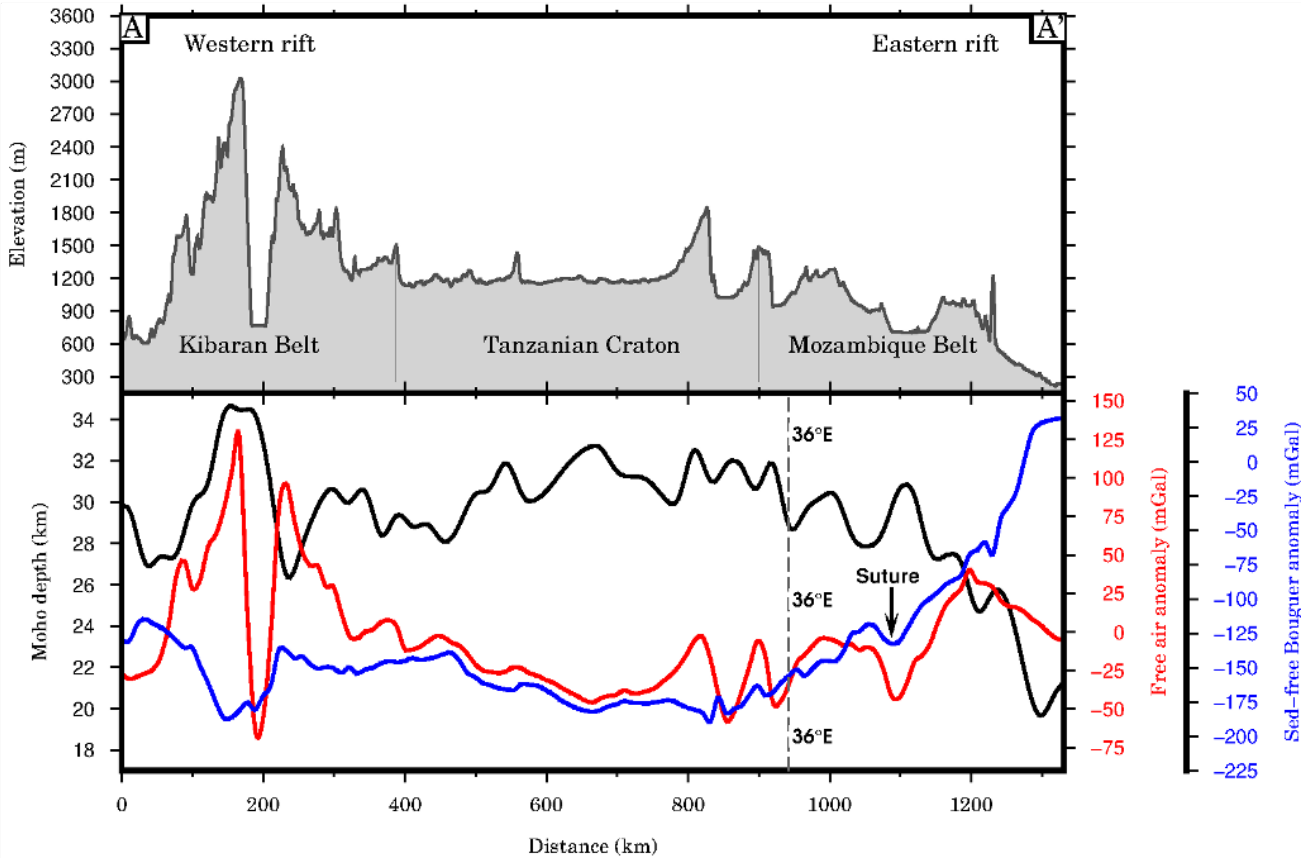

Figure 49: West-East profile showing the Bouguer gravity disturbances, the free-air disturbances, and the Moho depth across Congo and southeast Kenya (see Fig. 5 for profile location). The location of the craton-mobile belt suture is shown by the arrow. Surrounding craton is highly irregular topography associated with the deforming rifts and old orogenic belts.

Along this profile, the topographic elevations merely correlate with the free-air gravity disturbances between the Kibaran and Mozambique Belts. However, the Bouguer gravity disturbances are characterized by a short-wavelength minimum of −200 mGal in the Kibaran Belt across Lake Tanganyika section and coincide well with minima of the free-air gravity disturbances (−75 mGal). The free-air gravity disturbances and the Moho depth undulations along the profile vary in a similar mode

with a thicker crust beneath the Kibaran Belt (35 km), while weakening towards lowlands of the Mozambique Belt (20 km) comprising the Archean basement and several younger metasedimentary sequences through the Archean granitoids, metavolcanics, and metasediments of the Tanzanian Craton (33 km).

The topographic relief and the Moho depth of the Cenozoic West Rift, fully situated within the late Proterozoic mobile belt, varies strongly both across and along the rift. The isostatic compensation between the West and East Rifts is apparent based on comparing gravity disturbances with the Moho depth. The suture is well represented with gravity lows over the craton-mobile belt contact and gravity highs over the mobile belt.

3.3.7 Summary and concluding remarks

We have compiled a new regional model of the Moho depth beneath the rifted orogenic belts and the Archean cratons in Tanzania and Congo margins of the East African Plateau using gravity, topographic, bathymetric, and sediment models constrained by seismic data. The Moho depth estimates were carried out by applying a regularized inversion based on the Gauss-Newton formulation of the improved Bott method with regularization and tesseroid techniques involved.

Our study clearly reveals and highlights the ability of gravity data inversion constrained on available seismic results for studying the crustal configuration of geologically complex formations. Moreover, compared to previous studies, our Moho model shows a better agreement with available seismic estimates than those of global or continental-scale crustal models (such as GEMMA or Tedla11). The reason is that the interpolation of such (large-scale) models on local scales might very likely produce unrealistic Moho depth estimates. According to our model, the Moho depth beneath the East African Rift System ranges from 22 km in the eastern parts of Tanzania and Kenya along coastal regions of the Indian Ocean and deepens to more than 47 km under the Tanzanian Craton. The signature of the Congo Craton in the East African Rift System is marked by a thin crust with the Moho depth generally less than 30

km.

Our model generally agrees with broadband seismic constrained records along with existing gravimetric models. The Moho depth at EARS sites located on the Precambrian craton, including the Tanzanian and Congo Cratons, is generally shallower than at sites located at the Cenozoic orogens, e.g. in southwest Kenya. The Moho depth variations for the Cratonic blocks are from 32 to 47 km. Our study has shown that the orogenic rifted and cratonic geomorphology of the crustal structure beneath EARS sites can realistically be deciphered from gravity data analysis, thus possibly extrapolated even in seismically unconstrained areas. There is, however, an uncertainty involved in the fit between gravity and seismic results, indicating the influence of a fixed value of the Moho density contrast for the gravity inversion.

These disparities between gravimetric and seismological estimates of Moho depth may reflect the presence of other density anomalies in the crust or uppermost mantle. Particularly relevant to active rift zones are large lateral temperature variations within the uppermost mantle that could induce a significant difference between crust composition and density of craters and young areas.

Our result confirmed a non-collisional origin of the Rwenzori Mountains. This is explained by the fact that both, the Archean and Proterozoic uppermost mantle, have not been modified significantly by the rifting. Our Moho depth estimates agree with results from previous studies, especially for the craton and mobile belts. These results assert that the East African Craton is characterized by tectonic stability within a generally mobile and less stable lithosphere. Thus, regarding the Rwenzori Belt, it is considered as the consequence of extreme uplift that is the result of local viscoelastic response of the mantle.

Conclusions and outlook

Conclusions

During this PhD project, new insights on the present-day crustal structure of Atlas Region, Cameroon and surrounding regions, and the East African Rift System consistently with geological and geophysical data, and seismic estimate was developed.

First, we use gravity, topographic, bathymetric and sediment data together with results of seismic surveys to image the Moho topography beneath the Atlas region. The regional gravimetric Moho inversion constrained on seismic data is carried out by applying a regularized inversion technique based on Gauss-Newton's formulation of improved Bott's method, while adopting Earth's spherical approximation.

The numerical result reveals relatively significant Moho depth variations in the Moroccan Atlas, with minima of $\backsim$24 km along continental margins of the Mediterranean Sea and maxima exceeding 51 km beneath the Rif Cordillera. The Moho depth beneath the West African Craton varies from 32 km in its southern margin to 45 km beneath the Middle Atlas. The Tell Atlas is characterized by the shallow Moho depth of $\backsim$22 km and further deepening to 42 km towards the northern edge of the Aures Mountains.

Our findings indicate a limited tectonic shortening of the High Atlas with the crustal thickness mostly within $36 - 42$ km. Topographic discrepancies between the Rif Cordillera and the Atlas Mountains suggest that the hypothesis of isostatic compensation cannot be fully established.

As a second step, we develop a new crustal structure beneath Cameroon and adjoined geological regions based on gravity information obtained from the EIGEN−6C4

global gravitational model together with topographic, bathymetric and seismic data

The gravimetric Moho model obtained from the regularized non-linear gravity inversion constrained on seismic data reflects realistically a regional tectonic configuration and geological structure of this region, generally consisting of two major geological features of the Cameroon Volcanic Line and the Congo Craton. The validation of gravimetric result at sites of the Cameroon Broadband Seismic Experiment (CBSE) reveals overall similarities between gravimetric and seismic estimates. A similar comparison of our result is also conducted with previously published results. The cross-comparison of these results reveals a good agreement between them, particularly beneath the Cameroon Volcanic Line, the Adamawa Plateau and the Garoua Rift.

Nevertheless, some relatively large inconsistencies roughly reaching ± 10 km in estimated values of the Moho depth are also identified in geological regions of the Congo Craton and the Yaoundé domain. The spatial correlation analysis between the Moho geometry and the topography indicates an isostatic state of particular geological units, suggesting their compensation stage. Our result closely agrees with the assumption that most of isostatically over compensated geological structures were formed during a compressional tectonic regime, except for the Garoua Rift that was likely formed during an extensional regime.

Our findings indicate that the Yaoundé domain likely represents the crustal manifestation of the suture zone between the Adamawa-Yadé domain, acting as a microcontinent and the Congo Craton.

Furthermore, along the Tanzanian Craton (including parts of the East African Rift System and the Congo Craton) The Moho model exhibits the contrast between a thin Archean block compared to a thicker crust of the Phanerozoic orogenic block. The Moho depth beneath the Archean Tanzanian Craton is typically within 34 km in south and 45 km at its northern margin.

The maximum Moho deepening ($\backsim$ 47 km) is predicted under the southwest part of Kenya near the Eyasi Rift. Along the western branch of the East African Rift System, from Lake Tanganyika to the Rwenzori Mountains, the Moho depth varies

within $35 - 43$ km. Further south, in northern Tanzania, the Moho depth slightly decreases to $35 - 39$ km in the locus of rifting, then slightly increases to $36 - 39$ km along the Proterozoic Mozambique Orogenic Belt, and reaches $38 - 42$ km depth in the craton.

Along with the Cenozoic Kenya Rift structure, we observe crustal thinning and an anomalous mantle, widening northwards in agreement with existing studies, with the Moho depth shallowing from $\backsim$ 35 km in the south to only $\backsim$ 20 km in the north. According to our result, a thick lower crust beneath the Rwenzori Belt could be associated with a crustal modification occurring during rifting episodes that induced the delamination of the lithospheric mantle and consequently resulted in crustal uplift. These findings support a non-collisional origin of the central Rwenzori Mountains

The overall new crustal model presented here studying the density contrast of geologically- interesting formations, where the Bouguer anomaly data is combined with a priori information retrieved from sediments contribution and seismic datasets. Compared to previous studies, the developed gravity-based Moho model shows a better match with the available seismic studies than that of the global crustal model (e.g., the GEMMA, TUGUME and TEDLA), in which the interpolation of such global models on local scales might produce unrealistic Moho depth values.

In summary, this Thesis has provided new insights on the present-day crustal structure of three African hots consistently with geological and geophysical data, and seismic estimates. Hopefully, this work will help to better understand the mantle structure and its contribution to the present configuration of African Archean cratons and the Cameroon Volcanic Lines.

Outlook

The research conducted through this thesis has shown several issues and limitations which should be considered and solved in future research. In this section, some recommendations for future work are addressed.

▷ Development of fast numerical algorithms and software packages for the gravi-

metric forward and inverse modelling based on the modified Parker-Oldenburg method for Earth's spherical approximation and solved by employing the Fast Fourier Transformation (FFT) technique.

- ▷ Development of the new crustal density model for Africa (with the spatial resolution of about 10 km) based on the analysis of in situ measurements of rock density samples and geological maps, while incorporating also empirical density models (of seawater, marine sediments, etc.)

- ▷ Development of the new Moho depth model for Africa (with the spatial resolution of about 10 km and the expected accuracy of $3 - 5$ km) from gravity data and constrained on seismic estimates of the Moho depth.

Bibliography

Adams, A., A. Nyblade, and D. Weeraratne, 2012: Upper mantle shear wave velocity structure beneath the east African plateau: evidence for a deep, plateau wide low velocity anomaly. *Geophysical Journal International*, **189**, 123–142. doi: 10.1111/j.1365-246x.2012.05373.x.

Airy, 1855: III. on the computation of the effect of the attraction of mountain-masses, as disturbing the apparent astronomical latitude of stations in geodetic surveys. *Philosophical Transactions of the Royal Society of London*, **145**, 101–104. doi: 10.1098/rstl.1855.0003.

Albaric, J., J. Déverchère, C. Petit, J. Perrot, and B.L. Gall, 2009: Crustal rheology and depth distribution of earthquakes: Insights from the Central and Southern East African Rift System. *Tectonophysics*, **468**, 28–41. doi: 10.1016/j.tecto.2008.05.021.

Amante, C., and B.W. Eakins, 2009: Etopo1 arc-minute global relief model: procedures, data sources and analysis. pp. 19.

Andersen, O.B., P. Knudsen, and P.A.M. Berry, 2009: The DNSC08gra global marine gravity field from double retracked satellite altimetry. *Journal of Geodesy*, **84**, 191–199. doi: 10.1007/s00190-009-0355-9.

Anderson, E.G., 1976: The effect of topography on solutions of stokes' problem. *Kensington, NSW, Australia: School of Surveying, University of New South Wales.*

Anderson, J.E., 1996: The neogene structural evolution of the Western margin of the Pelagian platform, Central Tunisia. *Journal of Structural Geology*, **18**, 819–833. doi: 10.1016/s0191-8141(96)80015-0.

Anderson, K.F., F. Wall, G.K. Rollinson, and C.J. Moon, 2014: Quantitative mineralogical and chemical assessment of the Nkout iron ore deposit, Southern Cameroon. *Ore Geology Reviews*, **62**, 25–39. doi: 10.1016/j.oregeorev.2014.02.015.

Angue, M.L.C.O., S. Nguiya, R. Nouayou, A.P.T. Kamga, and E. Manguelle-Dicoum, 2011: Geophysical investigation of the transition zone between the Congo Craton and the Kribi-Campo sedimentary basin (southestern Cameroon). *South African Journal of Geology*, **114**, 145–158. doi: 10.2113/gssajg.114.2.145.

Arfaoui, M., A. Reid, and M.H. Inoubli, 2015: Evidence for a new regional NW-SE fault and crustal structure in Tunisia derived from gravity data. *Geophysical Prospecting*, **63**, 1272–1283. doi: 10.1111/1365-2478.12248.

Asfirane, F., and A. Galdeano, 1995: The aeromagnetic map of northern Algeria: Processing and interpretation. *Earth and Planetary Science Letters*, **136**, 61–78. doi: 10.1016/0012-821x(95)00043-4.

Asgharzadeh, M.F., R.R.B. von Frese, H.R. Kim, T.E. Leftwich, and J.W. Kim, 2007: Spherical prism gravity effects by Gauss-Legendre quadrature integration. *Geophysical Journal International*, **169**, 1–11. doi: 10.1111/j.1365-246x.2007.03214.x.

Ayarza, P., F. Alvarez-Lobato, A. Teixell, M. Arboleya, E. Tesón, M. Julivert, and M. Charroud, 2005: Crustal structure under the Central High Atlas mountains (Morocco) from geological and gravity data. *Tectonophysics*, **400**, 67–84. doi: 10.1016/j.tecto.2005.02.009.

Ayarza, P., R. Carbonell, A. Teixell, I. Palomeras, D. Martí, A. Kchikach, M. Harnafi, A. Levander, J. Gallart, M.L. Arboleya, J. Alcalde, M. Fernández, M. Charroud, and M. Amrhar, 2014: Crustal thickness and velocity structure across the Moroccan Atlas from long offset wide-angle reflection seismic data: The SIMA experiment. *Geochemistry, Geophysics, Geosystems*, **15**, 1698–1717. doi: 10.1002/2013gc005164.

Bagherbandi, M., R. Tenzer, L.E. Sjöberg, and P. Novák, 2013: Improved global crustal thickness modeling based on the VMM isostatic model and non-isostatic gravity correction. *Journal of Geodynamics*, **66**, 25–37. doi: 10.1016/j.jog.2013.01.002.

Balmino, G., F. Perosanz, R. Rummel, N. Sneeuw, and H. Sunkel, 1999: CHAMP, GRACE and GOCE: Mission concepts and simulations. *Bollettino di Geofisica Teorica ed Applicata*, **40**, 309–319.

Baranov, A., and A. Bobrov, 2018: Crustal structure and properties of archean cratons of Gondwanaland: similarity and difference. *Russian Geology and Geophysics*, **59**, 512–524. doi: 10.1016/j.rgg.2018.04.005.

Bastow, I.D., G.W. Stuart, J.M. Kendall, and C.J. Ebinger, 2005: Upper-mantle seismic structure in a region of incipient continental breakup: northern Ethiopian rift. *Geophysical Journal International*, **162**, 479–493. doi: 10.1111/j.1365-246x.2005.02666.x.

Begg, G., W. Griffin, L. Natapov, S.Y. O'Reilly, S. Grand, C. O'Neill, J. Hronsky, Y.P. Djomani, C. Swain, T. Deen, and P. Bowden, 2009: The lithospheric architecture of Africa: Seismic tomography, mantle petrology and tectonic evolution. *Geosphere*, **5**, 23–50. doi: 10.1130/ges00179.1.

Bird, P., 2003: An updated digital model of plate boundaries. *Geochemistry, Geophysics, Geosystems*, **4**. doi: 10.1029/2001gc000252.

Birt, C., P. Maguire, M. Khan, H. Thybo, G. Keller, and J. Patel, 1997: The influence of pre-existing structures on the evolution of the Southern Kenya rift valley — evidence from seismic and gravity studies. *Tectonophysics*, **278**, 211–242.

Blundell, D.J., R. Freeman, and S. Mueller (Eds.), 1992: *A Continent Revealed*. Cambridge University Press.

Bonjer, K.P., K. Fuchs, and J. Wohlenberg, 1970: *Crustal structure of the East African Rift System from spectral response ratios of long-period body waves.* Geophysical Inst.

Bott, M.H.P., 1960: The use of rapid digital computing methods for direct gravity interpretation of sedimentary basins. *Geophysical Journal International*, **3**, 63–67.

Bruinsma, S.L., C. Förste, O. Abrikosov, J.M. Lemoine, J.C. Marty, S. Mulet, M.H. Rio, and S. Bonvalot, 2014: ESA's satellite-only gravity field model via the direct approach based on all GOCE data. *Geophysical Research Letters*, **41**, 7508–7514. doi: 10.1002/2014gl062045.

Burke, K., and J.T. Wilson, 1972: Is the African plate stationary? *Nature*, **239**, 387–390. doi: 10.1038/239387b0.

Calais, E., C. Ebinger, C. Hartnady, and J. Nocquet, 2006: Kinematics of the east African rift from GPS and earthquake slip vector data. *Geological Society, London, Special Publications*, **259**, 9–22. doi: 10.1144/gsl.sp.2006.259.01.03.

Chisenga, C., and J. Yan, 2019: A new crustal thickness model for mainland china derived from EIGEN-6c4 gravity data. *Journal of Asian Earth Sciences*, **179**, 430–442. doi: 10.1016/j.jseaes.2019.05.011.

Chorowicz, J., 2005: The east African Rift System. *Journal of African Earth Sciences*, **43**, 379–410. doi: 10.1016/j.jafrearsci.2005.07.019.

Civiero, C., V. Strak, S. Custódio, G. Silveira, N. Rawlinson, P. Arroucau, and C. Corela, 2018: A common deep source for upper-mantle upwellings below the Ibero-Western Maghreb region from teleseismic P-wave travel-time tomography. *Earth and Planetary Science Letters*, **499**, 157–172.

Contrucci, I., F. Klingelhöfer, J. Perrot, R. Bartolome, M.A. Gutscher, M. Sahabi, J. Malod, and J.P. Rehault, 2004: The crustal structure of the NW Moroccan continental margin from wide-angle and reflection seismic data. *Geophysical Journal International*, **159**, 117–128. doi: 10.1111/j.1365-246x.2004.02391.x.

Cooper, C., and M. Miller, 2014: Craton formation: Internal structure inherited from closing of the early oceans. *Lithosphere*, **6**, 35–42. doi: 10.1130/l321.1.

Coulon, C., P. Vidal, C. Dupuy, P. Baudin, M. Popoff, H. Maluski, and D. Hermitte, 1996: The mesozoic to early Cenozoic magmatism of the Benue Trough (Nigeria); geochemical evidence for the involvement of the St Helena plume. *Journal of Petrology*, **37**, 1341–1358.

Dawson, J., 1992: Neogene tectonics and volcanicity in the north Tanzania sector of the gregory rift valley: contrasts with the Kenya sector. *Tectonophysics*, **204**, 81–92. doi: 10.1016/0040-1951(92)90271-7.

Delvaux, D., 2001: Tectonic and palaeostress evolution of the Tanganyika-Rukwa-Malawi rift segment, East African Rift System. *Peri-Tethys Memoir*, **6**, 545–567.

der Meijde, M.V., and A. Nyblade, 2013: Reply to "comment on 'A crustal thickness map of Africa derived from a global gravity field model using Euler deconvolution"'. *Geophysical Journal In-*

ternational, **196**, 96–99. doi: 10.1093/gji/ggt450.

der Meijde, M.V., and R. Pail, 2020: Impact of uncertainties of GOCE gravity model on crustal thickness estimates. *Geophysical Journal International*. doi: 10.1093/gji/ggaa073.

Diaz, J., J. Gallart, and R. Carbonell, 2016: Moho topography beneath the Iberian-Western mediterranean region mapped from controlled-source and natural seismicity surveys. *Tectonophysics*, **692**, 74–85. doi: 10.1016/j.tecto.2016.08.023.

Dugda, M.T., 2005: Crustal structure in Ethiopia and Kenya from receiver function analysis: Implications for rift development in Eastern Africa. *Journal of Geophysical Research*, **110**. doi: 10.1029/2004jb003065.

Ebinger, C., Y.P. Djomani, E. Mbede, A. Foster, and J.B. Dawson, 1997: Rifting Archean lithosphere: the Eyasi-Manyara-Natron rifts, East Africa. *Journal of the Geological Society*, **154**, 947–960. doi: 10.1144/gsjgs.154.6.0947.

Ebinger, C.J., D. Keir, I.D. Bastow, K. Whaler, J.O.S. Hammond, A. Ayele, M.S. Miller, C. Tiberi, and S. Hautot, 2017: Crustal structure of active deformation zones in Africa: Implications for global crustal processes. *Tectonics*, **36**, 3298–3332. doi: 10.1002/2017tc004526.

Elsheikh, A., S. Gao, and K. Liu, 2014: Formation of the Cameroon Volcanic Line by lithospheric basal erosion: Insight from mantle seismic anisotropy. *Journal of African Earth Sciences*, **100**, 96–108. doi: 10.1016/j.jafrearsci.2014.06.011.

Ennih, N., and J.P. Liégeois, 2008: The boundaries of the west African craton, with special reference to the basement of the Moroccan metacratonic anti-Atlas belt. *Geological Society, London, Special Publications*, **297**, 1–17. doi: 10.1144/sp297.1.

Eyike, A., and J. Ebbing, 2015: On the use of global potential field models for regional interpretation of the West and Central African Rift System. tectonophysics. *South African Journal of Geology*, **118**, 285–298. doi: 10.2113/gssajg.118.3.285.

Fairhead, J., 1976: The structure of the lithosphere beneath the Eastern rift, East Africa, deduced from gravity studies. *Tectonophysics*, **30**, 269–298. doi: 10.1016/0040-1951(76)90190-6.

Fishwick, S., and I.D. Bastow, 2011: Towards a better understanding of African topography: a review of passive-source seismic studies of the African crust and upper mantle. *Geological Society, London, Special Publications*, **357**, 343–371. doi: 10.1144/sp357.19.

Fitton, J.G., 1987: The Cameroon line, West Africa: a comparison between oceanic and continental alkaline volcanism. *Geological Society, London, Special Publications*, **30**, 273–291. doi: 10.1144/gsl.sp.1987.030.01.13.

Förste, C., S. Bruinsma, O. Abrikosov, J. Lemoine, T. Schaller, H. Götze, J. Ebbing, J. Marty, F. Flechtner, and G. Balmino, 2014: Eigen-6c4 the latest combined global gravity field model including GOCE data up to degree and order 2190 of GFZ Potsdam and GRGS Toulouse. *In: EGU General Assembly 2014, Vienna, 27 April–2 May 2014*. doi: 10.5880/icgem.2015.1.

Fritz, H., V. Tenczer, C.A. Hauzenberger, E. Wallbrecher, G. Hoinkes, S. Muhongo, and A. Mogessie, 2005: Central Tanzanian tectonic map: A step forward to decipher Proterozoic structural events in the East African orogen. *Tectonics*, **24**, 1–26. doi: 10.1029/2005tc001796.

Fuchs, K., 1997: Structure and dynamic processes in the lithosphere of the Afro-Arabian Rift System. *Tectonophysics*, **278**.

Fullea, J., M. Fernàndez, and H. Zeyen, 2008: FA2BOUG—a FORTRAN 90 code to compute Bouguer gravity anomalies from gridded free-air anomalies: Application to the Atlantic-Mediterranean transition zone. *Computers & Geosciences*, **34**, 1665–1681. doi: 10.1016/j.cageo.2008.02.018.

Gallacher, R.J., and I.D. Bastow, 2012: The development of magmatism along the Cameroon Volcanic Line: Evidence from teleseismic receiver functions. *Tectonics*, **31**. doi: 10.1029/2011tc003028.

Gao, S.S., K.H. Liu, C.A. Reed, Y. Yu, B. Massinque, H. Mdala, M. Moidaki, D. Mutamina, E.A. Atekwana, S. Ingate, and A.M. Reusch, 2013: Seismic arrays to study African rift initiation. *Eos, Transactions American Geophysical Union*, **94**, 213–214. doi: 10.1002/2013eo240002.

Gerlach, C., N. Sneeuw, P. Visser, and D. Švehla, 2003: CHAMP gravity field recovery with the energy balance approach: First results. In: *First CHAMP Mission Results for Gravity, Magnetic and Atmospheric Studies*, pp. 134–139. Springer Berlin Heidelberg. doi: 10.1007/978-3-540-38366-6_20.

Ghomsi, F.E.K., N. Sévérin, A. Mandal, F.E.A. Nyam, R. Tenzer, A.P.T. Kamga, and R. Nouayou, 2020: Cameroon's crustal configuration from global gravity and topographic models and seismic data. *Journal of African Earth Sciences*, **161**, 103657. doi: 10.1016/j.jafrearsci.2019.103657.

Ghomsi, F.E.K., R. Tenzer, N. Sévérin, A. Mandal, and R. Nouayou, 2019: Crustal thickness beneath Atlas region from gravity, topographic, sediment and seismic data. *Geodesy and Geodynamics*, **11**, 18–30. doi: 10.1016/j.geog.2019.08.002.

Giese, P., and V. Jacobshagen, 1992: Inversion tectonics of intracontinental ranges: High and middle Atlas, Morocco. *Geologische Rundschau*, **81**, 249–259. doi: 10.1007/bf01764553.

Gil, A., J. Gallart, J. Diaz, R. Carbonell, M. Torne, A. Levander, and M. Harnafi, 2014: Crustal structure beneath the Rif Cordillera, North Morocco, from the RIFSIS wide-angle reflection seismic experiment. *Geochemistry, Geophysics, Geosystems*, **15**, 4712–4733. doi: 10.1002/2014gc005485.

Gladkikh, V., and R. Tenzer, 2011: A mathematical model of the global ocean saltwater density distribution. *Pure and Applied Geophysics*, **169**, 249–257. doi: 10.1007/s00024-011-0275-5.

Globig, J., M. Fernàndez, M. Torne, J. Vergés, A. Robert, and C. Faccenna, 2016: New insights into the crust and lithospheric mantle structure of Africa from elevation, geoid, and thermal analysis. *Journal of Geophysical Research: Solid Earth*, **121**, 5389–5424. doi: 10.1002/2016jb012972.

Gomez, F., R. Allmendinger, M. Barazangi, A. Er-Raji, and M. Dahmani, 1998: Crustal shortening

and vertical strain partitioning in the Middle Atlas Mountains of Morocco. *Tectonics*, **17**, 520–533. doi: 10.1029/98tc01439.

Guidarelli, M., and A. Aoudia, 2016: Ambient noise tomography of the Cameroon Volcanic Line and Northern Congo craton: new constraints on the structure of the lithosphere. *Geophysical Journal International*, **204**, 1756–1765. doi: 10.1093/gji/ggv561.

Hebert, L., and C.A. Langston, 1985: Crustal thickness estimate at AAE (Addis-Ababa, Ethiopia) and NAI (Nairobi, Kenya) using teleseismic P-wave conversions. *Tectonophysics*, **111**, 299–327. doi: 10.1016/0040-1951(85)90290-2.

Henry, W.J., J. Mechie, P.K.H. Maguire, M.A. Khan, C. Prodehl, G.R. Keller, and J. Patel, 1990: A seismic investigation of the Kenya rift valley. *Geophysical Journal International*, **100**, 107–130. doi: 10.1111/j.1365-246x.1990.tb04572.x.

Hinze, W.J., 2003: Bouguer reduction density, why 2.67? *Geophysics*, **68**, 1559–1560.

Hodgson, I., F. Illsley-Kemp, R.J. Gallacher, D. Keir, C.J. Ebinger, and K. Mtelela, 2017: Crustal structure at a young continental rift: A receiver function study from the Tanganyika rift. *Tectonics*, **36**, 2806–2822. doi: 10.1002/2017tc004477.

Huerta, A.D., A.A. Nyblade, and A.M. Reusch, 2009: Mantle transition zone structure beneath Kenya and Tanzania: more evidence for a deep-seated thermal upwelling in the mantle. *Geophysical Journal International*, **177**, 1249–1255. doi: 10.1111/j.1365-246x.2009.04092.x.

Jacobsen, B.H., 1987: A case for upward continuation as a standard separation filter for potential-field maps. *GEOPHYSICS*, **52**, 1138–1148. doi: 10.1190/1.1442378.

Jallouli, C., and K. Mickus, 2000: Regional gravity analysis of the crustal structure of Tunisia. *Journal of African Earth Sciences*, **30**, 63–78. doi: 10.1016/s0899-5362(00)00008-7.

Jallouli, C., S. Mogren, K. Mickus, and M.M. Turki, 2013: Evidence for an east–west regional gravity trend in northern Tunisia: Insight into the structural evolution of northern Tunisian Atlas. *Tectonophysics*, **608**, 149–160. doi: 10.1016/j.tecto.2013.10.003.

Jessell, M.W., G.C. Begg, and M.S. Miller, 2016: The geophysical signatures of the west African craton. *Precambrian Research*, **274**, 3–24. doi: 10.1016/j.precamres.2015.08.010.

Julià, J., C.J. Ammon, and A.A. Nyblade, 2005: Evidence for mafic lower crust in Tanzania, east Africa, from joint inversion of receiver functions and Rayleigh wave dispersion velocities. *Geophysical Journal International*, **162**, 555–569. doi: 10.1111/j.1365-246x.2005.02685.x.

Kampunzu, A., M. Bonhomme, and M. Kanika, 1998: Geochronology of volcanic rocks and evolution of the Cenozoic Western Branch of the East African Rift System. *Journal of African Earth Sciences*, **26**, 441–461. doi: 10.1016/s0899-5362(98)00025-6.

Kim, J.H., 2009: Estimating classification error rate: Repeated cross-validation, repeated hold-out and bootstrap. *Computational statistics and data analysis*, **53**, 3735–3745.

Knapmeyer-Endrun, B., F. Kruger, and t. P. W. Group, 2014: Moho depth across the Trans-European

Suture Zone from P- and S-receiver functions. *Geophysical Journal International*, **197**, 1048–1075. doi: 10.1093/gji/ggu035.

Kosarian, M., 2006: *Lithospheric structure of North Africa and Western Eurasia.* Ph. D. thesis, The Pennsylvania State Univ.

KRISP, 1987: Structure of the Kenya rift from seismic refraction. *Nature*, **325**, 239–242. doi: 10.1038/325239a0.

Laske, G., G. Masters, Z. Ma, and M. Pasyanos, 2013: Update on CRUST1.0 - A 1-degree Global Model of Earth's Crust. In: *EGU General Assembly Conference Abstracts*, EGU General Assembly Conference Abstracts, pp. 2658.

Last, R.J., A.A. Nyblade, C.A. Langston, and T.J. Owens, 1997: Crustal structure of the East African Plateau from receiver functions and rayleigh wave phase velocities. *Journal of Geophysical Research: Solid Earth*, **102**, 24469–24483. doi: 10.1029/97jb02156.

Lee, D.C., A.N. Halliday, J. Fitton, and G. Poli, 1994: Isotopic variations with distance and time in the volcanic islands of the Cameroon line: evidence for a mantle plume origin. *Earth and Planetary Science Letters*, **123**, 119–138. doi: 10.1016/0012-821x(94)90262-3.

Leo, J.F.D., J. Wookey, J.M. Kendall, and N.D. Selby, 2015: Probing the edge of the West African craton: A first seismic glimpse from Niger. *Geophysical Research Letters*, **42**, 1694–1700. doi: 10.1002/2014gl062502.

Leonov, A., 2011: Extraoptimal a posteriori estimates of the solution accuracy in the ill-posed problems of the continuation of potential geophysical fields. *Izvestiya, Physics of the Solid Earth*, **47**, 531–540.

Liu, H.S., 1977: Convection pattern and stress system under the African plate. *Physics of the Earth and Planetary Interiors*, **15**, 60–68. doi: 10.1016/0031-9201(77)90010-3.

Macheyeki, A.S., D. Delvaux, M.D. Batist, and A. Mruma, 2008: Fault kinematics and tectonic stress in the seismically active Manyara–Dodoma Rift segment in Central Tanzania – implications for the East African Rift. *Journal of African Earth Sciences*, **51**, 163–188. doi: 10.1016/j.jafrearsci.2008.01.007.

Makris, J., A. Demnati, and J. Klussmann, 1985: Deep seismic soundings in Morocco and a crust and upper mantle model deduced from seismic and gravity data. In: *Annales geophysicae (1983)*, Volume 3, pp. 369–380.

Mancilla, F.d.L., and J. Diaz, 2015: High resolution moho topography map beneath Iberia and northern Morocco from receiver function analysis. *Tectonophysics*, **663**, 203–211. doi: 10.1016/j.tecto.2015.06.017.

Mancilla, F.d.L., D. Stich, J. Morales, J. Julià, J. Diaz, A. Pazos, D. Córdoba, J.A. Pulgar, P. Ibarra, M. Harnafi, and F. Gonzalez-Lodeiro, 2012: Crustal thickness variations in northern Morocco. *Journal of Geophysical Research: Solid Earth*, **117**. doi: 10.1029/2011jb008608.

Manya, S., and M. Maboko, 2003: Dating basaltic volcanism in the neoarchaean sukumaland greenstone belt of the tanzania craton using the sm–nd method: implications for the geological evolution of the tanzania craton. *Precambrian Research*, **121**, 35–45. doi: 10.1016/s0301-9268(02)00195-x.

Marcel, J., J.M.A. Essi, J.L. Meli'i, P.N. Nouck, A. Mahamat, and E. Manguelle-Dicoum, 2018: Geodynamic insights of the Cameroon Volcanic Line (Western Africa) from isostatic gravity anomalies. *Journal of Geodynamics*, **121**, 36–48. doi: 10.1016/j.jog.2018.07.002.

Mariani, P., C. Braitenberg, and N. Ussami, 2013: Explaining the thick crust in Paraná basin, Brazil, with satellite GOCE gravity observations. *Journal of South American Earth Sciences*, **45**, 209–223. doi: 10.1016/j.jsames.2013.03.008.

Mayer-Guerr, T., 2015: The combined satellite gravity field model GOCO05s. In: *EGU general assembly conference abstracts*, Volume 17.

McCall, G., 1957: The Menengai caldera, Kenya Colony. In: *Proceedings of the 20th International Geological Congress, Mexico*, pp. 55–69.

McConnell, R.B., 1972: Geological development of the Rift System of Eastern Africa. *Geological Society of America Bulletin*, **83**, 2549.

Mechie, J., G. Keller, C. Prodehl, M. Khan, and S. Gaciri, 1997: A model for the structure, composition and evolution of the Kenya rift. *Tectonophysics*, **278**, 95–119. doi: 10.1016/s0040-1951(97)00097-8.

Meng, X., L. Guo, Z. Chen, S. Li, and L. Shi, 2009: A method for gravity anomaly separation based on preferential continuation and its application. *Applied Geophysics*, **6**, 217–225. doi: 10.1007/s11770-009-0025-y.

Mickus, K., and C. Jallouli, 1999: Crustal structure beneath the Tell and Atlas Mountains (Algeria and Tunisia) through the analysis of gravity data. *Tectonophysics*, **314**, 373–385. doi: 10.1016/s0040-1951(99)00225-5.

Möller, A., K. Mezger, and V. Schenk, 2000: U–pb dating of metamorphic minerals: Pan-African metamorphism and prolonged slow cooling of high pressure granulites in Tanzania, East Africa. *Precambrian Research*, **104**, 123–146. doi: 10.1016/s0301-9268(00)00086-3.

Mueller, S., and K.P. Bonjer, 1973: Average structure of the crust and upper mantle in East Africa. *Tectonophysics*, **20**, 283–293. doi: 10.1016/0040-1951(73)90117-0.

Ngako, V., 1999: Les déformations continentales panAfricaines en afrique Centrale: résultat d'un poinçonnement de type himalayen. *Th ese Doctorat d'Etat, Univ. Yaoundé I*, 241.

Ngako, V., E. Njonfang, F.T. Aka, P. Affaton, and J.M. Nnange, 2006: The North–South Paleozoic to Quaternary trend of alkaline magmatism from Niger–Nigeria to Cameroon: Complex interaction between hotspots and Precambrian faults. *Journal of African Earth Sciences*, **45**, 241–256. doi: 10.1016/j.jafrearsci.2006.03.003.

Ngalamo, J.F.G., M. Sobh, D. Bisso, M.G. Abdelsalam, E. Atekwana, and G.E. Ekodeck, 2018: Lithospheric structure beneath the Central Africa Orogenic Belt in Cameroon from the analysis of satellite gravity and passive seismic data. *Tectonophysics*, **745**, 326–337. doi: 10.1016/j.tecto.2018.08.015.

Ngatchou, E.H., L. Genyou, T.C. Tabod, J. Kamguia, S. Nguiya, A. Tiedeu, and K. Xiaoping, 2014: Crustal structure beneath Cameroon from EGM2008. *Geodesy and Geodynamics*, **5**, 1–10.

Nkoumbou, C., P. Barbey, C. Yonta-Ngouné, J. Paquette, and F. Villiéras, 2014: Pre-collisional geodynamic context of the Southern margin of the Pan-African fold belt in Cameroon. *Journal of African Earth Sciences*, **99**, 245–260. doi: 10.1016/j.jafrearsci.2013.10.002.

Nnange, J., V. Ngako, J. Fairhead, and C. Ebinger, 2000: Depths to density discontinuities beneath the Adamawa Plateau region, Central Africa, from spectral analyses of new and existing gravity data. *Journal of African Earth Sciences*, **30**, 887–901. doi: 10.1016/s0899-5362(00)00058-0.

Nolet, G., and S. Mueller, 1982: A model for the deep structure of the East African Rift System from simultaneous inversion of teleseismic data. *Tectonophysics*, **84**, 151–178. doi: 10.1016/0040-1951(82)90158-5.

Novak, O., C. Prodehl, A. Jacob, and W. Okoth, 1997: Crustal structure of the southeastern flank of the Kenya rift deduced from wide-angle P-wave data. *Tectonophysics*, **278**, 171–186. doi: 10.1016/s0040-1951(97)00100-.

Nunn, J.A., and J.R. Aires, 1988: Gravity anomalies and flexure of the lithosphere at the Middle Amazon Basin, Brazil. *Journal of Geophysical Research: Solid Earth*, **93**, 415–428. doi: 10.1029/jb093ib01p00415.

Nyblade, A.A., 2002: Crust and upper mantle structure in East Africa: Implications for the origin of Cenozoic rifting and volcanism and the formation of magmatic rifted margins. In: *Volcanic Rifted Margins*. Geological Society of America. doi: 10.1130/0-8137-2362-0.15.

Nyblade, A.A., C.A. Langston, R.J. Last, C. Birt, and T.J. Owens, 1996: Seismic experiment reveals rifting of craton in Tanzania. *Eos, Transactions American Geophysical Union*, **77**, 517. doi: 10.1029/96eo00339.

Nyblade, A.A., and H.N. Pollack, 1992: A gravity model for the lithosphere in Western Kenya and northeastern Tanzania. *Tectonophysics*, **212**, 257–267. doi: 10.1016/0040-1951(92)90294-g.

Nzenti, J.P., B. Kapajika, G. Wörner, and T.R. Lubala, 2006: Synkinematic emplacement of granitoids in a Pan-African shear zone in Central Cameroon. *Journal of African Earth Sciences*, **45**, 74–86. doi: 10.1016/j.jafrearsci.2006.01.005.

Ojo, A.O., S. Ni, J. Xie, and L. Zhao, 2019: Further constraints on the shear wave velocity structure of Cameroon from joint inversion of receiver function, rayleigh wave dispersion and ellipticity measurements. *Geophysical Journal International*, **217**, 589–619. doi: 10.1093/gji/ggz008.

Ojo, A.O., L. Zhao, and X. Wang, 2019: Estimations of sensor misorientation for broadband seismic

stations in and around Africa. *Seismological Research Letters*, **90**, 2188–2204. doi: 10.1785/0220190103.

Okereke, C.S., 1988: Contrasting modes of rifting: The Benue Trough and Cameroon Volcanic Line, West Africa. *Tectonics*, **7**, 775–784. doi: 10.1029/tc007i004p00775.

Oldenburg, D.W., 1974: The inversion and interpretation of gravity anomalies. *Geophysics*, **39**, 526–536. doi: 10.1190/1.1440444.

Owens, T.J., A.A. Nyblade, H. Gurrola, and C.A. Langston, 2000: Mantle transition zone structure beneath Tanzania, East Africa. *Geophysical Research Letters*, **27**, 827–830. doi: 10.1029/1999gl005429.

Pail, R., T. Fecher, D. Barnes, J. Factor, S. Holmes, T. Gruber, and P. Zingerle, 2016: The experimental gravity field model XGM2016. In: *International Symposium on Gravity, Geoid and Height System 2016-1st Joint Commission 2 and IGFS Meeting*.

Pail, R., H. Goiginger, W.D. Schuh, E. Höck, J.M. Brockmann, T. Fecher, T. Gruber, T. Mayer-Gürr, J. Kusche, A. Jäggi, and D. Rieser, 2010: Combined satellite gravity field model GOCO01S derived from GOCE and GRACE. *Geophysical Research Letters*, **37**, 1–5. doi: 10.1029/2010gl044906.

Pasyanos, M.E., and A.A. Nyblade, 2007: A top to bottom lithospheric study of Africa and Arabia. *Tectonophysics*, **444**, 27–44. doi: 10.1016/j.tecto.2007.07.008.

Pavlis, N.K., S.A. Holmes, S.C. Kenyon, and J.K. Factor, 2012: The development and evaluation of the Earth Gravitational Model 2008 (EGM2008). *Journal of Geophysical Research: Solid Earth*, **117**. doi: 10.1029/2011jb008916.

Poudjom, Y.D., M. Diament, and M. Wilson, 1997: Lithospheric structure across the Adamawa plateau (Cameroon) from gravity studies. *Tectonophysics*, **273**, 317–327. doi: 10.1016/s0040-1951(96)00280-6.

Poudjom, Y.H.D., J.M. Nnange, M. Diament, C.J. Ebinger, and J.D. Fairhead, 1995: Effective elastic thickness and crustal thickness variations in West Central Africa inferred from gravity data. *Journal of Geophysical Research: Solid Earth*, **100**, 22047–22070. doi: 10.1029/95jb01149.

Priem, H., N. Boelrijk, E. Hebeda, E. Verdurmen, R. Verschure, I. Oen, and L. Westra, 1979: Isotopic age determinations on granitic and gneissic rocks from the Ubendian-Usagaran system in Southern Tanzania. *Precambrian Research*, **9**, 227–239. doi: 10.1016/0301-9268(79)90004-4.

Prodehl, C., A. Jacob, H. Thybo, E. Dindi, and R. Stangl, 1994: Crustal structure on the northeastern flank of the Kenya rift. *Tectonophysics*, **236**, 271–290. doi: 10.1016/0040-1951(94)90180-5.

Rapp, R.H., 1998: Past and future developments in geopotential modeling. In: *Geodesy on the Move*, pp. 58–78. Springer.

Reguzzoni, M., and D. Sampietro, 2015: GEMMA: An Earth crustal model based on GOCE satellite data. *International Journal of Applied Earth Observation and Geoinformation*, **35**, 31–43. doi:

10.1016/j.jag.2014.04.002.

Reid, A.B., J. Ebbing, and S.J. Webb, 2012: Comment on 'a crustal thickness map of Africa derived from a global gravity field model using Euler deconvolution' by Getachew E. Tedla, M. Van der Meijde, A. A. Nyblade and F. D. van der Meer. *Geophysical Journal International*, **189**, 1217–1222. doi: 10.1111/j.1365-246x.2012.05353.x.

Reusch, A.M., A.A. Nyblade, D.A. Wiens, P.J. Shore, B. Ateba, C.T. Tabod, and J.M. Nnange, 2010: Upper mantle structure beneath Cameroon from body wave tomography and the origin of the Cameroon Volcanic Line. *Geochemistry, Geophysics, Geosystems*, **11**, Q10W07. doi: 10.1029/2010gc003200.

Ring, U., 2008: Extreme uplift of the Rwenzori Mountains in the East African Rift, Uganda: Structural framework and possible role of glaciations. *Tectonics*, **27**, 1–19. doi: 10.1029/2007tc002176.

Sandvol, E., D. Seber, A. Calvert, and M. Barazangi, 1998: Grid search modeling of receiver functions: Implications for crustal structure in the Middle East and North Africa. *Journal of Geophysical Research: Solid Earth*, **103**, 26899–26917. doi: 10.1029/98jb02238.

Shako, R., C. Förste, O. Abrikosov, S. Bruinsma, J.C. Marty, J.M. Lemoine, F. Flechtner, H. Neumayer, and C. Dahle, 2013: EIGEN-6C: A high-resolution global gravity combination model including GOCE data. In: *Advanced Technologies in Earth Sciences*, pp. 155–161. Springer Berlin Heidelberg. doi: 10.1007/978-3-642-32135-1_20.

Silva, J.B.C., D.F. Santos, and K.P. Gomes, 2014: Fast gravity inversion of basement relief. *GEOPHYSICS*, **79**, G79–G91. doi: 10.1190/geo2014-0024.1.

Simiyu, S.M., and G.R. Keller, 1998: Upper crustal structure in the vicinity of Lake Magadi in the Kenya Rift Valley region. *Journal of African Earth Sciences*, **27**, 359–371. doi: 10.1016/s0899-5362(98)00068-2.

Simiyu, S.M., and G.R. Keller, 2001: An integrated geophysical analysis of the upper crust of the Southern Kenya rift. *Geophysical Journal International*, **147**, 543–561. doi: 10.1046/j.0956-540x.2001.01542.x.

Sippel, J., C. Meeßen, M. Cacace, J. Mechie, S. Fishwick, C. Heine, M. Scheck-Wenderoth, and M.R. Strecker, 2017: The Kenya rift revisited: insights into lithospheric strength through data-driven 3-D gravity and thermal modelling. *Solid Earth*, **8**, 45–81. doi: 10.5194/se-8-45-2017.

Sobh, M., J. Ebbing, A.H. Mansi, and H.J. Götze, 2019: Inverse and 3D forward gravity modelling for the estimation of the crustal thickness of Egypt. *Tectonophysics*, **752**, 52–67. doi: 10.1016/j.tecto.2018.12.002.

Spieker, K., I. Wölbern, C. Thomas, M. Harnafi, and L.E. Moudnib, 2014: Crustal and upper-mantle structure beneath the Western Atlas mountains in SW Morocco derived from receiver functions. *Geophysical Journal International*, **198**, 1474–1485. doi: 10.1093/gji/ggu216.

Stuart, G.W., J.D. Fairhead, L. Dorbath, and C. Dorbath, 1985: A seismic refraction study of the

crustal structure associated with the Adamawa Plateau and Garoua Rift, Cameroon, West Africa. *Geophysical Journal International*, **81**, 1–12. doi: 10.1111/j.1365-246x.1985.tb01346.x.

Tadili, B., M. Ramdani, D. Ben Sari, K. Chapochnikov, and A. Bellot, 1986: Structure de la croûte dans le nord du Maroc. In: *Annales geophysicae. Series B. Terrestrial and planetary physics*, Volume 4, pp. 99–104.

Tadjou, J.M., R. Nouayou, J. Kamguia, H.L. Kande, and E. Manguelle-Dicoum, 2009: Gravity analysis of the boundary between the Congo Craton and the Pan-African belt of Cameroon. *Austrian Journal of Earth Sciences*, **102**, 71–79.

Tapley, B.D., 2004: GRACE measurements of mass variability in the earth system. *Science*, **305**, 503–505. doi: 10.1126/science.1099192.

Taylor, K.E., 2001: Summarizing multiple aspects of model performance in a single diagram. *Journal of Geophysical Research: Atmospheres*, **106**, 7183–7192. doi: 10.1029/2000jd900719.

Tchameni, R., K. Mezger, N. Nsifa, and A. Pouclet, 2000: Neoarchæan crustal evolution in the Congo Craton: evidence from K-rich granitoids of the Ntem Complex, Southern Cameroon. *Journal of African Earth Sciences*, **30**, 133–147. doi: 10.1016/s0899-5362(00)00012-9.

Tedla, G.E., M. van der Meijde, A.A. Nyblade, and F.D. van der Meer, 2011: A crustal thickness map of Africa derived from a global gravity field model using Euler deconvolution. *Geophysical Journal International*, **187**, 1–9. doi: 10.1111/j.1365-246x.2011.05140.x.

Tenzer, R., and W. Chen, 2019: Mantle and sub-lithosphere mantle gravity maps from the LITHO1.0 global lithospheric model. *Earth-Science Reviews*, **194**, 38–56. doi: 10.1016/j.earscirev.2019.05.001.

Tenzer, R., W. Chen, D. Tsoulis, M. Bagherbandi, L.E. Sjöberg, P. Novák, and S. Jin, 2014: Analysis of the refined CRUST1.0 crustal model and its gravity field. *Surveys in Geophysics*, **36**, 139–165. doi: 10.1007/s10712-014-9299-6.

Tenzer, R., and V. Gladkikh, 2014: Assessment of density variations of marine sediments with ocean and sediment depths. *The Scientific World Journal*, **2014**, 1–9. doi: 10.1155/2014/823296.

Tenzer, R., K. Hamayun, and P. Vajda, 2009: Global maps of the CRUST 2.0 crustal components stripped gravity disturbances. *Journal of Geophysical Research*, **114**. doi: 10.1029/2008jb006016.

Tenzer, R., P. Novák, and V. Gladkikh, 2011: On the accuracy of the bathymetry-generated gravitational field quantities for a depth-dependent seawater density distribution. *Studia Geophysica et Geodaetica*, **55**, 609–626. doi: 10.1007/s11200-010-0074-y.

Tenzer, R., N. Pavel, and G. Vladislav, 2012: The bathymetric stripping corrections to gravity field quantities for a depth-dependent model of seawater density. *Marine Geodesy*, **35**, 198–220. doi: 10.1080/01490419.2012.670592.

Tenzer, R., P. Vajda, and P. Hamayun, 2010: A mathematical model of the bathymetry-generated

external gravitational field. *Contributions to Geophysics and Geodesy*, **40**, 31–44. doi: 10.2478/v10126-010-0002-8.

Tikhonov, A.N., and V.Y. Arsenin, 1977: Solutions of ill-posed problems. *New York*, 1–30.

Tokam, A.P.K., C.T. Tabod, A.A. Nyblade, J. Julià, D.A. Wiens, and M.E. Pasyanos, 2010: Structure of the crust beneath Cameroon, west Africa, from the joint inversion of Rayleigh wave group velocities and receiver functions. *Geophysical Journal International*, **183**, 1061–1076. doi: 10.1111/j.1365-246x.2010.04776.x.

Toteu, S., W.V. Schmus, J. Penaye, and A. Michard, 2001: New u–pb and sm–nd data from north-central Cameroon and its bearing on the pre-Pan African history of Central Africa. *Precambrian Research*, **108**, 45–73. doi: 10.1016/s0301-9268(00)00149-2.

Toteu, S.F., J. Penaye, and Y.P. Djomani, 2004: Geodynamic evolution of the Pan-African belt in Central Africa with special reference to Cameroon. *Canadian Journal of Earth Sciences*, **41**, 73–85. doi: 10.1139/e03-079.

Tugume, F., A. Nyblade, and J. Julià, 2012: Moho depths and Poisson's ratios of Precambrian crust in East Africa: Evidence for similarities in Archean and Proterozoic crustal structure. *Earth and Planetary Science Letters*, **355-356**, 73–81. doi: 10.1016/j.epsl.2012.08.041.

Tugume, F., A. Nyblade, J. Julià, and M. van der Meijde, 2013: Precambrian crustal structure in Africa and arabia: Evidence lacking for secular variation. *Tectonophysics*, **609**, 250–266. doi: 10.1016/j.tecto.2013.04.027.

Uieda, L., and V.C. Barbosa, 2016: Fast nonlinear gravity inversion in spherical coordinates with application to the South American moho. *Geophysical Journal International*, **208**, 162–176. doi: 10.1093/gji/ggw390.

Uieda, L., V.C.F. Barbosa, and C. Braitenberg, 2016: Tesseroids: Forward-modeling gravitational fields in spherical coordinates. *Geophysics*, **81**, F41–F48. doi: 10.1190/geo2015-0204.1.

Urchulutegui, J.F., M. Fernàndez, and H. Zeyen, 2006: Lithospheric structure in the atlantic–mediterranean transition zone (Southern spain, northern Morocco): a simple approach from regional elevation and geoid data. *Comptes Rendus Geoscience*, **338**, 140–151. doi: 10.1016/j.crte.2005.11.004.

Van der Meijde, M., I. Fadel, P. Ditmar, and M. Hamayun, 2015: Uncertainties in crustal thickness models for data sparse environments: A review for South America and Africa. *Journal of Geodynamics*, **84**, 1–18. doi: 10.1016/j.jog.2014.09.013.

Van der Meijde, M., J. Julià, and M. Assumpção, 2013: Gravity derived Moho for South America. *Tectonophysics*, **609**, 456–467. doi: 10.1016/j.tecto.2013.03.023.

Vicat, J.P., J.M. Léger, E. Nsifa, P. Piguet, and J.P. Nzenti, 1996: Distinction, au sein du craton Congolais du sud-ouest du Cameroun, de deux épisodes doléritiques initiant les cycles orogéniques éburnéen (paléoprotérozoïque) et panAfricain (néoprotérozoïque). *Comptes Rendus*

de l'Académie des Sciences. Série 2. Sciences de la terre et des planètes, **323**, 575–582.

Viele, G.W., W.A. Thomas, and I.W.D. Dalziel, 1998: Neoproterozoic-Paleozoic geography and tectonics: Review, hypothesis, environmental speculation: Discussions and reply. *Geological Society of America Bulletin*, **110**, 1615–1620.

Wadge, G., J. Biggs, R. Lloyd, and J.M. Kendall, 2016: Historical volcanism and the state of stress in the East African Rift System. *Frontiers in Earth Science*, **4**. doi: 10.3389/feart.2016.00086.

Walker, K.T., A.A. Nyblade, S.L. Klemperer, G.H.R. Bokelmann, and T.J. Owens, 2004: On the relationship between extension and anisotropy: Constraints from shear wave splitting across the East African Plateau. *Journal of Geophysical Research: Solid Earth*, **109**. doi: 10.1029/2003jb002866.

Wallner, H., and H. Schmeling, 2011: Sensitivity analysis of rift induced delamination with application to Rwenzori mountains. *Geophysical Journal International*, **187**, 1135–1145. doi: 10.1111/j.1365-246x.2011.05237.x.

Weeraratne, D.S., D.W. Forsyth, K.M. Fischer, and A.A. Nyblade, 2003: Evidence for an upper mantle plume beneath the Tanzanian craton from Rayleigh wave tomography. *Journal of Geophysical Research: Solid Earth*, **108**. doi: 10.1029/2002jb002273.

Wigger, P., G. Asch, P. Giese, W.D. Heinsohn, S.O. el Alami, and F. Ramdani, 1992: Crustal structure along a traverse across the Middle and High Atlas mountains derived from seismic refraction studies. *Geologische Rundschau*, **81**, 237–248. doi: 10.1007/bf01764552.

Wilson, M., and R. Guiraud, 1992: Magmatism and rifting in Western and Central Africa, from Late Jurassic to Recent times. *Tectonophysics*, **213**, 203–225. doi: 10.1016/0040-1951(92)90259-9.

Wölbern, I., G. Rümpker, A. Schumann, and A. Muwanga, 2010: Crustal thinning beneath the Rwenzori region, Albertine rift, Uganda, from receiver-function analysis. *International Journal of Earth Sciences*, **99**, 1545–1557. doi: 10.1007/s00531-009-0509-2.

Woollard, G.P., 1959: Crustal structure from gravity and seismic measurements. *Journal of Geophysical Research*, **64**, 1521–1544. doi: 10.1029/jz064i010p01521.

Yoder, C., J. Williams, J. Dickey, B.E. Schutz, R.J. Eanes, and B.D. Tapley, 1983: Secular variation of Earth's gravitational harmonic J2 coefficient from LAGEOS and nontidal acceleration of Earth rotation. *Nature*, **303**, 757–762.

List of Publications

Peer-Reviewed

1. **Franck Eitel Kemgang Ghomsi**, Nelson Ribeiro-Filho, Raissa Baldez, Robert Tenzer, Cristiano Mendel Martins, Chikondi Chisenga, Sévérin Nguiya, Robert Nouayou. (2021): **Identification of Cameroon's geological structures through a gravity separation and using seismic crustal models**. *Journal of African Earth Sciences.* **173**. DOI: 10.1016/j.jafrearsci.2020.104027 . (*Impact Factor: 1,713*);

2. **Franck Eitel Kemgang Ghomsi**, Nguiya Sévérin, Animesh Mandal, Françoise Enyegue A. Nyam, Robert Tenzer, Alain P.Tokam Kamga and Robert Nouayou. (2020): **Cameroon's crustal configuration from global gravity and topographic models and seismic data**. *Journal of African Earth Sciences.* **161**. DOI: 10.1016/j.jafrearsci.2019.103657. (*Impact Factor: 1,713*);

3. **Franck Eitel Kemgang Ghomsi**, Robert Tenzer, Sévérin Nguiya, Animesh Mandal, Robert Nouayou. (2019): **Crustal thickness beneath Atlas region from gravity, topographic, sediment and seismic data**. *Geodesy and Geodynamics.* DOI: 10.1016/j.geog.2019.08.002. (*Impact Factor: 1,470*);

Journal of African Earth Sciences 173 (2021) 104027

Contents lists available at ScienceDirect

Journal of African Earth Sciences

journal homepage: www.elsevier.com/locate/jafrearsci

Identification of Cameroon's geological structures through a gravity separation and using seismic crustal models

Franck Eitel Kemgang Ghomsi [a,b,*], Nelson Ribeiro-Filho [c], Raissa Baldez [c], Robert Tenzer [d], Cristiano Mendel Martins [c], Chikondi Chisenga [e], Sévérin Nguiya [f], Robert Nouayou [b]

[a] Institute of Geological and Mining Research (IRGM), Branch for Geophysical and Volcanological Research (ARGV), P.O. Box 370, Buea, Cameroon
[b] Department of Physics, University of Yaoundé 1, P.O. Box 812, Yaoundé, Cameroon
[c] Centro de Pós Graduação Em Geofísica (CPGF), Universidade Federal Do Pará (UFPA), Belém, Brazil
[d] Department of Land Surveying and Geo-Informatics, Hong Kong Polytechnic University, Hong Kong
[e] Department of Earth Sciences, Ndata School of Climate and Earth Sciences, Malawi University of Science and Technology, Box 5196, Limbe, Malawi
[f] National Advanced School of Engineering of Douala, University of Douala, Douala, Cameroon

ARTICLE INFO

Keywords:
Crust
Forward modelling
Geology
Gravity
Cameroon

ABSTRACT

Residual gravity data provide useful information for a geophysical interpretation of geological sources. Several techniques have been developed and applied to separate a different content in gravity data. Nevertheless, few methods actually incorporate factual geophysical or geological information in gravity data processing. Instead, most of these methods relay only on mathematical techniques that do not necessarily reflect the actual geological composition and problems inherent to gravity inversion, most notably a non-uniqueness of solutions to gravimetric inverse problems (i.e. infinity many geological configurations could theoretically provide the same gravity solution) as well as the fact that gravimetric inverse solutions are generally ill-posed problems that require employment of regularization techniques. To partially address this issue, we apply a gravimetric forward modelling based on available seismic crustal structure models to separate a residual gravity signal from observed gravity data in order to interpret more realistically detailed geological and tectonic features. This procedure involves the estimation of the uppermost mantle gravity contribution that is treated as a regional gravity data. The residual gravity data is then obtained by subtracting the regional gravity data from observed gravity data. In addition, observed gravity data are typically corrected for the gravitational contributions of topography and bathymetry (and possibly other known crustal density heterogeneities, such as sediments and density variations within the underlying consolidated crust). The application of these gravity corrections to observed (free-air) gravity data yields the Bouguer gravity data. We employ this forward modelling approach to the Bouguer gravity disturbances over Cameroon. Furthermore, we apply a regional-residual separation based on a spectral analysis and a robust polynomial fitting. The performance of these three techniques is compared in terms of their interpretational quality. The numerical analysis reveals that the residual gravity disturbance map obtained by applying the forward modelling technique resembles main known geological and tectonic configuration and closely reproduces even more detailed features. The results from using a spectral analysis could to some extent reproduce realistically tectonic and geological structures, except for more localized features otherwise seen in the forward modelling result. A robust polynomial fitting, on the other hand, fails to provide residual gravity disturbances that realistically reflect geological and tectonic configuration of the study area. The reason is that this method produces either only positive or only negative gravity disturbances, but not both. Moreover, this merely mathematical technique does not take into consideration available geological and geophysical information.

* Corresponding author. Institute of Geological and Mining Research (IRGM), Branch for Geophysical and Volcanological Research (ARGV), P.O. Box 370, Buea, Cameroon.

E-mail addresses: franckeitel@gmail.com (F.E. Kemgang Ghomsi), nelsondelimar@gmail.com (N. Ribeiro-Filho), raissabaldez1@gmail.com (R. Baldez), robert.tenzer@polyu.edu.hk (R. Tenzer), mendelmartins@gmail.com (C.M. Martins), cchisenga@must.ac.mw (C. Chisenga).

https://doi.org/10.1016/j.jafrearsci.2020.104027
Received 25 July 2020; Received in revised form 18 September 2020; Accepted 5 October 2020
Available online 8 October 2020

Journal of African Earth Sciences 161 (2020) 103657

Contents lists available at ScienceDirect

Journal of African Earth Sciences

journal homepage: www.elsevier.com/locate/jafrearsci

Cameroon's crustal configuration from global gravity and topographic models and seismic data

Franck Eitel Kemgang Ghomsi[a], Nguiya Sévérin[b], Animesh Mandal[c], Françoise Enyegue A. Nyam[a], Robert Tenzer[d], Alain P. Tokam Kamga[a], Robert Nouayou[a,*]

[a] Laboratory of Geophysics and Geoexploration, Department of Physics, The University of Yaoundé I, Yaoundé, Cameroon
[b] Faculty of Industrial Engineering, University of Douala, Douala, Cameroon
[c] Department of Earth Sciences, Indian Institute of Technology, Kanpur, India
[d] Department of Land Surveying and Geo-Informatics, Hong Kong Polytechnic University, Hong Kong

ARTICLE INFO

Keywords:
Cameroon
Crust
Gravity inversion
Moho
Seismic data

ABSTRACT

We use gravity information obtained from the XGM2016 global gravitational model together with topographic, bathymetric and seismic data to interpret the crustal structure beneath Cameroon and adjoined geological regions. For this purpose, we apply the regularized non-linear gravity inversion for a gravimetric determination of the Moho depth utilizing existing results of seismic data analysis as constraints. The estimated Moho model reflects regional tectonic configuration and geological structure of this region, mainly consisting of two major geological units, i.e. the Cameroon Volcanic Line and the Congo Craton. A validation of gravimetric result at sites of the Cameroon Broadband Seismic Experiment (CBSE) reveals overall similarities between gravimetric and seismic estimates. A comparison of our result is also conducted with previously published results. The cross-comparison of these results reveals a good agreement between them, particularly beneath the Cameroon Volcanic Line, the Adamawa Plateau and the Garoua Rift. Nevertheless, some relatively large inconsistencies roughly reaching ± 10 km in estimated values of the Moho depth are identified in geological regions of the Congo Craton and the Yaoundé domain. The spatial correlation analysis between the Moho geometry and the topography indicates an isostatic state of particular geological units, suggesting their compensation stage. Our result closely agrees with the assumption that most of isostatically over compensated geological structures were formed during a compressional tectonic regime, except for the Garoua Rift that was likely formed during an extensional regime. We also computed the Bouguer gravity data at different constant elevations above sea level in order to supress a gravitational signature of shallower sources, while enhancing a gravitational signature from deeper crustal and lithospheric structures, focusing primarily on cores of major cratonic formations. The Bouguer gravity maps indicate that the Yaoundé domain likely represents the crustal manifestation of the suture zone between the Congo Craton and the Adamawa-Yadé domain, acting as a micro-continent.

1. Introduction

The first gravimetric survey in Cameroon had begun between 1963 and 1968. Since then, several detailed gravity surveys in parts of Cameroon and surrounding central African countries were undertaken by the Office de la Recherche Scientifique et Technique Outre-Mer (ORSTOM) between 1970 and 1990 (Collignon, 1968) as well as by other geophysical campaigns (Poidevin, 1983). Despite this effort, the high-resolution gravity data are mostly limited to oil-producing sedimentary basins, typically concentrated in the Gulf of Guinea and the main Chad basin zones, while also usually being the property of petroleum companies. Consequently, most of the detailed gravity datasets are currently not available for a scientific community. Furthermore, the region is covered by a thick forest and highlands with few roads. This restricted access further limits possibilities of collecting terrestrial gravity data that could sufficiently cover the whole region and allow a more detailed gravimetric interpretation. As consequence, the existing gravity data distribution is highly uneven, while largely concentrated along major roads and tracks (Tadjou et al., 2009). Moreover, their patchy distribution does not allow derivation of large-scale interpretational models. Thus, big data gaps exist in inaccessible areas and areas without an indication of valuable minerals. The

* Corresponding author. The Department of Land Surveying and Geo-Informatics, The Hong Kong Polytechnic University, 181 Chatham Road South, Kowloon, Hong Kong.
E-mail address: robert.tenzer@polyu.edu.hk (R. Nouayou).

https://doi.org/10.1016/j.jafrearsci.2019.103657
Received 13 June 2019; Received in revised form 26 September 2019; Accepted 27 September 2019
Available online 04 October 2019
1464-343X/

Geodesy and Geodynamics 11 (2020) 18–30

Contents lists available at ScienceDirect

Geodesy and Geodynamics

journal homepage: http://www.keaipublishing.com/geog

Crustal thickness beneath Atlas region from gravity, topographic, sediment and seismic data

Franck Eitel Kemgang Ghomsi [a], Robert Tenzer [b, *], Sévérin Nguiya [c], Animesh Mandal [d], Robert Nouayou [a]

[a] Department of Physics, The University of Yaoundé I, Yaoundé, Cameroon
[b] Department of Land Surveying and Geo-Informatics, Hong Kong Polytechnic University, Hong Kong, China
[c] Faculty of Industrial Engineering, University of Douala, Douala, Cameroon
[d] Department of Earth Sciences, Indian Institute of Technology, Kanpur, India

ARTICLE INFO

Article history:
Received 19 May 2019
Accepted 8 August 2019
Available online 6 November 2019

Keywords:
Atlas
Gravity
Inversion
Moho
Seismic data

ABSTRACT

The Atlas region in northwest Africa is characterized by the Quaternary volcanism and elevated topography with past complex tectonic mitigation between the African and European plates. Geodynamics of this atypical region has left indubitably imprints in crustal architectonics, mainly regarding the crustal thickness as well as the crustal density structure. The knowledge of crustal thickness variations is of a significant interest, since it provides a crucial constraint to geodynamic and geophysical modelling of this region. In this study, we use gravity, topographic, bathymetric and sediment data together with results of seismic surveys to image the Moho topography beneath the Atlas region. The Bouguer gravity anomalies used for a gravimetric Moho recovery are obtained from the free-air gravity anomalies after subtracting the gravitational contributions of topography, bathymetry and sediments. The regional gravimetric Moho inversion constrained on seismic data is carried out by applying a regularized inversion technique based on Gauss-Newton's formulation of improved Bott's method, while adopting Earth's spherical approximation. The numerical result reveals relatively significant Moho depth variations in the Moroccan Atlas, with minima of approximately 24 km along continental margins of the Mediterranean Sea and maxima exceeding 51 km beneath the Rif Cordillera. The Moho depth beneath the West African Craton varies from 32 km in its southern margin to 45 km beneath the Middle Atlas. The Tell Atlas is characterized by the shallow Moho depth of approximately 22 km and further deepening to 42 km towards the northern edge of the Aures Mountains. Our findings indicate a limited tectonic shortening of the High Atlas with the crustal thickness mostly within 36–42 km. Topographic discrepancies between the Rif Cordillera and the Atlas Mountains suggest that the hypothesis of isostatic compensation cannot be fully established.

1. Introduction

The Atlas Mountains evolved through a long and complex geological history, which formed an intra-continental mountain belt that resulted from the convergence between the African and Eurasian plates. This process began in the Late Caenozoic and continues to present times [1–3]. As the result, the crustal structure of this region is composed of a variety of different geological units. The crustal variability is one of the most important factor that manifests a tectonic evolution of this region. Its nature and geodynamic settings have been the subject of numerous studies, especially over last few decades. Among published results, we

* Corresponding author. The Department of Land Surveying and Geo-Informatics, The Hong Kong Polytechnic University, 181 Chatham Road South, Kowloon, Hong Kong, China.
E-mail address: robert.tenzer@polyu.edu.hk (R. Tenzer).

Peer review under responsibility of Institute of Seismology, China Earthquake Administration.

Production and Hosting by Elsevier on behalf of KeAi

https://doi.org/10.1016/j.geog.2019.08.002